HUGHES

NEUTRON CROSS SECTIONS

INTERNATIONAL SERIES OF
MONOGRAPHS ON NUCLEAR ENERGY

NEUTRON CROSS SECTIONS

by

DONALD J. HUGHES

BROOKHAVEN NATIONAL LABORATORY

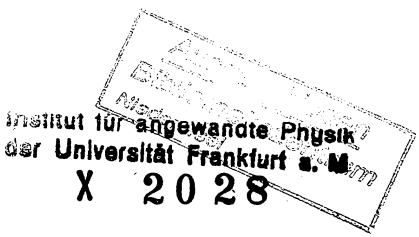

PERGAMON PRESS

LONDON · NEW YORK · PARIS

1957

PUBLISHED BY
PERGAMON PRESS
4 & 5 Fitzroy Square, London W.1
122 East 55th Street, New York 22, N.Y.
*24 Rue des Écoles, Paris V^e^*

Printed in Great Britain by Page Bros. (Norwich) Ltd., Norwich

International Series of Monographs on Nuclear Energy

Division II. NUCLEAR PHYSICS

Volume 1

NEUTRON CROSS SECTIONS

The International Series of Monographs on Nuclear Energy

GENERAL EDITORS

R. A. CHARPIE and J. V. DUNWORTH

Monographs will be published in the following divisions

I. Economics of Nuclear Energy
II. Nuclear Physics
III. Biology
IV. Isotopes and Radiation
V. Health Physics
VI. Medicine
VII. Reactor Engineering
VIII. Materials
IX. Chemical Engineering
X. Reactor Design Physics
XI. Reactor Operational Problems
XII. Chemistry
XIII. Reactor Theory

TO VAL

CONTENTS

PREFACE

THE writing of this book is a direct result of experiences connected with the collection and evaluation of cross-section data during the past eight years at "Sigma Centre", Brookhaven National Laboratory. Here, experimental results received from laboratories throughout the world are carefully evaluated and compiled in the curves and tables of the large volume *Neutron Cross Sections*. The most recent version of the compilation, known as BNL 325, appeared 1 July 1955, and Supplement 1 to BNL 325 was published on 1 January 1957.

Hundreds of requests have come to Sigma Centre, concerning not only specific cross sections but the way in which to use them in practical applications or to assess their accuracy. Many people are now in a position where they must use cross-section data in their work but are handicapped because they have not had training in nuclear theory. Many of the cross-section requests can be answered by recourse to simple theoretical principles but of course this information, not being included in the compilation, is not easily available to those without nuclear training. Actually, it is often true that basic knowledge is needed even to *ask* a question in clear form about a cross section; again this information cannot be gained from the compilation itself.

Thus it became clear that there was a definite need for a clear and concise explanation of the principles of cross-section theory, measurement, and use that underly the compilation, in other words, a manual that would assist in the understanding and use of BNL 325. The compilation itself consists almost completely of cross sections at specific energies, shown in the form of curves or tables, with only brief explanatory texts. The present monograph, it is hoped, will be an answer to the need that has become evident in the course of compilation work. Its objective is to present the principles of cross-section measurement and use, as well as sufficient theory so that the general behaviour of cross sections is made understandable.

After a brief view of the most general properties of cross sections, Chapter 1, the book goes on to a discussion of the theory of cross sections and of nuclear structure. Here an attempt is made to present the basic facts of cross sections, without going into more details than are necessary for a clear and correct understanding. It is impossible to treat the theory of cross sections without some description of current views of nuclear structure, for the interactions

of neutrons with nuclei obviously are determined by the latter's structure. Those principles of nuclear structure that are particularly important to the understanding of cross-section behavior are therefore included in Chapter 2.

The specific techniques for measurement of cross sections and a consideration of the experimental results are then presented, beginning with fast neutrons in Chapter 3 and continuing with resonance neutrons in Chapter 4, resonances in fissionable materials in Chapter 5, and concluding with thermal neutrons in Chapter 6. In the discussions of experimental results in these chapters, actual cross sections are presented for illustrative purposes only, for the present monograph is not a compilation of data. It deals rather with the principles of cross-section measurement, behavior, and use, which hopefully will lose their pertinence only very slowly. The actual experimental results, which at times change rapidly, can be found in BNL 325 and its supplements and future editions. Frequent reference is made to BNL 325, however, for it is hoped that the present monograph will increase the usefulness of the compilation to a great extent.

Because this volume is intended for the many individuals who must use cross sections but do not have training in advanced nuclear theory, it was not felt desirable or necessary to include numerous references to original literature. For those with advanced training the compilation alone is probably sufficient, as it does contain references to the original sources of data. General references have been listed at the ends of the various chapters in the present volume that can be used for further reading and study.

I should like to express my gratitude to J. A. Harvey for his careful reading of the manuscript and valuable suggestions, as well as to G. Cox for many of the original drawings and to A. Marshall for preparation of the manuscript.

D. J. HUGHES

Brookhaven National Laboratory,
Long Island, New York

CHAPTER 1

TYPES OF CROSS SECTIONS AND PRINCIPLES OF MEASUREMENT

THE subject of the interaction of neutrons with matter contains an astonishing diversity of phenomena. The basic reason for the great variety in their behaviour is that neutrons of an extremely wide energy range are able to interact effectively with nuclei. As the neutron carries no net electrical charge, there is no Coulomb repulsion to prevent its interaction with nuclei and it is thus able to cross the nuclear boundary even when moving at less than thermal velocity. Because of the lack of charge, the energy region over which neutrons cause nuclear interactions is much wider than it is for protons. Primarily because of this simple fact, a broad field of *neutron physics* exists—contrasted to which, of course, we cannot point to an equally wide field of "proton physics". From nuclear reactors alone, neutron beams are available in sufficient intensity to make possible effective studies of interactions with matter from energies as low as 10^{-4} eV to an upper limit at about 10^{7} eV, an astonishingly large range in energy—a 10^{11}-fold spread. Actually, including the most powerful accelerating machines presently available increases the energy spread only slightly, that is up to a few times 10^{9} eV, the energy available with the Bevatron accelerator at the University of California.

Corresponding to the enormous range in energy over which neutrons exhibit appreciable interactions with matter, there is a great variety in the types of interactions that are observed. As the neutron energy increases throughout this energy range its wavelength decreases, from a value much greater than the distance between atoms in ordinary matter at the lowest energies, until at the upper limit the wavelength becomes much smaller than the size of the nucleus, eventually reaching a size about equal to the range of nuclear forces. Considering the 10^{11} energy factor, it is not at all surprising that in this range the properties of neutrons in their interactions with matter can also vary greatly.

At the low energy or long wavelength limit of available intensity, the optical properties of neutrons predominate and we can demonstrate refraction and reflection of neutrons in ordinary matter. As the energy increases and the neutron wavelength decreases, the particle

characteristics of neutrons become more dominant until at the highest energies it seems most natural to think of neutrons as point projectiles colliding with the individual particles that make up the nuclei.

The measure of the interaction of neutrons with matter is the neutron *cross section*, and the great range of phenomena is reflected in the range of types of cross sections that can be measured. The collection of neutron cross sections shown as curves in the compilation* BNL 325 illustrates this variety. For some cross sections there exist great differences from element to element or even from isotope to isotope, while for other cross sections there are striking regularities as one moves through the Periodic Table or from energy to energy within a single nuclide. The numerical magnitudes of the cross sections vary from values as large as millions of barns down to millionths of barns, that is, from *megabarns* to *microbarns*.

The matter of neutron cross sections is the very heart of neutron physics, for in one sense almost the whole of neutron physics is just the study of cross sections. Every neutron interaction can be described as a particular type of cross section, hence the measurement of any phenomenon with neutrons is automatically a cross-section measurement of some type. Fortunately, the great range of cross-section types exhibited in the compilation have a close connection with underlying theory, which, although it is not sufficiently exact to predict cross sections, nevertheless is of great value in correlating, interpolating between measured points, and even "guessing" many of them with fair accuracy.

SIMPLE DEFINITION OF CROSS SECTION AS NUCLEAR AREA

Cross sections are measured in units of area, the almost universally used "barn" (the basis for the cover design of BNL 325) being equal to 10^{-24} cm^2. Although in Chapter 2 we shall be concerned with the more exact quantum mechanical analysis of cross sections, at the present time a simple dimensional definition related to area is useful. The simple concept of cross section in terms of area is not only useful for its illustrative purposes, but is exact enough so that for practically all applications one can consider cross sections simply as target areas, with no error arising as a result. In this elementary sense, the cross section of a nucleus is just the target area presented by that nucleus to an approaching neutron. The target area or cross section

* *Neutron Cross Sections*, D. J. Hughes and J. A. Harvey, July 1, 1955, Brookhaven National Laboratory Report BNL 325, and BNL 325–Supplement No. 1, D. J. Hughes and R. B. Schwartz, January 1, 1957, Superintendent of Documents, Government Printing Office, Washington 25, D. C. ($3.50 and $1.75).

is measured as area on a plane normal to the motion of the neutron, and can be considered simply as the area of the projection of the actual nucleus on the plane.

This picture of course must not be taken too literally because the cross section changes, and often very rapidly, with the velocity of the neutron, whereas it is obvious that the actual size of the nucleus is not dependent on the velocity of the incoming neutron. The cross section defined as the projected area of the nucleus is a measure of the probability that a neutron will hit that nucleus regardless of what happens after the collision. This type of cross section is called the *total cross section*, which is proportional to the total probability of interaction, of whatever kind, for the nucleus.

The total cross section can be subdivided into *partial cross sections*, each proportional to the probability of a particular event ensuing, of the various possible end-results following the collision of the neutron with the nucleus. For instance, the neutron may collide elastically and not be absorbed at all, it may be captured by the nucleus followed by emission of gamma radiation, it may emerge from the nucleus with its energy decreased, or it may even cause the nucleus to split, with the emission of perhaps a proton or an alpha particle or, for several heavy nuclei, by the more violent phenomenon that is fission. The partial cross sections are all measured in terms of area, as is the total cross section, and the sum of the partial cross sections of course must add to the total cross section itself. In this simple picture the target may be considered as divided into different sections, each corresponding to a particular type of reaction, and a neutron hitting a particular section resulting in the corresponding reaction. If the total cross section were always reasonably constant with energy, as it is at high energy, this picture of a subdivided nuclear area would seem reasonable enough. In the intermediate and low energy regions, however, the total target area itself must be considered to be changing rapidly with neutron energy, a property that is a bit difficult to reconcile with such a simple model.

From the model we have just considered, even if far too crude in some respects, the basic properties of neutrons in interacting with matter are nevertheless easily and correctly derived. Thus, as shown in Fig. 1–1, the number of interactions taking place per unit time when N' nuclei are bombarded by neutrons of density n per cm^3 and velocity v, cm per sec, is given by:

$$\text{interactions per second} = N'nv\sigma_T \,, \qquad (1\text{–}1)$$

assuming that N' is small enough so that the nuclei do not change the neutron density appreciably. Thus the interaction rate is proportional to the product of neutron density n and velocity v, which is the

neutron flux. Although strictly speaking nv should be called the flux density, wide acceptance of the shorter term has standardized its usage. Thus a unit cross section is one that gives one interaction per unit time when a unit neutron flux is incident on a single nucleus. It is to be noted that the interaction rate depends on the total number of nuclei, N', not on the number per cm^3, N, which we shall use in many other connections later.

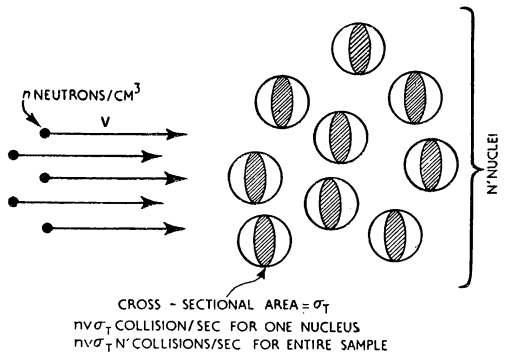

FIG. 1–1. The simple concept of neutron cross section as nuclear area. The number of neutrons in the volume $v\sigma_T$ will hit a given nucleus per second. This number is $nv\sigma_T$ for one nucleus or $N'nv\sigma_T$ for all nuclei, regardless of the density of the sample or orientation, if N' is sufficiently small so that there is no self-shielding.

Although the practical utility of the concept of a cross section as nuclear area is obvious, its unreality is clearly shown by the variation in size of cross sections, enormous compared to the relatively constant true nuclear size. Only for high energy neutrons, for which the wavelength, which can be thought of as the neutron's size, is less than that of the nucleus, is the cross section about equal to the geometrical size of the nucleus itself. For a nucleus of radius R the area projected on a plane is πR^2, which for a heavy nucleus is about 3×10^{-24} cm^2 or 3 barns. Thus the total cross section for fast neutrons is typically of the order of a few barns, though the way in which this cross section is divided into various partial cross sections may differ greatly from element to element. The similarity of cross sections for fast neutrons from nuclide to nuclide and the very gentle change with energy is a direct result of the fact that for short wavelength the particle aspects of the neutrons are dominant. For a small, almost a point particle, hitting a strongly interacting sphere the total cross section should be approximately πR^2. That the total cross sections are not precisely this value is a matter of great importance to modern nuclear theory, as we shall see, and reveals that the

nucleus is a much more weakly interacting object than had been long assumed.

At lower neutron energy, where the neutron *wavelength* is larger than the nucleus, the situation becomes much more complicated, as the wave properties begin to emerge. When the neutron is much larger than the nucleus, it is quite reasonable to conclude that the chance of interaction is given not by the size of the nucleus but by the size of the neutron itself, which is about $\pi\lambda\!\!\!^{-2}$ rather than πR^2 where λ is the neutron wavelength ($\lambda\!\!\!^{-} = \lambda/2\pi$). For non-relativistic velocities, the neutron wavelength is given by the formula

$$\lambda = \frac{h}{mv} \quad , \tag{1–2}$$

where h is Planck's constant and mv is the momentum of the neutron. The wavelength is expressed in terms of the neutron energy, E(eV), as

$$\begin{aligned} \lambda &= h/\sqrt{(2mE)} \\ &= 2{\cdot}86 \times 10^{-9}/\sqrt{(E)}\ \text{cm} \\ &= 0{\cdot}286/\sqrt{(E)}\ \text{Ångstrom units (Å)} \ . \end{aligned} \tag{1–3}$$

The equations for the neutron wavelength are given in the simple non-relativistic form because the neutron energies with which we shall be concerned are sufficiently low so that the relativistic corrections are negligible. The wavelength is much larger than the nuclear radius for intermediate and low energy neutrons, for example $\lambda\!\!\!^{-}$ is $4{\cdot}6 \times 10^{-10}$ cm for a one eV neutron, several hundred times larger than a typical nuclear radius.

In actuality, as a glance at BNL 325 will show, the cross section does not turn out to be simply the slowly varying $\pi\lambda\!\!\!^{-2}$, but is vastly more complicated. In general, it is much smaller than $\pi\lambda\!\!\!^{-2}$, but does reach values as large as $4\pi\lambda\!\!\!^{-2}$ under very special circumstances, as we shall see later. The reason for the low cross-section values and the rapid variations in energy is that the wave properties of the neutron necessitate a wave-mechanical treatment of the nuclear interaction and the results are not at all what one would expect from a classical view of an object of cross-sectional area $\pi\lambda\!\!\!^{-2}$ hitting one of area πR^2. In addition, the variation in cross section from nuclide to nuclide is extremely great, and at first sight may seem to be rather capricious. However, modern theory has gone a long way toward the understanding of neutron cross sections even in the energy region where the variations with energy and nuclide are abrupt and large.

CROSS-SECTION NOMENCLATURE

With such an enormous range of types of cross sections and numerical magnitudes it becomes a rather difficult task to distinguish

clearly the cross sections for specific interactions and to correlate measured results. Even the question of nomenclature of types of cross sections has given rise to increasing confusion as measurement techniques have become more subtle, and it is only recently that the nomenclature has begun to be well codified. Much of the difficulty in cross-section terminology arises because the terms sometimes refer to the phenomenon or manifestation by which the cross section is measured, such as capture cross section (detection of capture gamma rays), activation cross section (radioactivity of end product), etc., and at times to the theoretical picture that is used to describe the interactions, such as compound nucleus formation cross section, reaction cross section, etc. Whereas it is true that in many cases a cross-section type, based on a theoretical model, can be clearly identified with a specific cross section as it is manifested experimentally, in general a careful distinction must be made between a theoretical interpretation of what is going on and the phenomena as they are actually measured in experiments. For our purposes it is best to emphasize those cross-section types that are based on the principle of measurement primarily, rather than on theoretical constructs. The collection, correlation and evaluation of measured cross sections, as is done in BNL 325, for example, is in the frame of reference of experiments, with only a few general theoretical concepts as guides.

Even for cross-section terms that refer only to experimental conditions, however, there is a wide variety, reflecting the range of phenomena that are observed at various energies. Many of these refer to specific interactions that are observed in limited energy bands only, such as "phonon gain scattering" or "spin-dependent incoherent scattering" and these we shall consider later, in appropriate chapters. But in spite of the variety, there are some cross section terms of rather general meaning that are useful throughout the entire energy range, and it is desirable to define these before proceeding. Certainly the most universally measured cross section is the *total cross section*, which as we have seen represents all the interaction processes that may result from the collision of a neutron with an atom, and is thus the sum of all the *partial cross sections*. Simple as this definition may seem, its interpretation, especially at low energy, requires careful attention. At energies above one eV or so, the individual atoms do not affect each other and the cross section of a particular atom is the same whether it is isolated or associated with other atoms in a crystal. At lower energy, however, the neutron waves scattered by different atoms interfere and the observed scattering, hence cross section, can be a strong function of the physical state of the material, for example whether it is crystalline or liquid. In this case, as in all

others, the total cross section found in BNL 325 is obtained from Eq. (1–1), which means that it is averaged over the atoms as they exist in the sample and is not the cross section of an isolated atom. For exactness, we have referred in this paragraph to the "atom", although most of the cross section is contributed by the nucleus, particularly at energies above one eV. There is an appreciable magnetic interaction between the neutron and the atomic electrons, as well as a very small electrostatic interaction, but these are observable only at low energy where the atomic electrons have an appreciable form factor.

Of the various partial cross sections, the *scattering cross section* has a very definite meaning, being the cross section for all processes in which the only *particle* emitted in the interaction is a neutron. If this neutron should have energy identical with the incoming neutron energy the scattering is then called *elastic scattering*, and in the case that the energy changes it is *inelastic scattering*. The usual type of inelastic scattering is that in which energy is lost by the neutron and emitted as gamma radiation.

In general, neutron scattering is not isotropic, hence it is useful to specify a cross section as a function of the direction in which the neutron is emitted. Thus the *differential scattering cross section*, which of course in turn may be elastic or inelastic, gives the cross section for emission of the neutron at a particular angle. This differential scattering cross section is expressed as the scattering per unit solid angle and its integral over the total solid angle must equal the scattering cross section, elastic or inelastic. It is tempting in this connection to refer to the "total scattering cross section" but ambiguity is reduced if the adjective "total" is reserved for the total cross section alone.

For those interactions other than scattering, there are of course a number of corresponding partial cross sections, the *capture cross section*, for example, for those interactions in which the neutron is absorbed by the nucleus, and followed by emission of gamma rays.

The capture cross section is sometimes called the *absorption cross section*, but this term has been used with such a variety of meanings that it is wise to discourage its general use, and to define it on the spot if its use is desired. Another particular type of cross section, the *activation cross section*, refers to those interactions measured by the resulting radioactivity of the nucleus formed. The activation cross section *usually* is the same as the capture cross section, but activation can sometimes be a result of reactions other than neutron capture, such as the (n,p) and (n,α) reactions, which are not considered capture cross sections. It is also true that neutron

capture can result in a stable nucleus, which strictly speaking, has zero activation cross section.

A very special cross section is that for *fission*, which occurs only for the heaviest elements, whose isotopes are called *fissionable* if fission occurs for slow neutrons. The cross-section term much used for fissionable isotopes is the absorption cross section, which has such a variety of meanings that its use has often led to ambiguities. The current meaning with regard to fissionable isotopes, such as U^{235}, is reasonably well established, however. For slow neutrons the total cross section of U^{235} is made up of scattering plus fission plus capture, where by capture we here of course mean the (n,γ) reaction only. In this case the fission cross section plus the capture cross section is usually called the absorption cross section, that is, the total cross section minus scattering. This "absorption cross section" is particularly valuable for comparison with theory and is found plotted for the fissionable isotopes in BNL 325, p. 298, for example.

A type of cross section that is analogous to the absorption cross section, as just described, is the *nonelastic cross section.* It has been defined in a number of ways but agreement seems now about reached that it signifies the total cross section minus the *elastic* scattering cross section. The fundamental raison d'etre for it is that a particular technique, the "*sphere transmission*", described in Chapter 3, gives just this cross section. It often is identical with the inelastic scattering cross section, but in addition will include other processes, such as capture, (n,α), (n,p), fission, etc., if they are appreciable. In the energy region where nonelastic cross sections are usually measured, several MeV, they are approximately equal to inelastic scattering, for the other processes mentioned are in general much smaller.

As the phenomena observed with neutrons change with neutron energy, various types of cross sections, useful only in certain energy regions, appear. Thus, at a few eV, we talk about "free atom cross sections", whereas for neutrons of about 10^{-4} to 10^{-1} eV, where we are interested in the phenomena of neutron optics, such as reflection and diffraction, there is much discussion of the "coherent" and "incoherent" cross sections. There is usually no difficulty in terminology with these cross sections, which apply only in special circumstances, but the more general types of cross sections such as capture, total, nonelastic and inelastic, etc., are sufficiently general so that care should be used in applying them.

The nomenclature used for cross sections has until recently not existed in a universally accepted form and as a result a certain amount of confusion has arisen. However, the Nuclear Cross Sections Advisory Group of the U.S. Atomic Energy Commission

has now proposed some rules of nomenclature to unify cross-section definitions and notation. The recommendations apply to the notation with regard to experimentally determined quantities rather than the theoretical significance of the cross sections. The type of reaction is indicated by subscripts, such as σ_{np} for the (n,p) reaction and σ_{nT} for the total cross section. Of course, when neutrons only are considered as incident particles, the n can be omitted in the subscript, thus in the present monograph we shall use σ_T as the total cross section and σ_p as the (n,p) cross section. The experimental variables that apply to the particular cross section are indicated in the parentheses following the cross section symbol, thus E in the parentheses refers to the energy of the neutron, as $\sigma_T(E)$, and θ in the parentheses denotes the differential cross section at the angle θ, as $\sigma_n(E; \theta)$ for differential elastic scattering.

Even though the notation is kept to a minimum in this system, it can still become rather complicated, especially when reactions emitting several products occur. An example is the $(n,2n)$ reaction for an incident neutron of energy E, written in full as

$$\sigma_{n2n}(E; E', \theta) ,$$

which gives the differential cross section for emission of a neutron of energy E' at the angle θ, with no specification for the other emitted neutron. However, for most of the reactions that we shall be considering the terminology retains its simplicity as we shall see in later chapters. Examples are $\sigma_{nn}(E)$ for the cross section for elastic scattering, and $\sigma_{nn}(E; \theta)$ for the differential elastic scattering at angle θ, which we can simplify to $\sigma_n(E)$ and $\sigma_n(E; \theta)$.

A cross section of some importance is the total minus the elastic cross section, which we have already defined as the *nonelastic cross section*; it is denoted by $\sigma_{nX}(E)$ or $\sigma_X(E)$,

$$\sigma_X = \sigma_T - \sigma_n . \tag{1-4}$$

The *inelastic scattering cross section*, for the process in which a neutron is emitted from a nucleus with an energy different from the incident energy, is denoted by $\sigma_{nn'}(E)$. If we wish to specify the energy of the emitted neutron E', we then have the cross section $\sigma_{nn'}(E; E')$ and further to specify the angle of emission we have the differential cross section $\sigma_{nn'}(E; E', \theta)$. Of course the first n in the subscript, which we have included for the moment, can be omitted if neutron cross sections only are under consideration. We shall not concern ourselves at the moment with the additional but straightforward complications of the inelastic scattering notation arising from the specification of the energies and angles of emission of the gamma rays produced in inelastic scattering. The real advantage of a universally adopted

system of notation is not in its capability of handling complex, but infrequent, situations but in attaining consistency for the frequently measured cross-section types.

GENERAL PRINCIPLES OF CROSS-SECTION MEASUREMENT

There is a close correspondence between the methods by which cross sections are measured and their terminology because cross sections are classified in a way based closely on the methods of measurement. Perhaps when cross-section and nuclear theories are

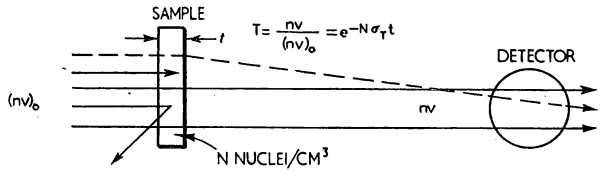

FIG. 1–2. The principle of the transmission measurement of the total cross section, σ_T. As the equation shown is based on the assumption that every interaction in the sample prevents a neutron from reaching the detector, correction must be made for the small angle scattering, shown by the dotted line, for which the neutron is still detected.

completely developed, cross sections may be described and discussed more in terms of their theoretical implication, that is, in terms of what is going on in the nucleus itself, rather than the experimental methods. However, at the present time, when the cross-section field is still somewhat in the empirical stage, the methods of measurement are still the important criteria for distinguishing types of cross sections. At present, we shall consider briefly the general principles of measurement techniques that apply throughout the entire energy range, reserving those specific to limited energies for later discussion.

By far the simplest type of cross section to measure, and furthermore, the one that can be measured most accurately, is the total cross section. In order to illustrate the principle of the measurement, let us for simplicity assume that we have a monoenergetic neutron source and also that the neutrons from the source are moving in a parallel incident beam as shown in Fig. 1–2. In this case the total cross section measurement is made simply by determining the *transmission* of the sample, T, that is, the ratio of the counting rate of the detector with the sample in the beam to that with no sample in place. The total cross section then follows from the relationship

$$T = \exp(-N\sigma_T t) \ , \qquad (1\text{–}5)$$

where N is the number of atoms per cm³ and t is the sample thickness.

A useful arithmetical time-saver is accomplished by writing Avogadro's number as 0·603 (omitting the 10^{-24}) and the cross section in barns, thus

$$N\sigma_T = 0{\cdot}603 \frac{\rho}{A} \sigma_T \ , \tag{1-6}$$

with ρ the density of the sample and A the atomic weight. For iron, for example, and 1 eV neutrons,

$$\begin{aligned} N\sigma_T &= 0{\cdot}603 \times 7{\cdot}8 \times 11{\cdot}6/55{\cdot}9 \ , \\ &= 0{\cdot}98, \end{aligned}$$

and the transmission of a 1 cm thickness would be $e^{-0{\cdot}98}$ or 0·38.

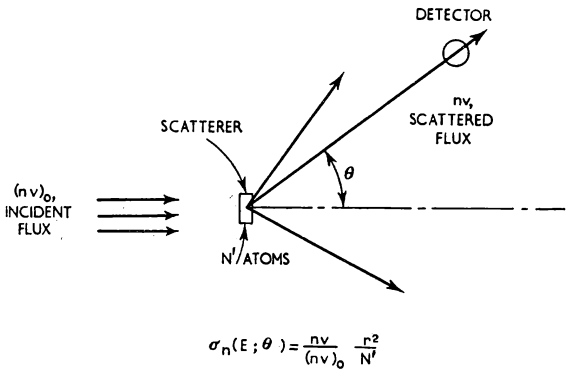

FIG. 1–3. The principle of the measurement of the differential scattering by detection of the scattered neutrons. The equation shown is based on the assumption that the sample is thin, hence does not attenuate the incident beam appreciably.

It is easy to see that any interaction in the sample that removes neutrons from the beam in any way, whether by scattering or a particular reaction, contributes to the total cross section measured in this way. We are not concerned at the moment with minor difficulties, such as correction for the fact that, with a finite size detector, the neutrons that are scattered by only a small angle will still hit the detector and hence their effect will be missed in the measurement. This, and other difficulties, can be avoided and the total cross section measured with extremely high accuracy, primarily because no absolute calibration of the detector is necessary, only the ratio of counting rates, T, entering the equation.

In principle, the elastic scattering cross section can be measured by moving the detector out of the direct beam, Fig. 1–3, so that it measures only the scattered neutrons at a particular angle. In this way the differential cross section is measured but, in contrast to the

total cross section, the absolute efficiency of the detector must usually be known. Furthermore, it must respond only to elastically scattered neutrons. The cross section cannot be obtained simply from a ratio of counting rates with the sample in place to an open beam because of the difference in shape and intensity of the direct and scattered neutron distributions. It is necessary to know $\Delta\omega$, the solid angle subtended by the detector at the scattering sample, in order to evaluate the scattered flux, hence the differential scattering cross section, in absolute terms. Thus the neutron flux measured at the angle θ, relative to the incident flux, gives the differential elastic scattering cross section $\sigma_n(E; \theta)$:

$$\sigma_n(E; \theta) = \frac{nv}{(nv)_0} \frac{r^2}{N'} , \tag{1-7}$$

where r is the scatterer-detector distance and N' the total number of atoms in the scatterer.

In a differential scattering measurement t must be sufficiently small so that there is little chance for neutrons to scatter more than once in the sample (i.e., negligible *multiple scattering*). Comparison of Eq. (1–7) for scattering with Eq. (1–5) shows that Eq. (1–7) contains the assumption that t is so small that there is negligible decrease in beam intensity in the sample (T near unity). Only a small fraction of the beam is scattered, and only $\Delta\omega/4\pi$ of this fraction (if isotropic scattering) enters the detector, hence the lack of intensity in scattering measurements is easily appreciated. The elastic scattering cross section σ_n is determined from the integral over 4π solid angle of the differential cross section, which, for isotropic scattering, is given simply as $4\pi\sigma_n(E; \theta)$.

Because of the complications mentioned, scattering cross sections in general are much more poorly known than total cross sections. We shall not discuss the methods used for the distinction of inelastic from elastic scattering at present for they are specific to fast neutrons primarily and will be taken up in detail in Chapter 3.

Even more difficult types of experiments are involved in the measurement of other partial cross sections such as capture, (n,p), (n,α), $(n,2n)$, fission, etc. In the case of neutron capture it is necessary to detect the capture process by some specific property, the most direct being the emission of radiation. Determination of an absolute cross section, however, involving Eq. (1–1), means that the reaction rate must be obtained in absolute terms. The absolute rate is difficult to determine because the gamma rays emitted at neutron capture are usually unknown with regard both to energy and number per capture. Similar complications arise in connection with the other reactions listed, although for some, primarily fission, the absolute

efficiency of a detector is much easier to calibrate than in the case of gamma radiation. For all the reactions whose cross sections are measured in terms of reaction rates, however, it is essential that the absolute strength of the incident flux be known, a determination that is not at all simple. Without going further into the actual experimental details at the present time, this brief description should suffice to show why total cross sections can be measured simply and directly, at times with accuracies of the order of a few tenths of a per cent, while differential cross sections are much more difficult and the reaction cross sections more difficult still. In later chapters we shall consider the techniques and results of partial cross section measurements by a variety of methods useful for specific energy ranges only.

SURVEY OF EXPERIMENTAL RESULTS

Before proceeding to the more detailed discussions of cross section techniques and results, it seems wise to make a rapid survey of existing cross-section data as they are exhibited in the large compilation, BNL 325. We can thus gain a bird's-eye view of the types of cross sections, their variation with energy and with element, the accuracy with which they can be measured, and the extent to which information is available for the various cross-section categories.

At extremely low energies neutrons move so slowly that the manner in which they are scattered is affected greatly by the *thermal motion* of the atoms in the sample under investigation. Because of the important effect of the thermal agitation on scattering, the cross section for very slow neutrons varies greatly with the temperature of the sample. A striking example of this behaviour is afforded by the cross section of beryllium, shown in Fig. 1–4, which is a reproduction of the low energy curve for beryllium as given in BNL 325. The rapid variation of the total cross section with temperature is illustrated by the fact that the cross section at 440° K is 15 times greater than the cross section at 100° K. Because of the low capture cross section of beryllium, the total cross section is mainly scattering, which at very low energy is a type of inelastic scattering in which the neutron picks up energy from the lattice vibrations. In this type of scattering the neutron moves into the crystal very slowly, is then hit by a moving nucleus, and is knocked out of the crystal with much higher energy than its incident energy. A characteristic of lattice vibration scattering is that it increases with decreasing neutron energy, simply because the chance of a neutron's being hit by a moving nucleus is proportional to the time the neutron is in the scattering sample.

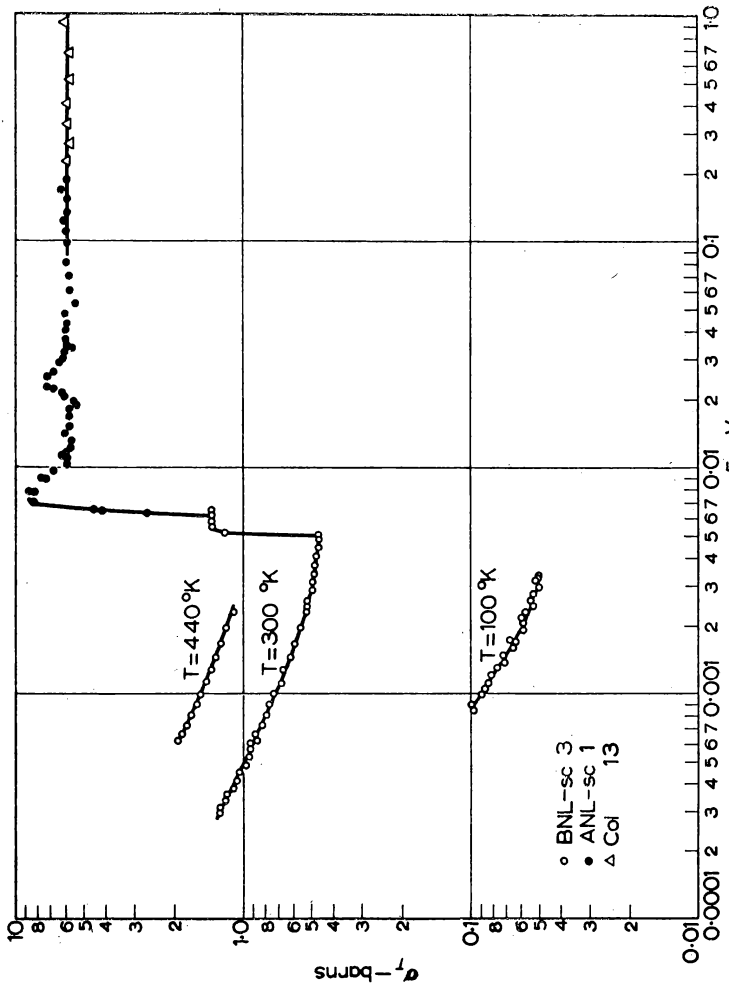

FIG. 1–4. The total cross section of beryllium in the low energy region, based on BNL 325; the references given by the code are listed at the end of the present volume. The rapid change of cross section with sample temperature is evidence for lattice vibration, or thermal inelastic, scattering.

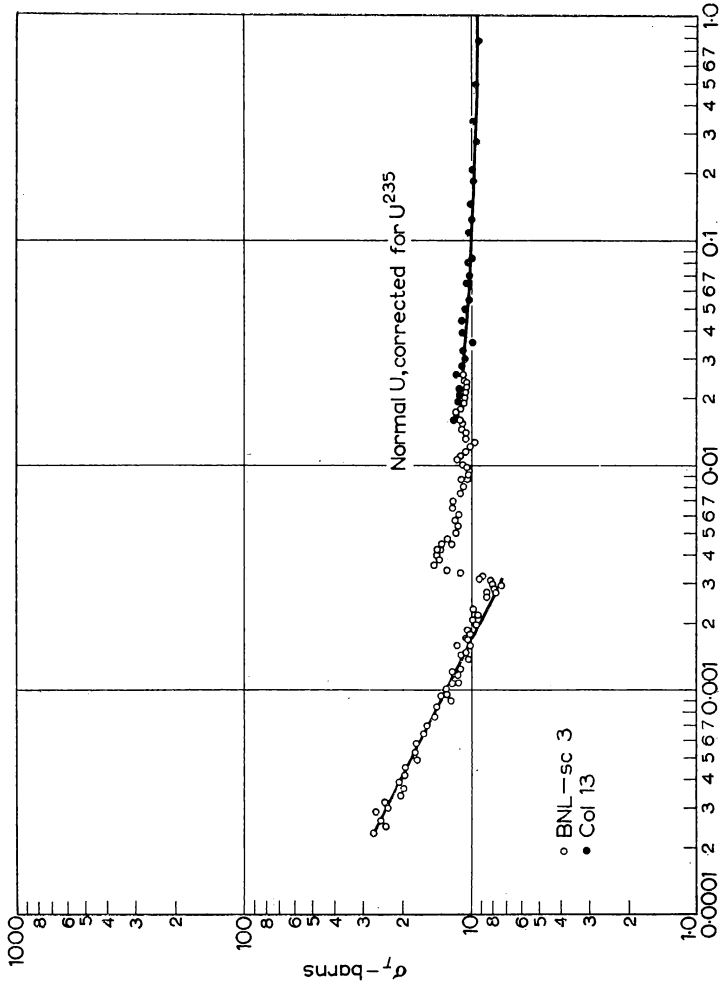

FIG. 1–5. The total cross section of U^{238} in the low energy region, showing the $1/v$ capture cross section at low energy.

The cross section for beryllium in Fig. 1–4 also illustrates very well another type of cross section, that for *coherent elastic scattering*, in which the neutron waves from many nuclei add together, exhibiting interference effects. The rapid rise in cross section at 0·005 eV marks the onset of coherent elastic scattering, and the location of this rise, as well as another to be noted at 0·006 eV, represents effects directly dependent on the crystal structure of the beryllium, that is, on the distance between the lattice planes of the crystal. These effects are typical of *neutron diffraction* and represent the phenomena that are used to study the structure of crystals by means of neutron scattering. Several additional discontinuities in the total cross section of beryllium, also ascribable to neutron diffraction effects, are seen in the energy region 0·01 to 0·1 eV. Above this energy the cross section is remarkably constant, for beryllium has very little capture, which would vary with energy. In the region above 0·1 eV the beryllium nucleus acts as if it is free in the scattering process and the constant cross section observed in this region is called the *free atom cross section.*

In contrast to beryllium, the cross section of U^{238}, Fig. 1–5, shows additional complications because it has appreciable neutron capture. The crystal discontinuity, or *cut-off*, occurs at about 0·003 eV; below this point the cross section rises with decreasing energy about as it does for beryllium. However, this rising cross section for U^{238} is not inelastic lattice vibration scattering, but is simply neutron capture, for experiments show that it does not vary with sample temperature. Above the neutron diffraction region, that is above about 0·03 eV, the cross section decreases very slowly with increasing neutron energy because the capture cross section, although small at this point, is still not negligible, and it decreases slowly with increasing neutron energy. An example of a material with very large neutron capture, gold, is shown in Fig 1–6. Here the capture cross section is so large that it dominates the total cross section. Even though there is a scattering cross section of about 8 barns, and a discontinuity of this order of magnitude at about 0·004 eV, the large capture cross section, which varies as $1/v$, obscures the small discontinuity at the cut-off.

As we go to somewhat higher neutron energies we enter the region where sharp *resonances* are observed. For various atomic weights resonances become important at different energies. Thus for very heavy elements the resonances are so closely spaced that they are obvious even in the region of thermal neutrons, that is, about 0·02 eV. For light elements, on the other hand, such as beryllium and carbon, the resonances are so widely spaced that they are usually not seen until neutron energies of several MeV are reached. It is for this

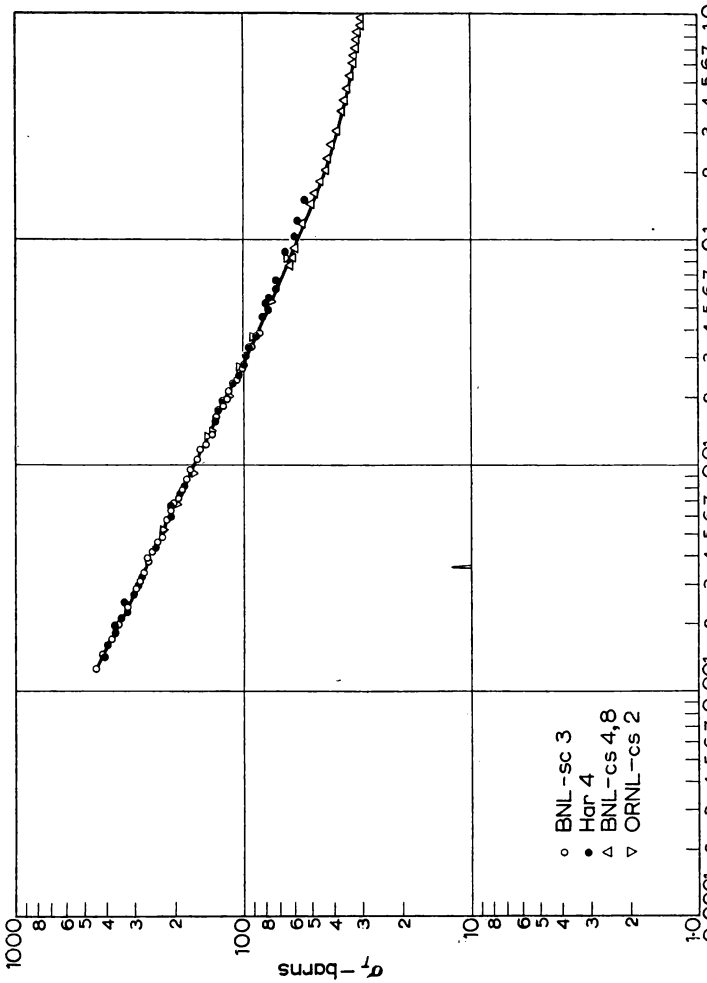

FIG. 1–6. The total cross section of gold at low energy; the capture cross section is so large that the crystal discontinuity at 0·004 eV is barely discernible.

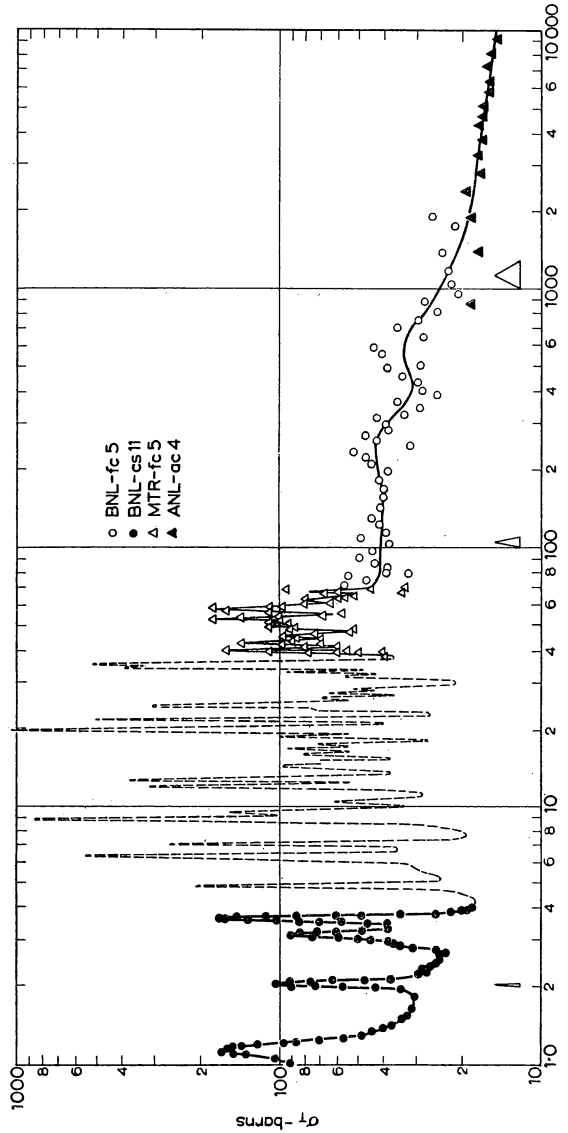

FIG. 1-7. The total cross section of U^{235} in the eV region. The small level spacing of U^{235} results in an extremel complicated resonance spectrum for this isotope. As the energy is increased the presently available resolving power, show by the triangles, fails to separate resonances, even though they are still actually present.

reason, the lack of resonances, that the cross section in the thermal and sub-thermal region for beryllium is as simple as it appears in Fig. 1–4. A rather striking example of the opposite extreme, the richly populated resonance region of U^{235}, is given in Fig. 1–7. Each of the resonances in this figure represents an excitation state of the compound nucleus formed after addition of a neutron to U^{235}. Each such state, or energy level, of the nucleus has definite properties, which can be ascertained by careful study of the neutron resonances. These results have a direct bearing on basic nuclear theory, as well as being of vital importance to the design of nuclear reactors. Because of the extreme importance of the resonance region, both for nuclear theory and reactor design, we shall examine it in much more detail in Chapter 4.

As the neutron energy is increased the resonances apparently disappear. Most of this disappearance is not real, however, and were we to repeat the measurements with increased resolving power we would find that the apparently smooth cross-section curve is really made up of resonances, spaced even more closely than they are in the lower energy region where they can be seen individually. The apparent disappearance of resonances with increasing energy, or decreasing resolution, is shown well in Fig. 1–7 for U^{235}. Even with infinite resolution, however, we would eventually reach an energy where the levels would actually merge and thus average to a smooth curve, in spite of indefinite increase in resolution. This effect occurs because the width of the levels increases with increasing neutron energy, and eventually attains a value equal to the spacing between levels. We then reach a *continuum region* where the properties of the neutron cross sections become much simpler, because of the merging or averaging of levels, than in the lower energy resonance region.

The energy region where individual resonances have become completely merged occurs at different neutron energies depending on atomic weight. Thus for the lightest elements, resonances are still seen for neutrons of several million volts, whereas for the heaviest elements we would not see individual resonances, even with infinite resolution, at energies above about 10 keV because of their close spacing. The energy at which resonances merge decreases in general with increasing atomic weight, but there are a few notable exceptions, the heavy nuclei containing magic numbers of neutrons behaving as if they were much lighter, as can be seen from the cross-section curves in the MeV region of bismuth and lead, Figs. 3–13 and 3–7, compared with neighbouring elements, shown in BNL 325.

Where individual resonances have become merged, the cross-section curve is relatively constant but does show a residual very slow variation with energy. This slow wave-like variation, exemplified

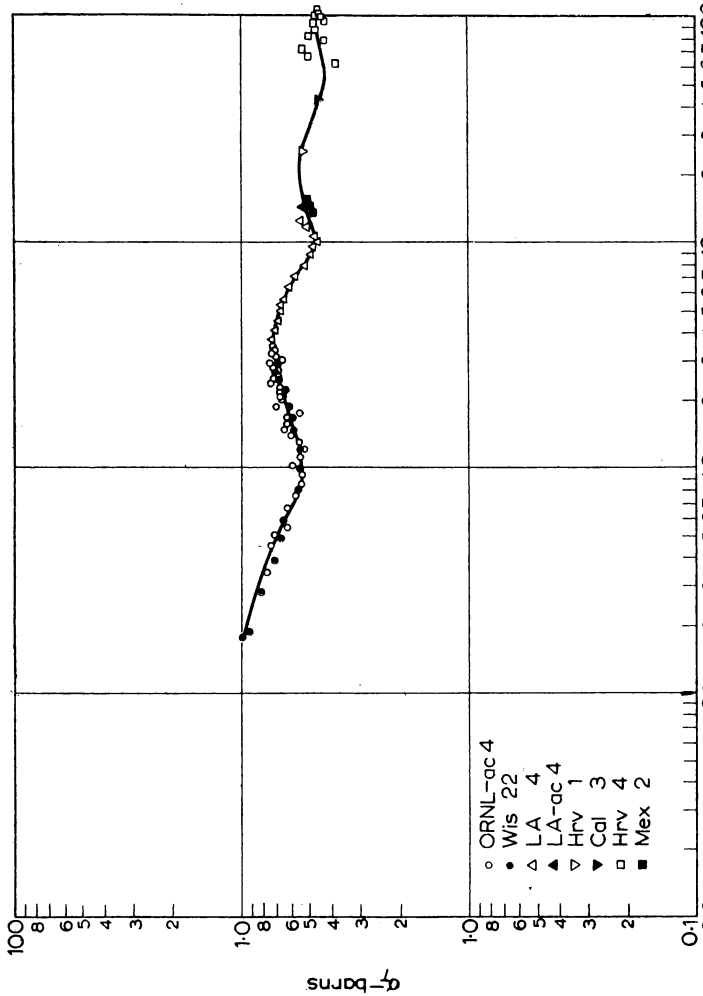

FIG. 1–8. The total cross section of mercury in the MeV region. The smooth cross section, averaged over resonances, exhibits the slowly varying optical behaviour of the neutron waves in the nucleus.

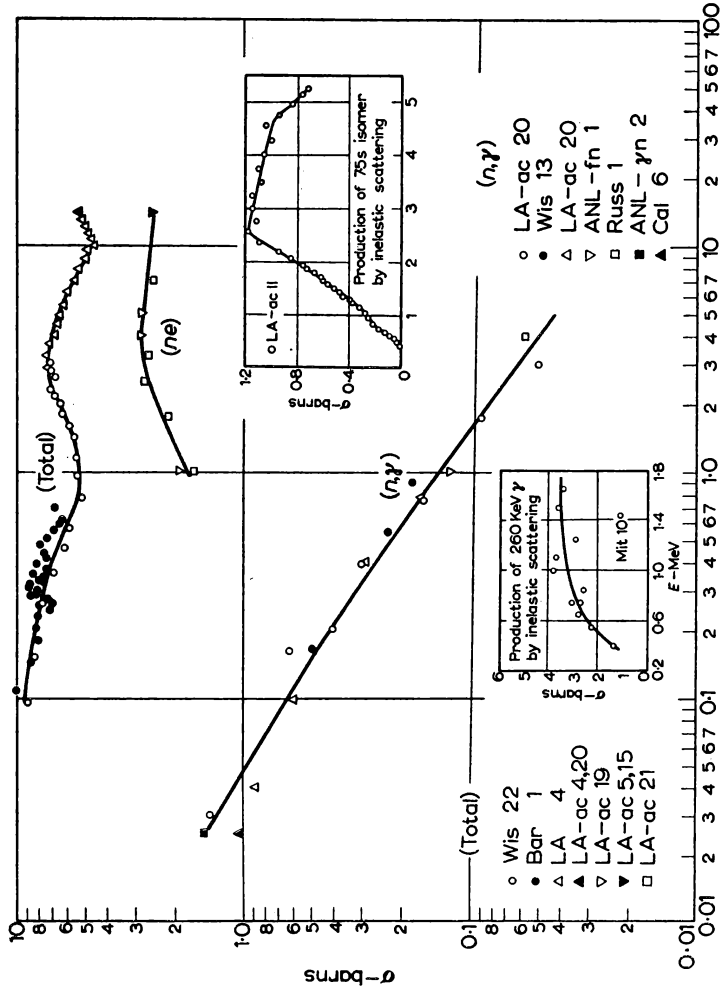

FIG. 1-9. Various cross sections of gold in the MeV region. Results for the total, capture, inelastic, and nonelastic cross sections are shown.

by the MeV curve for mercury, Fig. 1–8, for example, is an optical effect and actually represents diffraction of the neutron wave in the individual nucleus. The variation is a result of the fact that the neutron wave penetrates the nucleus, and then re-emerges producing coherent optical effects, which at some energies cause the cross section to increase and at others to decrease relative to its value for a strongly absorbing, or "black" nucleus.

The cross sections that we have been discussing so far in this quick survey have been total cross sections only, although in certain energy regions the total cross sections consist almost completely of one component only, such as thermal inelastic scattering for beryllium at low energy, or the scattering cross section for mercury at high energy. Because of the simplicity and high attainable accuracy typical of total cross section measurements, more of them are available than the various partial cross sections, as can be seen by an examination of the data presented in BNL 325. However, certain partial cross sections have been measured for some elements, an example being furnished by the case of gold for which the capture cross section has been measured in the million volt region, Fig. 1–9. Here the capture cross section is much smaller that the total cross section, but its measurement is possible because the nucleus formed is radioactive and can be measured by activation methods. Another partial cross section that has been measured in the fast neutron region for a number of nuclides is the *nonelastic cross section*, which is also shown for gold in Fig. 1–9.

Cross sections have been most completely measured for a particular energy region of great practical importance, the energy region of *thermal neutrons*, that is, those in equilibrium with matter at ordinary temperature. Because of the very high neutron densities available in the thermal region in nuclear reactors, extensive measurements have been made in this energy region and important techniques have been developed for use of thermal neutrons. The large amount of cross-section information available in this one energy region necessitates a table of thermal cross sections in the compilation. In this table, p. 1 of BNL 325, the cross sections are listed at one particular energy, 0·0253 eV, which corresponds to a neutron velocity of 2200 m/sec. Actually, in many cases thermal cross sections are measured or used, not for a single velocity of 2200 m/sec, but for the entire Maxwell distribution of velocities that obtains in a moderating material in which the neutrons have reached thermal equilibrium with the moderator. In Chapter 6 we shall discuss the measurement and use of cross sections for the entire Maxwell distribution, but at the present time we wish to limit ourselves to monoenergetic neutron sources for simplicity.

The great variation of thermal absorption cross sections is obvious in the table, with absorption cross sections sometimes much less than scattering cross section and sometimes much greater. In the thermal region, the term "absorption cross section" is widely used, and usually does not lead to ambiguity; it refers to the sum of all interactions except scattering, and is thus given by:

$$\sigma_{abs} = \sigma_T - \sigma_n \ . \tag{1-8}$$

For neutron optical behaviour, that is, neutron diffraction, refraction, and reflection, the properties of neutron scattering with regard to *coherence* and *incoherence* are important. It is for this reason that in the thermal cross section table the coherent scattering cross section is listed as well as the complete scattering cross section, which is sometimes called the *bound atom cross section.* It is this latter cross section that is listed under the symbol $\sigma_{fa}\left(\frac{A+1}{A}\right)^2$, and the difference between it and the listed coherent cross section gives the fraction of the cross section that is incoherent, i.e. the fraction of the scattering that does not lead to optical effects. In most cases the coherent scattering is nearly as large as the bound atom cross section, but there are a few major exceptions, mainly hydrogen and vanadium, in which the scattering is primarily incoherent. The reasons for the incoherence of scattering in certain materials we shall discuss in Chapter 6.

This rapid survey of cross sections, while allowing no leisurely examination, does illustrate the great variety that is present with regard to energy variation and actual quantitative magnitude of cross sections. In succeeding chapters we shall describe how these variations are related to basic theory, theory that in some cases is sufficiently good to allow rather accurate predictions of cross sections. Thus far in our quick survey we have talked as if cross sections are always measured and used for monoenergetic neutrons; unfortunately in actual practice we must be concerned with cross-section averages and as we later describe the theory and measurement of cross sections in various energy regions, we shall also consider the meaning and use of various average cross sections.

BASIC APPLICATIONS OF CROSS SECTIONS

Because of the great variety in types and magnitudes of cross sections it is fairly obvious that in their use, for instance in predicting reaction rates and behaviour of nuclear reactors, many standard formulas, approximation methods, and computational techniques, will also exist. Although these matters, which would fill several volumes, are not our concern, there are a few simple general principles

that apply to use of cross sections. While we are still introducing cross-section concepts in a simple and general way, it might be useful to cover these principles, which are applicable so often in practice. Again, we shall think only of cross sections for monoenergetic neutrons, leaving the complicated questions of averaging until later. The two general cases of interest in cross-section use refer to the *transmission* of neutrons through, and the *activation* or reaction rate in, a material. For neutron transmission, where we are considering monoenergetic neutrons, the rate at which the neutron flux drops off in intensity as it passes through the sample is given by an exponential law,

$$nv = (nv)_0 \exp(-N\sigma_T t) \ , \qquad (1\text{–}9)$$

where $(nv)_0$ is the incident flux, nv the flux at thickness t, N the number of nuclei per cm^3 and σ_T the total cross section. The transmission T is defined as $nv/(nv)_0$ and is thus

$$T = \exp(-N\sigma_T t) \ . \qquad (1\text{–}10)$$

In actual practice, the exponential law is observed to hold extremely well for monoenergetic neutrons, especially under the good experimental conditions that are available with modern high intensity neutron sources.

It is because of the simplicity of this law that total cross sections are so easily measured by transmission. Actually, of course, a strictly monoenergetic flux is never available but the exponential law will still hold if the cross section is constant over the actual energy spread in the beam. If the cross section changes over the energy spread the transmission will be exponential for each individual energy value but the net effect will be a gradual "*hardening*" of the beam, as the neutrons of higher cross section are preferentially removed. For materials of rapidly changing cross section, the absorption will be rather complicated but still tractable in analysis, as we shall see in connection with neutron resonances in Chapter 4.

In the case of reaction rates, such as the amount of *activity* produced in a sample, the fundamental equation again is very simple:

$$\text{activations per sec} = \mathrm{d}N_a/\mathrm{d}t = nv\sigma_{\text{act}}N' \ , \qquad (1\text{–}11)$$

where N' is the total number of atoms that are in the neutron flux nv, and N_a is the number of activated atoms. The *activation cross section*, σ_{act}, pertains to the production of the particular radioactive species regardless of the reaction involved, which is usually the (n,γ) but may be (n,p), (n,α) or other reactions. Although the flux in Eq. (1–11) is the number of neutrons that cross a square centimetre per second, the activation rate, $\mathrm{d}N_a/\mathrm{d}t$, depends on the total number

of atoms present, N' regardless of the volume over which they are distributed.

We have considered thus far only beams of neutrons, but Eq. (1–11) holds for isotropic fluxes, such as those within a pile, equally well. If a range of velocities is present, it is necessary to consider appropriate average values of flux, which are discussed later. Whereas the transmission equation often holds extremely well in practice, the activation involves at least minor difficulties. The fundamental reason for the difficulties is that the neutron flux is often disturbed by the sample itself, the atoms in the centre not receiving the full neutron flux. This effect is usually called *self-absorption* or *self-protection*, and unfortunately its estimation is not in general very simple. In accurate measurement of a cross section by reaction rate it is necessary to use small enough samples so that self-absorption is negligible, but in the practical case of manufacture of radioisotopes, for example, a delicate balance must be maintained between self-absorption, which lessens the *specific activity* (N_a/N'), and total sample size, which increases the *total activity* produced (N_a).

After a time t the number of activated atoms will, of course, be given by $nv\sigma_{act}N't$, if the number of activated atoms that have decayed by time t is negligible, that is, the activation will at first increase linearly with time. If the activated atoms have a reasonably large radioactive *decay constant* λ, then decay of the activated atoms will decrease the rate of formation as time progresses. The number of activated atoms present, N_a, will increase until the rate of radioactive decay, given by $N_a\lambda$, is equal to the rate of formation,

$$N_a\lambda = nv\sigma_{act}N' \ . \tag{1–12}$$

The number of activated atoms will then remain constant with further irradiation. The *disintegration rate* of the sample, or intensity of radioactivity, will be equal to $nv\sigma_{act}N'$ if the sample remains in the neutron flux until equilibrium is attained. This equilibrium activity is called the *saturation activity*.

Before saturation is reached, the rate of change of the number of activated atoms is given by

$$dN_a/dt = nv\sigma_{act}N' - N_a\lambda \tag{1–13}$$

and the growth of the number of activated atoms, or of the *activity* ($I = N_a\lambda$), is obtained by integration of Eq. (1–12),

$$I = I_0(1 - e^{-\lambda t}) \ , \tag{1–14}$$

where $I_0 = nv\sigma_{act}N'$. The formation of a typical radioisotope, Na^{24}, by neutron irradiation is given in Fig. 1–10. The "half-life" of Na^{24}

is 14·8 hr, hence its mean life is 14·8/0·693 or 21·3 hr and its disintegration constant λ equals $1/21{\cdot}3 = 0{\cdot}047$ hr^{-1}. It is seen in Fig. 1–10 that half the final activity is produced in one half-life, three-quarters in two half-lives, etc., and that the amount of activity formed approaches the saturation amount, I_0 very slowly after the first few half-lives.

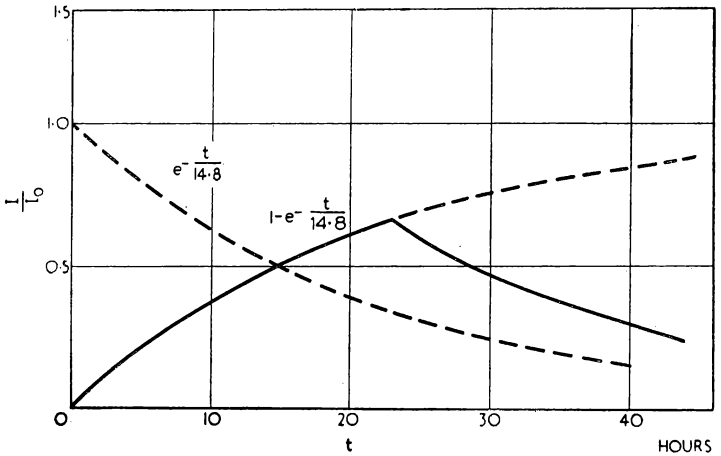

FIG. 1–10. The formation and decay characteristics of the radioisotope Na^{24}. The solid line shows the formation of the radioisotope in a neutron flux and its decay when removed before saturation is attained. The approach to saturation if not removed, as well as the decay of a sample initially fully saturated are also shown (dotted lines).

The decay of a radioisotope of initial activity I_0 is usually quite simple, as compared with natural radioactivity, because there are few complicated parent-daughter relationships. If the radioisotope gives rise to a stable daughter, as is usually the case, the activity will be observed to decay as

$$I = I_0 e^{-\lambda t} \ . \tag{1–15}$$

The decay curve for Na^{24} is also shown in Fig. 1–10, as well as the decay for the case of removal before the attainment of saturation. Combination of Eqs. (1–14) and (1–15) gives a useful result for the calculation of the saturated activity of a radioisotope when the actual activity I is produced in a neutron flux for a time t_1, and then measured for activity at a time t_2 after the end of the irradiation:

$$I_0 = \frac{I}{e^{-\lambda t_2}(1 - e^{-\lambda t_1})} \ . \tag{1–16}$$

The activation cross section, in terms of the observed activity and flux, is given simply by

$$\sigma_{act} = I_0/nvN_t \ . \qquad (1\text{–}17)$$

Equations (1–16 and (1–17) are those commonly used in measurement of activation cross sections.

The few cases in which radioisotopes give rise to daughters that are also radioactive can be handled by solution of the differential equations* for the particular situation involved. When the half-lives of parent and daughter are markedly different, one may be negligible compared with the other, with the result that the situation is greatly simplified. For instance, a parent of extremely short half-life can be studied by measuring the long-lived daughter, if the latter has a more convenient half-life. A long-lived parent followed by a short-lived daughter will exhibit the parent's half-life and activity just double that of the parent.

The general equations concerning cross sections in transmission and activation calculations that we have just outlined are encountered constantly in the measurement and application of neutron cross sections. In addition there are often specific applications, many of which we shall consider in appropriate places, as well as inevitable complications that necessitate corrections, often complex, for departure from the ideal conditions assumed in this section. These specific applications and corrections for non-ideal circumstances, however, do not usually involve new and different concepts, but rather mathematical complications only. Before beginning the detailed description of cross sections at various energies, we shall now consider the basic theory of nuclei and of their interactions with neutrons that are manifested as cross sections.

REFERENCES FOR ADDITIONAL INFORMATION

1. B. T. FELD, *Experimental Nuclear Physics*, Vol. II (E. SEGRÉ, editor), (Wiley, 1953), pp. 209–247. The basic properties of neutrons, including accounts of early significant discoveries.
2. W. HEITLER, *Elementary Wave Mechanics*, (Oxford, 1944), Chapters I and II. An interesting elementary treatment of the wave-particle dualism of matter.
3. D. J. HUGHES and J. A. HARVEY, *Neutron Cross Sections*, Brookhaven National Laboratory Report 325 (July 1955), (Superintendent of Documents, Government Printing Office, Washington 25, D.C.). Introductions to the various sections. Explanation of the criteria for selection, evaluation and presentation of the neutron cross-section data.

* The general equations are discussed in Rutherford, Chadwick, and Ellis, *Radiations from Radioactive Substances*, (Cambridge, 1930), pp. 8–30.

CHAPTER 2

CROSS SECTIONS AND NUCLEAR STRUCTURE

IF THE matter of dealing with neutron cross sections were completely empirical, if the experimental results were simply collected with no resort to theory as a means of correlation, there would then be no need to relate cross sections to the structure of the nucleus. They would be treated merely as numbers to be measured, evaluated for accuracy only, compiled in convenient form, then used in various equations, such as those given in the previous chapter.

The manner of treating cross sections that is actually used in the compilation BNL 325 resembles this empirical approach closely because the compilation is designed primarily for evaluation of experimental accuracy and convenient listing, rather than comparison of results with theory. For some types of cross sections, of course, little more can be done, even if desired, simply because there are no adequate theoretical guides by which the cross sections can be correlated. However, for many types of cross sections, the theory is sufficiently well developed and verified so that it serves not only as a guide for methods of correlating measured values but actually can be used to predict cross sections as well. The predictions are extremely valuable for substances for which no measurements are available, even if at times they serve only as an aid in intelligent interpolation between measured materials or cross sections measured at certain energies.

In the theory-experiment relationship, the flow of information is twofold, both from theory to cross sections as a means of predicting practical results, and from measured cross sections to theory as a means of providing the fundamental data on which theory is built. What we can properly call the "theory" of cross sections, that is, the way in which cross sections are expressed in terms of wave functions and various types of amplitudes, is not a very involved matter in itself. However, the quantitative evaluation of these amplitudes, which is necessary in order to predict actual cross sections, depends on the much deeper and more fundamental theory of nuclear structure. Thus the theory of cross sections supplies the principles and mathematical formalism underlying the general behaviour of cross sections, but does not allow us to evaluate such fundamental

quantities as the amplitudes for scattering and for capture necessary to specify actual cross sections.

These fundamental quantities cannot be easily computed because they are intimate and detailed properties of the structure of the nucleus, actually being determined by the nature of the actual energy levels that exist for the particular nucleus under consideration. We of course do not have space to describe what is now known of nuclear structure in anything but the simplest terms. However, since any discussion of cross sections becomes trivial if it is not related to the basic facts of nuclear structure, it is extremely desirable that we consider some of the simple principles of the structure of the nucleus. The properties we wish to consider now are those that are of such a fundamental nature that they come up continually in discussion of cross sections, regardless of the neutron energy. They are important to the determination and systematization of cross sections whether for extremely slow neutrons or those in the high MeV region.

RADII AND MASSES OF NUCLEI

There are certain simple, but fundamental, properties of nuclei that have an obvious importance to the matter of neutron cross sections. Such fundamentals as the size of the nucleus, its shape, and its density, by themselves help greatly to explain the simplest facts of neutron cross sections. We shall not be concerned with the origin of these properties, for example the actual reason why the nucleus has a constant density, which is one of the most fundamental properties of the forces between nucleons. Rather we are interested in the basic properties of nuclei only inasmuch as they affect neutron cross sections. Actually, it is a bit surprising that it is only in very recent times that it has been possible to measure with accuracy such apparently simple properties as the size and shape of nuclei. In fact there are still many uncertainties in our knowledge of the details of the nuclear shape.

Nuclei have been known for many years to be composed of neutrons and protons, in approximately equal numbers for light nuclei, but with a growing excess of neutrons as nuclei become heavier, until for example in U^{238} there are 146 neutrons and 92 protons, a total of 238 *nucleons*.

Nuclear density is remarkably constant over a great range of nuclear sizes. This constancy of density, that is, proportionality of the nucleus to the number of particles it contains, is shown by the equation that gives the radius of the nucleus, R, in terms of the number of nucleons it contains, or its mass number, A:

$$R = r_0 A^{\frac{1}{3}} , \qquad (2\text{–}1)$$

where r_0 is a constant about $1{\cdot}35 \times 10^{-13}$ cm in magnitude. Until the last year or so it was assumed, with no better knowledge being available, that the nucleus had a sharp boundary, with a density that was constant out to the radius R at which point it suddenly becomes zero.

It was more or less obvious that things could hardly be as simple as is indicated by Eq. (2–1), but it has been only recently that experimental evidence has revealed that the surface of the nucleus is not sharp, and that the density decreases gradually to zero in a surface layer of about 10^{-13} cm thickness. Fig. 2–1 gives the

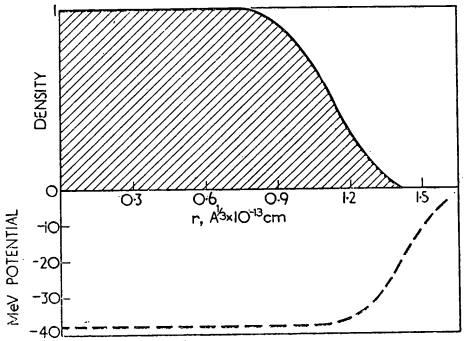

FIG. 2–1. The nuclear charge distribution for gold compared with the distribution of the potential experienced by an incoming proton. Both experimental distributions reveal that the nucleus has a diffuse rather than a sharp edge.

distribution of matter in a typical nucleus, revealing the constant density of most of the nucleus and the "diffuse boundary". The distribution of protons alone has been measured by studying the scattering of high energy electrons, whereas the distribution of the total content of the nucleus, neutrons and protons, is known from the scattering of protons, which are affected by both the neutrons and protons in the nucleus.

The distributions in Fig. 2–1 reveal that the so-called *charge distribution*, obtained from electron scattering, is smaller than the *potential distribution* "seen" by an incoming proton. The reasons for this difference are still not well understood, but it seems most likely at the moment that the potential affecting an incoming proton is larger than the charge distribution, seen by an incoming electron, because of the finite range of nuclear forces, which makes the potential experienced by a proton somewhat larger than the actual distribution of matter in the nucleus. There is some possibility of course that the neutrons and protons are not distributed equally within the nucleus. From this standpoint the larger potential distribution could be

explained by the protons being more concentrated at the centre of the nucleus than the neutrons. However, while the correct explanation of the different curves in Fig. 2–1 is still not available, the facts of the charge and potential distributions are reasonably well established at present.

A matter of great importance to neutron cross sections is the *stability* of different nuclei. The energy content of a nucleus is expressed most simply in terms of its mass, and the mass, relative to that of neighbouring nuclei, readily gives the available energy in the nucleus, by use of Einstein's mass-energy equation. In ordinary nuclear reactions only a small fraction of the mass of the nucleus changes into energy or vice versa, but very large amounts of energy result. Einstein's equation gives, for the energy equivalent of 1 g, for example:

$$\begin{aligned} E &= mc^2 \text{ ergs}, \\ &= 9 \times 10^{20} \text{ ergs}, \\ &= 9 \times 10^{13} \text{ watt sec}, \\ &= 2{\cdot}5 \times 10^{7} \text{ kWh}. \end{aligned} \qquad (2\text{–}2)$$

All of the energy considerations in nuclear changes, such as the energy absorbed or evolved in a nuclear reaction, the energy produced when an unstable nucleus emits radiation and becomes a stable nucleus, the amount of energy released when a heavy nucleus fissions —all involve energies that follow directly from comparison of the masses of the interacting particles. In any nuclear change, of whatever sort, the energy evolved or absorbed in the process is given simply by comparison of the mass of the final products with the mass of the initial products. The masses of atoms are always expressed in terms of the O^{16} atom as the fundamental standard, which is assigned the *atomic mass* 16·000. If the final products in a reaction are lighter than the initial constituents, the mass that disappears represents the energy evolved in the process, which usually appears as kinetic energy of the products or as gamma radiation. If the final products are heavier, on the other hand, the difference in mass represents the energy that must be added to make the reaction take place. The energy needed to make a reaction go is usually supplied as kinetic energy of the incoming particle, or in some cases, in the form of a gamma ray.

The conversion of mass to energy is extremely simple—one unit of atomic mass is the equivalent of 931·1 MeV of energy:

$$\frac{1 \times (2{\cdot}998)^2 \times 10^{20}}{0{\cdot}6025 \times 10^{24} \times 1{\cdot}602 \times 10^{-12}} = 9{\cdot}311 \times 10^{8} \text{ eV} = 931{\cdot}1 \text{ MeV} \quad ,$$

the denominator containing Avogadro's number and the conversion factor from ergs to eV. As an example, let us consider several reactions that are possible, in addition to elastic scattering, when a neutron is incident on the Al^{27} nucleus:

$$(1)\ Al^{27}(n,\gamma)Al^{28} + Q_1\ ,$$
$$(2)\ Al^{27}(n,p)Mg^{27} + Q_2\ ,$$
$$(3)\ Al^{27}(n,\alpha)Na^{24} + Q_3\ ,$$

where the Q's represent energies evolved or absorbed. For reaction (1), let us consider an incident neutron so slow that it contributes negligible kinetic energy. We have, using masses from the table in Appendix 2:

$$\begin{array}{r} 26{\cdot}990081 \text{ mass* of } Al^{27} \\ 1{\cdot}008986 \text{ mass of neutron} \\ \hline 27{\cdot}999067 \text{ total} \\ -\ 27{\cdot}990771 \text{ mass of } Al^{28} \\ \hline 0{\cdot}008296\ Al^{27} + n - Al^{28} \end{array}$$

These figures show that there is a mass excess of 8·296 millimass units (mmu) for the initial particles relative to Al^{28}, which excess must appear as energy in the Al^{28} formed. The amount of energy, Q, corresponding to this mass excess is of course equal to $8{\cdot}296 \times 0{\cdot}931$, or 7·72 MeV. A similar calculation shows that $Al^{27} + n$ is lighter than $Mg^{27} + p$ and lighter than $Na^{24} + \alpha$, and that $Q_2 = -2{\cdot}03$ MeV and $Q_3 = -3{\cdot}18$ MeV. Thus reactions (2) and (3) are both endothermic, and additional energy in the amount $-Q_2$ or $-Q_3$ must be supplied by the incident neutron to make the reactions occur.

The masses of the many existing nuclei, both stable and unstable, have either been measured with mass spectrometers, which utilize the deflection of ions in an electromagnetic field or they have been determined from the energies involved in nuclear reactions. Many of the nuclear masses, particularly for low A, have been accurately fixed, and a recent set appears in Appendix 2. Unfortunately, not all of the masses have been accurately measured, particularly for high A, and resort must be made to a *semi-empirical formula* to obtain values for those nuclear masses that have not as yet been measured accurately.

The semi-empirical formula, which expresses masses in terms of

* The masses actually used are the atomic masses, which include the orbital electrons. No error results from use of atomic masses because conservation of charge ensures that the number of electrons before and after the reaction is the same.

mass number A and *charge Z*, contains terms whose dimensional form is based on theory, i.e. on a particular model, the *liquid drop model* of nuclear structure. The empirical aspect of the mass formula is related to its quantitative features, for the numerical factors are fixed to match known masses. There is a term in the formula that corresponds to the energy of surface tension, and is hence proportional to the surface area, or R^2, or $A^{\frac{2}{3}}$ in terms of mass number, A. The complete formula, see references, includes other terms, for the Coulomb potential energy, for example, and various odd-even effects:

$$M(A,Z) = 1{\cdot}01464A + 0{\cdot}014A^{\frac{2}{3}} - 0{\cdot}041905Z_A + \frac{0{\cdot}041905}{Z_A}(Z - Z_A)^2 + \lambda\frac{0{\cdot}036}{A^{\frac{1}{2}}}\,, \qquad (2\text{–}3)$$

where

$$Z_A = \frac{A}{1{\cdot}980670 + 0{\cdot}0149624A^{\frac{2}{3}}}\,,$$

and

$$\lambda = \begin{cases} +1 \text{ for } A \text{ even, } Z \text{ odd.} \\ -1 \text{ for } A \text{ even, } Z \text{ even.} \\ 0 \text{ for } A \text{ odd.} \end{cases}$$

Numerical values of M for a large range of A and Z have been calculated from this formula by N. Metropolis and G. Reitwiesner.*

The formula obviously varies slowly with atomic weight and charge, with no abrupt discontinuities at particular values of A or Z. This behaviour gives the general characteristics of nuclear masses correctly but does not exhibit a property that has been only recently well established. A careful study of mass values, as well as other nuclear phenomena, for example, the level spacing, Fig. 2–2, shows that for specific numbers of particles in the nucleus great stability is attained. These *closed shells* in nuclei occur for 50, 82 or 126 particles, the "magic numbers" whether they are neutrons or protons. In other words a nucleus containing 50 protons, 82 neutrons, etc., will be exceptionally stable, thus its mass, which is its fundamental measure of stability, will be less than the semi-empirical formula would indicate. In some work on neutron cross sections it is necessary to take into account these discontinuities in nuclear masses or stability at the closed nuclear shells. We shall later note in several connections, the great importance of keeping these discontinuities in mind in correlating and predicting cross-section behaviour.

* N. Metropolis and G. Reitwiesner, Report NP 1980, available from the Technical Information Service, AEC, Oak Ridge, Tennessee.

THE COMPOUND NUCLEUS

If a neutron is absorbed by a target nucleus a rather large amount of energy is made available, as can easily be seen by comparison of the masses involved. Thus if Al^{27} absorbs a slow neutron, as we have seen, energy is made available in the Al^{28} nucleus equal to the *binding energy*, representing the excess in mass of Al^{27} plus one neutron over Al^{28} in its stable or ground state. For this comparison we do not need to use the mass formula because masses of most light nuclei have been measured with higher accuracy than could be obtained from the formula. Our previous calculation of the Al neutron

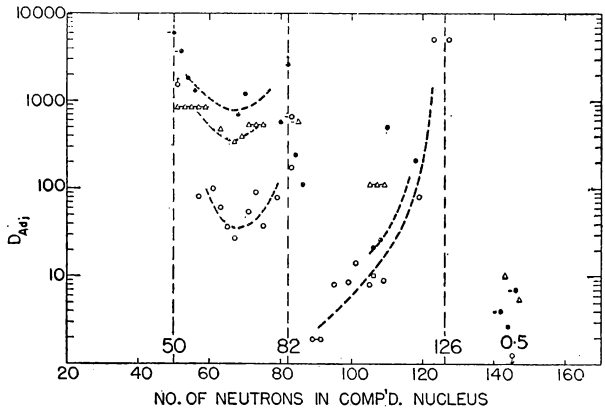

FIG. 2–2. The spacing of nuclear energy levels as a function of neutron number, exhibiting the high values at the magic numbers, 50, 82, and 126. The determination of the level spacing, D, by the methods of neutron spectroscopy is discussed in Chapter 4.

reactions has already given us the required information—the mass energy made available is 7·7 MeV, assuming the incident neutron carries negligible kinetic energy.

Of course this energy is usually emitted as gamma radiation, the Al^{28} falling to its ground state in the process, i.e. by the emission of 7·7 MeV in gamma-ray energy. However the nucleus has the possibility of disintegrating in various ways, not only by radiation; for example a proton or alpha particle may be emitted if sufficient energy is available. Before the nucleus disintegrates it is in an *excited state* because it has extra energy within it, present as kinetic and potential energy of its constituents. The nucleus in this state is called the *compound nucleus* and its properties are of extreme importance in determining the entire course of nuclear reactions. The *excitation energy* of the compound nucleus is given by the binding energy of the incident particle, which we have calculated as 7·7 MeV for Al^{27}, plus

any kinetic energy the incident particles may possess. Examination of the mass table shows that, while the binding energy of an incident neutron varies somewhat with atomic mass, it is always in the range of about 5 to 8 MeV.

A fundamental principle of the theory of the compound nucleus is that its properties, such as its lifetime and type of disintegration products, are independent of the manner in which it was formed. Thus the same compound nucleus could be formed by capture of a neutron in a particular target nucleus or by capture of a proton in a different target nucleus. The essence of the compound nucleus theory is that the compound nucleus, containing about six MeV of energy, is in a highly excited state and the particles within the nucleus are moving in complicated ways. Furthermore, the compound nucleus lives a sufficiently great time so that it can be said to forget the manner in which it was formed. The precise manner of disintegration of the compound nucleus then is simply a matter of chance, the relative probability of emission of different particles being determined by the energy with which these particles emerge, the penetrability of the barrier surrounding the nucleus, etc., properties that we shall examine in more detail later.

Following the development of the idea of the compound nucleus by Niels Bohr in the middle '30s, it has been extremely successful in correlating and predicting the properties of nuclear reactions. However, in the last few years, increasing evidence has been found that the compound nucleus theory does not apply in the simple manner in which it was first envisaged. The deviations from simplicity are primarily cases for which the course of a nuclear reaction is determined to some extent by the nature of the incident particle, contrary to the supposition of the lack of memory of the compound nucleus. These are reactions in which the incident particle does not amalgamate its energy fully with the nucleus, but interacts with one part of the nucleus only, for example, a particle in the outer surface layer of the nucleus. However, for most nuclear reactions the compound nucleus theory does apply with accuracy, especially at low energies. The deviations tend to occur for higher energy particles, which, because of their small wavelength, can be thought of as interacting with parts of the nucleus only, such as the surface layer. For the energy range of most interest to the compilation BNL 325, that is for energies particularly applicable to reactors, the compound nucleus concept is extremely useful for interpretation of the neutron reactions observed.

As we shall see later when we study the more detailed theory of nuclear reactions, the compound nucleus concept is so useful because it unifies the cross-section behaviour from nucleus to nucleus. In its

simplest terms, the course of a nuclear reaction according to the compound nucleus theory is this: The amount of excitation energy present in the compound nucleus is given by the table of mass values or the empirical formula we have discussed. This excitation energy is thought of as being present as energy of agitation of the nuclear particles, in much the same manner for all nuclides regardless of the particular nucleus involved. Furthermore, the type of particle emitted is determined simply by the energy of the particle, which in turn is given by the nuclear reaction mass values, and its ability to get out of the nucleus. The probability of emergence is related to very simple properties of the nuclear surface, again varying smoothly with atomic weight.

We shall see that these elementary nuclear principles go surprisingly far in predicting the general behaviour of various types of nuclear reactions for an extremely wide range of neutron energies and atomic weights. They cannot predict the specific rapid variation of cross section with energy but the values averaged over the sharp fluctuations can be predicted remarkably well.

NUCLEAR ENERGY LEVELS

The six MeV or so of excitation energy contained in the compound nucleus is not present as a continuum, in other words, the compound nucleus cannot exist with an arbitrary energy content, but only in definite *energy states*. These states or *energy levels* of the compound nucleus are typically rather sharp with a width much less than the separation of the levels. The reason why the compound nucleus exists only in definite sharp energy levels is because of the quantum characteristics of the excitation. The excitation of the nucleus actually exists as energy of excitation added over several, perhaps many, particles in the nucleus that are excited above their normal energy levels, which they occupy in the *ground state*, or lowest energy state of the nucleus. Because the individual particles have definite quantum levels in the nucleus, being particles held in a potential well, the total energy, although it may have many possible values, exists only as discrete, sharply defined, energy states. It is because the compound nucleus can exist only for sharply defined energy levels that its formation is very probable, or its formation cross section high, only when the incident neutron has just the right amount of energy to form the compound nucleus in one of its many energy states.

These energy levels do not represent true bound states of the nucleus, because the compound nucleus can always emit a neutron of the same energy as the incident neutron that formed the compound nucleus, and thus decay. Because this mode of disintegration

is always possible, the state is not truly bound and the excited nucleus will inevitably decay after a sufficient length of time. However, because the nuclear motion is so complicated the level may live a long time before disintegrating. Thus the states, while not truly stationary states, are *quasi-stationary states*, which live a finite length of time. Of course, there are in addition many energy levels lying below the excitation energy represented by the neutron binding energy plus its kinetic energy, and these states can be reached from the initial excitation state if the compound nucleus emits a gamma

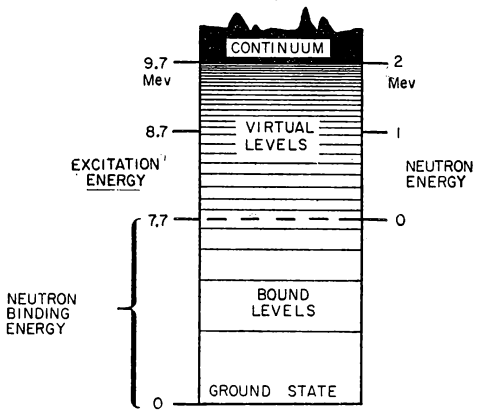

FIG. 2–3. The excitation energy of the compound nucleus Al^{28} formed by absorption of a neutron in Al^{27}; the excitation energy is equal to the neutron binding energy plus its kinetic energy. It is seen that the density of energy levels increases rapidly with excitation energy.

ray. The compound nucleus then falls to an energy level that is usually less than the neutron binding energy, that is to a state that is a true *bound* state. The bound state cannot emit a neutron, but still has a finite *width*, that is a finite *disintegration probability*, because of the possibility of emitting gamma radiation and falling to a still lower and finally to the ground state.

The energy relations and levels for the compound nucleus that we have just described are illustrated in Fig. 2–3 for the case of a neutron incident on Al^{27}. For a 1-MeV neutron, the excitation energy of the compound nucleus Al^{28} is 1 MeV plus the binding energy, or 8·7 MeV, so the nucleus is excited well into the region of virtual energy levels. It is seen that there are some widely spaced levels at excitation energies less than the neutron binding energy. These low-lying levels can be reached if the excited nucleus radiates energy in the form of a gamma ray of energy less than the excitation energy. The levels near ground (zero excitation energy) are, of course, true bound states because the energy is insufficient for dissociation.

The "*width*" (finite spread in excitation energy) of an energy level is related to its lifetime by the Heisenberg *uncertainty principle*, which states:

$$\Delta E \, \Delta t = \hbar \ . \tag{2–4}$$

That is, the uncertainty (or spread in the numerical value) of the energy (in ergs) multiplied by that of the time is given by $\hbar$. As applied to the lifetime of nuclear energy states, this principle shows that the lifetime of a state, Δt, is given by $\hbar/\Delta E$, where ΔE is its width. The *probability of disintegration* of a state per second is then given by $\Delta E/\hbar$, with ΔE in ergs.

The widths of levels, see Fig. 1–7, are usually expressed in eV and written as Γ, the full width at half-maximum. A "wide" level (large Γ) has a large disintegration probability, hence a short lifetime, while a "sharp" level lives a relatively long time. The actual value of the lifetime τ for a Γ in eV is given by,

$$\begin{aligned} \tau \text{ (sec)} &= \frac{\hbar}{\Gamma(\text{ergs})} \\ &= \frac{1{\cdot}05 \times 10^{-27}}{\Gamma(\text{eV}) \times 1{\cdot}60 \times 10^{-12}} \\ &= \frac{6{\cdot}56 \times 10^{-16}}{\Gamma(\text{eV})} \ . \end{aligned} \tag{2–5}$$

A wide level, with a Γ of 10^4 eV (appropriate for a light nucleus) has a lifetime of $6{\cdot}56 \times 10^{-20}$ sec, while a typical sharp level with a Γ of 0·1 eV lives for the relatively long time of $6{\cdot}56 \times 10^{-15}$ sec.* In Chapter 4 we shall see how widths are obtained directly from neutron cross sections as functions of velocity.

There is, of course, one disintegration probability for each possible disintegration product, hence a Γ_x, or a *partial width*, for each product. The *total width*, Γ, which gives the total disintegration probability, is then the sum of the individual particle widths:

$$\Gamma = \Gamma_\gamma + \Gamma_\alpha + \Gamma_n + \ldots \ . \tag{2–6}$$

The cross section for the process (n,x) is just

$$\sigma_{nx} = \sigma_c \ \Gamma_x/\Gamma \ , \tag{2–7}$$

where σ_c represents the cross section for formation of the compound nucleus. The theoretical treatment of various cross sections as functions of energy is developed on the basis of nuclear models that allow calculation of σ_c, as well as theoretical computations of the widths for various modes of disintegration of the compound

* A nucleon traverses the nucleus in about 10^{-21} sec.

nucleus. Before considering models and widths, however, we shall describe briefly some of the basic concepts of the quantum-mechanical formulation of neutron interactions.

QUANTUM-MECHANICAL ANALYSIS OF CROSS SECTIONS

We have already briefly discussed the rather simple-minded picture of the neutron cross section as the target area presented by the nucleus to the incoming neutron. This picture, although useful in many situations, does not have sufficient accuracy or basic validity to make it applicable for general use. It is necessary to examine the basic quantum-mechanical interpretation of neutron interactions in order to establish a more useful and more exact definition of neutron cross sections. The more exact quantum-mechanical treatment of neutron cross sections has extensive validity, and the basic properties of cross sections, as expressed in terms of this treatment, are of great value in correlating and predicting cross sections. It is well worth the effort expended to understand the basic definition of cross sections and the way in which the cross sections are expressed as functions of various types of *amplitudes.* We shall consider briefly the fundamental principles of neutron cross-sections theory, those characteristics that are common to neutron reactions whatever the energy involved. Later, in connection with cross sections at specific energies, we shall describe the specific characteristics of neutron cross sections at these energies. At the present time, however, we are interested only in general principles that apply at all energies.

In the quantum-mechanical analysis of cross sections the incident neutrons are considered as a plane wave that interacts with the potential field of the nucleus, producing a secondary scattered wave. The differential scattering cross section is then proportional to the square of the amplitude of the scattered wave. If the nuclear potential can be considered as spherically symmetrical, the amplitude of the scattered wave can be expressed as the sum of several *partial waves.* Mathematically, the amplitude is expanded in terms of Legendre polynomials and each partial wave corresponds to a particular polynomial. The *differential scattering cross section* is the square of the amplitude,

$$\sigma_n(\theta) = \left| \frac{\lambda}{2i} \sum_{l=0}^{\infty} (2l+1)\,[\exp(2i\delta_l) - 1]\,P_l(\cos\theta) \right|^2, \qquad (2\text{–}8)$$

$$= \lambda^2 \left| \sum_{l=0}^{\infty} (2l+1)\, e^{i\delta} \sin\delta_l P_l(\cos\theta) \right|^2, \qquad (2\text{–}9)$$

where $\sigma_n(\theta)$ is the scattering cross section per unit solid angle at the scattering angle θ, λ is the neutron wavelength divided by 2π, and P_l is the Legendre polynominal of order l. Thus the P_l's give the angular distribution of the scattered neutrons. These distributions are more complicated for higher l's, for example, $P_0 = 1$, $P_1 = \cos\theta$, so $l = 0$ scattering is isotropic and $l = 1$ is $\cos^2\theta$. The quantity δ_l, which is real for the case of scattering we are considering (no absorption), is the *phase shift* of the lth partial wave resulting from the nuclear potential, and its value determines the magnitude of the lth partial wave. All the symbols in Eq. (2–8) refer to the centre of mass system, which is essentially the same as the laboratory system when we are considering scattering from heavy nuclei.

The *scattering cross section*, valid in both the centre of mass and laboratory system, is obtained by integration of $\sigma_n(\theta)$:

$$\sigma = 2\pi \int_0^{\pi} \sigma_n(\theta) \sin\theta d\theta = 4\pi\lambda^2 \sum_{l=0}^{\infty} (2l+1) \sin^2 \sigma_l \ , \qquad (2\text{–}10)$$

and it is easily seen that the contribution to the cross section of any partial wave is zero if the corresponding phase shift is 0 or π. The physical significance of the decomposition into partial waves is that each corresponds to a certain *angular momentum* $l\hbar$, that is, l is the angular momentum quantum number, see Fig. 2–4. An angular

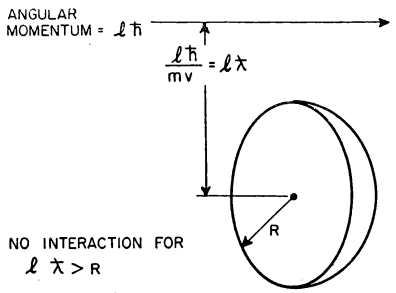

FIG. 2–4. The interpretation of the angular momentum quantum number l in terms of the classical distance of closest approach. Appreciable interaction occurs only if the latter is smaller than the nuclear radius.

momentum $l\hbar$, from a classical viewpoint, corresponds to a closest distance of approach equal to $l\hbar/mv = l\lambda$. If the radius of the nucleus is less than $l\lambda$, the amplitude for the lth partial wave, and the phase shift, will be zero, simply because the neutron passes so far from the nucleus that it "misses". In other words, λ for the neutron must be less than R/l for appreciable scattering of angular momentum l, where R is the nuclear radius. In analogy with spectroscopic notation,

scattering for which $l = 0, 1, 2$, etc. is referred to as *s*, *p*, *d*, etc. scattering and the partial waves as *s*, *p*, *d*, etc. waves.

For neutrons of low energy (less than 10^4 eV) the wavelength is so large that only $l = 0$, or *s* scattering, is possible. The scattering is then isotropic and the cross section is given simply by

$$\sigma = 4\pi\lambda\!\!\!^{-2} \sin^2 \delta_0. \tag{2–11}$$

If the nucleus is considered as an impenetrable sphere of radius R, the cross section for slow neutrons is readily obtained from Eq. (2–11). The wave is obviously shifted by the distance R, for it must go to zero at the surface of the sphere, see Fig. 2–5, hence the resultant

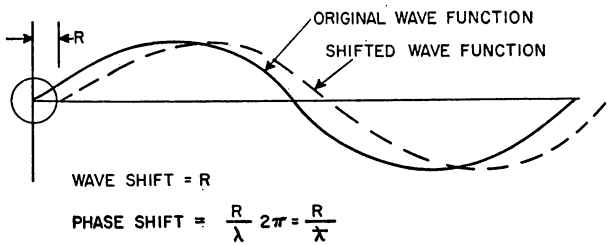

FIG. 2–5. The scattering cross section for slow neutrons at an impenetrable sphere of radius R. The scattering amplitude is just R and the potential scattering is $4\pi R^2$.

shift in phase is $2\pi R/\lambda = R/\lambda\!\!\!^{-}$. As $R \ll \lambda\!\!\!^{-}$ for slow neutrons, $\sin^2 \delta_0 = R^2/\lambda\!\!\!^{-2}$, the scattering amplitude ($\lambda\!\!\!^{-} \sin \delta_0$) is just R, and

$$\sigma = 4\pi R^2 \ , \tag{2–12}$$

an extremely useful evaluation, usually called the *potential scattering*.

Experimentally it is found that slow neutron scattering cross sections agree well with the result of Eq. (2–12), which is four times the expected classical value πR^2. Even if the nucleus is not impenetrable, but has a surface that constitutes an appreciable potential change, either attraction or repulsion, Eq. (2–12) will still apply because an abrupt change in potential will cause the wave function to go essentially to zero, unless the neutron is in resonance. These matters are particularly important to the resonance region, and we shall return to them in Chapter 4.

While the partial wave analysis is principally used for scattering, it can easily be extended to the case of absorption as well. If the phase shift in Eq. (2–10) is considered as a complex number, $\delta_{lr} + i\delta_{li}$, with δ_{lr} and δ_{li} real numbers, the scattering cross section becomes for δ small,

$$\sigma_n = 4\pi\lambda^2 \sum_{l=0}^{\infty} (2l + 1)\,(\delta_{rl}^2 + \delta_{li}^2)\ . \tag{2–13}$$

The absorption cross section σ_a, determined by comparing the total outward flux of neutrons with the incident flux, is a function of the imaginary part of the phase shift alone:

$$\sigma_a = 4\pi\lambda^2 \sum_{l=0}^{\infty} (2l + 1)\delta_{li}\,(1 - 2\delta_{li})\ . \tag{2–14}$$

However, as we shall see immediately, the absorption of neutrons into the nucleus is actually a complicated process and it is not profitable to pursue further the description of the absorption simply as the imaginary part of a phase shift with no reference to the absorption mechanism.

NUCLEAR MODELS

In the preceding discussion of the quantum-mechanical definition of cross sections we made no attempt to evaluate the actual amplitudes for various interactions. It is not the purpose of the theory to evaluate these amplitudes for they are not properly part of the scattering theory but rather an intimate part of the nuclear structure itself. It is the nature of the nucleus that determines the amplitudes for various processes, and the way in which they vary with neutron energy and with atomic weight. It is essentially impossible to compute the amplitudes for the various interactions by a consideration of the motions, energy states, and interactions of the individual particles in the nucleus. Not only would the computation be extremely complex because of the large number of particles in the nucleus, but it is rendered almost impossible because the basic law of force between nuclear particles is still unknown. The problem is much more complicated than atomic interactions, where the law of force is completely known, being of course just the Coulomb inverse square law.

Because of the complexity and the unknown nature of nuclear forces, the manner in which nuclear theory has been developed in order to predict neutron cross sections is in terms of what are called *nuclear models*. The purpose of a nuclear model is to provide a convenient, admittedly over-simplified, structure from which quantitative results can actually be computed, results that it is hoped will compare well with experiment. If the results, based on a particular model, do compare well with experiments where they are available, it gives confidence in the "truth" of the particular model,

and is hoped of course that the model can then be used with some confidence to make predictions for cross sections that have not been measured as yet.

The relationship between measured cross sections and the theoretical model is actually twofold, calculated results proceeding from the model to be compared with the cross sections, and the cross-section results proceeding to the model to be used to substantiate or to modify it, if necessary. Actually the specific nuclear model may be devised primarily to "explain" known cross section behaviour, rather than being based on nuclear *theory*, independent of measured cross sections. A good example of the effect of measurements on theory is the observed wave-like behaviour of fast neutron cross sections, which led to the inclusion of nuclear transparency in the models.

For many years the nuclear model that seemed to be closest to reality was one based closely on the idea of the compound nucleus, strongly absorbing, long-living, and forgetful of its mode of formation. In the usual compound nucleus theory, the incident particle is absorbed very quickly by the nucleus and the contributed energy of excitation, equal to its binding energy plus kinetic energy, rapidly shared with many nuclear particles. This strongly absorbing nuclear model is sometimes called the *black nucleus*. In recent years, however, evidence has come to light that incoming particles are not rapidly absorbed in nuclear matter, in fact, they may travel a distance equal to several nuclear diameters before losing their identity and sharing their energy with other nuclear particles. This weakly absorbing or transparent nuclear model has had a large share of success in the last few years. At the present time, one of the principal tasks of nuclear theory is to combine properties of the strongly absorbing or black nucleus with those of the partially transparent or *cloudy crystal ball nucleus*. Both models have a certain validity and we shall see in our later discussions that we must often refer to both in order to correlate the measured cross sections and guess intelligently with regard to unknown cross sections.

THE BLACK NUCLEUS

The concept of a black or completely absorbing nucleus was such a logical conclusion, both from experiment and theory, when neutron cross sections were first being measured, that its validity seemed beyond question. The sharpness of the observed neutron resonances showed that the lifetime of the compound nucleus was extremely long relative to the time required for a single nucleon to cross the nucleus. A typical resonance has a width of about 0·1 eV thus, by Heisenberg's uncertainty principle, Eq. (2–5), implying a

lifetime of $6{\cdot}6 \times 10^{-15}$ sec. This lifetime is more than a millionfold longer than the time required by a neutron to cross the nucleus, which is about 10^{-21} seconds. For such a long-lived nucleus, it would seem impossible that the energy of the incident neutron would not be shared with the other nuclear particles and the identity of the incoming neutron completely obliterated. Because of the high density of particles in the nucleus it also seemed extremely likely that the neutron would share its energy before it penetrated beyond the first surface layer of the nucleus. This blackness of the nucleus was also in accord with the theory of nuclear forces, for the neutron-proton and proton-proton forces, based on the exchange of mesons, could be predicted as having a range of only about 10^{-13} cm, following from the known meson mass.

Thus the compound nucleus would have properties completely independent of the method of formation, simply because the incident particle would lose its identity so quickly. The properties of the compound nucleus were then predicted by analogy with the properties of a *liquid drop*, in which the heat energy is shared among all the molecules of the drop, and is present as various types of liquid waves in the surface layer and interior of the drop. In predicting the characteristics of the energy levels in the excited nucleus, the liquid drop analogy is used in much the same way we have already seen that it forms the basis of the terms in the semi-empirical mass

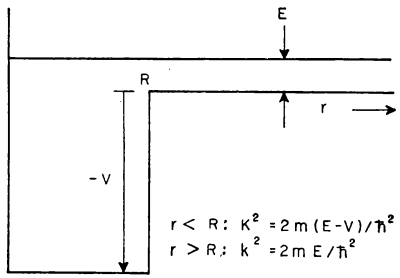

FIG. 2–6. The rectangular potential well, used to compute the average cross section for formation of the compound nucleus. The wave numbers for the neutron outside the nucleus, k, and inside the nucleus, K are shown.

formula. Thus there is, correspondingly, a "semi-empirical" *energy level density formula*, which gives the number of levels per unit energy interval as a function of various parameters. This formula, although admittedly a rough approximation, is valuable in the consideration of the neutron resonance structure of nuclei (Chapter 4).

The chance of a slow neutron, $l = 0$ only, forming a compound nucleus can be calculated quite easily for the black nucleus model.

The surface of a nucleus can be represented in this model by a sharp discontinuity in the potential experienced by the neutron, the potential dropping at the surface of the nucleus from zero to a value of approximately − 40 MeV. For simplicity this change in potential is often assumed to be extremely sharp, in other words the nucleus is represented as a rectangular potential well, as shown in Fig. 2–6. If we neglect for the moment the sharp resonance character of the neutron cross section we can obtain the *average* cross section for formation of the compound nucleus, σ_c.

The cross section σ_c is easily measured because it is observed directly if the resolution is poor enough so that individual resonances cannot be resolved; it is also a valuable cross section because of its significant theoretical implication. It is given, on the simplest theoretical basis, by the size of the nucleus or neutron, whichever is larger, multiplied by the chance of the incoming neutron wave for penetration of the potential discontinuity at the nuclear surface. The penetrability of the "barrier", which is represented by the sharp discontinuity, is a function of the wave number of the neutron outside and inside the nucleus. Outside the nucleus, the wave number $k(= 1/\lambda\!\!\!^{-})$ is given by

$$k^2 = 2mE/\hbar^2 \tag{2–15}$$

where E is the neutron energy, this formula actually being the same as Eq. (1–3), whereas the wave number inside the nucleus, where the kinetic energy is increased tremendously, is

$$K^2 = 2m(E - V)/\hbar^2 , \tag{2–16}$$

with V the nuclear well depth, Fig. 2–6, about − 40 MeV. The penetrability, p, of the surface is

$$p = \frac{4kK}{(k + K)^2} , \tag{2–17}$$

which, because $| \mathrm{V} | \gg E$ for slow neutrons, becomes simply

$$p = 4k/K = 4(E/ | \mathrm{V} |)^{\frac{1}{2}} . \tag{2–18}$$

The value of K for a 42 MeV well depth, currently in favour, is a useful constant to have in mind, and is, for negligible E,

$$K_{42\ \mathrm{MeV}} = (2m | \mathbf{V} |)^{\frac{1}{2}}/\hbar = \\ = 1{\cdot}42 \times 10^{13}\ \mathrm{cm}^{-1} ,$$

much greater than the k of a 100 eV incident neutron, for example, which is $2{\cdot}25 \times 10^{10}\ \mathrm{cm}^{-1}$.

The cross section for formation of the compound nucleus is now seen to be just the neutron "size", $\pi\lambda\!\!\!^{-2}$, which for a slow neutron is much larger than the nucleus, multiplied by the penetrability, or

$$\sigma_c = 4\pi\lambda^2(E/\mid V \mid)^{\frac{1}{2}}, \qquad (2\text{–}19)$$

and it is clear that this average cross section decreases monotonically with increasing neutron energy, in fact it varies as $1/v$, where v is the neutron velocity, because λ varies as $1/v$, and $E^{\frac{1}{2}}$ as v.

As the neutron energy increases and R is no longer negligible relative to λ, nor E relative to V, the cross section, more or less obviously, becomes

$$\sigma_c = \pi(R + \lambda)^2 \frac{4kK}{(k + K)^2}, \qquad (2\text{–}20)$$

which reduces to Eq. (2–19) at low energy and to πR^2 at high energy, thus to the classical picture of a point projectile hitting a sphere of radius R. The monotonically decreasing cross section for compound nucleus formation typical of the black nucleus is sketched in Fig. 2–7.

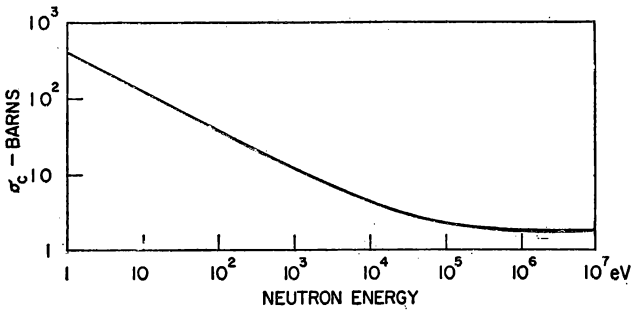

FIG. 2–7. The computed average cross section for formation of a compound nucleus computed from the reactangular potential well shown in Fig. 2–6; the monotonic behaviour is characteristic of the "black nucleus".

Actually, of course, the energy region about 100 eV is rich in resonances for heavy nuclei, see Fig. 1–7, but Eq. (2–20) correctly gives the *average* over these resonances to the extent that the black nucleus model is correct.

In addition to the behaviour of the average cross section, important as it is to nuclear theory, there is much more to be learned about the compound nucleus when the properties of individual cross-section resonances are examined. Each resonance in the neutron cross section corresponds to an energy level of the compound nucleus, at excitation energy equal to the neutron resonance energy plus its binding energy. The *parameters* of the resonance, measured as described in Chapter 4, give direct information on the compound nucleus energy level, such as its neutron width, radiation width and angular momentum.

The *neutron width*, Γ_n, of a resonance level is related to the mean

lifetime, τ_n, of the state relative to disintegration by emission of a neutron,

$$\Gamma_n = \hbar/\tau_n \ . \tag{2–21}$$

The width can be considered crudely as being determined by the time required for concentration of the excitation energy on a particular neutron and by the probability that this neutron will penetrate the nuclear potential barrier. Thus the neutron width is given by

$$\Gamma_n = \hbar p/t_0 \ , \tag{2–22}$$

where t_0 is the time spent by the nucleus in the particular excitation state before the energy is concentrated on a single neutron, and p is the barrier *penetrability*. Because neutron widths contain a factor proportional to neutron velocity it is useful to convert Γ_n's to their values at 1 eV, this reduced neutron width being thus (with E in eV)

$$\Gamma_n^0 = \Gamma_n/(E)^{\frac{1}{2}} \ . \tag{2–23}$$

Hence Γ_n^0 is given conveniently in terms of the penetrability of a 1 eV neutron, p^0,

$$\Gamma_n^0 = \hbar p^0/t_0 \ , \tag{2–24}$$

thus Γ_n^0 is determined by the nuclear surface (through p^0) and the intrinsic nuclear level structure (through t_0).

As the barrier penetrability p^0 is expected to be practically the same from one level to another in a particular nucleus, the wide range in neutron widths that is observed, Chapter 4, must indicate a corresponding wide range of lifetimes for the individual nuclear states. The barrier penetration, p^0, is of the order of 10^{-3}, Eq. (2–18), hence the intrinsic nuclear lifetime, t_0, varies from about 10^{-13} to 10^{-16} sec for the observed range in Γ_n^0, Chapter 4, of 0·01 mV to 10 mV for "heavy" elements, $A > 100$. In spite of this wide range, however, the values of t_0 are always much greater than the time required for a nucleon to cross the nucleus, about 10^{-21} second.

The wide range in t_0 observed reflects the variation in intrinsic properties of individual nuclear levels; hence some information can be obtained from the experimental data on the nature of the distribution of the nuclear lifetimes, or more simply, as they are expressed by the reduced neutron widths. However, in connection with the question of nuclear models, it is more significant to discuss the average reduced neutron widths, $\overline{\Gamma_n^0}$, in a particular nuclide, especially as it is related to the average spacing of levels, D, in the nuclide. Whenever we are considering level spacings we shall signify by D the average spacing of levels of a single angular

momentum value, J. For resonance neutrons incident on any but a zero-spin target nucleus, two values of J can result and D is usually taken to be twice the observed spacing on the assumption that D is independent of J, not completely a safe procedure, however, we must remember.

In addition to the intrinsic interest of $\overline{\Gamma_n^0}$ and D individually, their ratio has an important bearing at present on nuclear models. The significance of the $\overline{\Gamma_n^0}/D$ ratio follows directly from the relationship of the neutron width to the intrinsic lifetime of a nuclear state and the penetrability of the nuclear surface, Eq. (2–24). As the intrinsic lifetime of a state, t_0, is approximately given by h/D, it follows that division of the neutron width by D removes the specific nuclear part, leaving only the penetrability of the nuclear surface,

$$\overline{\Gamma_n^0}/D = p^0/2\pi \ . \qquad (2\text{–}25)$$

The relationship $t_0 = h/D$ follows directly from considerations of the nuclear configuration as a superposition of states (reference 1, p. 386), if the levels are considered to have equal spacing and it can be taken to hold approximately for actual level spacings as well, with D the average spacing.

For the strongly absorbing nucleus that we are considering, the penetrability of the sharp potential discontinuity that represents the nuclear surface is given simply by Eq. (2–18) for slow neutrons. Thus the ratio of the average reduced neutron width to the spacing D, or the *strength function*, turns out to be a function of the well depth alone,

$$\frac{\overline{\Gamma_n^0}}{D} = \frac{\overline{\Gamma_n/E^{\frac{1}{2}}}}{D} = \frac{4}{2\pi}\left(\frac{1}{V}\right)^{\frac{1}{2}}, \qquad (2\text{–}26)$$

a ratio that is $1{\cdot}0 \times 10^{-4}$ for a 42-MeV well depth, for example. Before considering how well this prediction of the black nucleus fits observations on the strength function for slow neutrons, we shall turn to another nuclear model, one that in some ways directly contradicts the basic assumptions of the black nucleus model.

THE CLOUDY CRYSTAL BALL

During the period when neutron cross sections were first being measured, the results seemed to fit very well into the predictions of the black nucleus model that we have just discussed. The observed cross sections in the energy region where individual resonances could not be seen seemed to decrease reasonably monotonically with increasing energy. In the lower energy region, where individual resonances were found, their neutron width relative to the spacing of the levels seemed to be about 10^{-4}, the ratio expected for a well depth

of about 40 MeV. The total cross sections were not measured accurately enough nor over a wide enough energy region to see if there were any departures from the monotonic behaviour predicted by the black nucleus model, nor were the number of resonances observed at low energies sufficiently great so that the ratio $\overline{\Gamma_n^0}/D$, or in other words, the cross section for formation of the compound nucleus, could be determined with great accuracy. Nevertheless, to the accuracy with which the measurements were made the predictions of the black nucleus or liquid drop model seemed to be adequately fulfilled. Furthermore, there seemed to be no reason to doubt that the nucleus should act as a strongly opaque body to the incoming neutron, simply because of the great density of particles within the nucleus and the large interaction that was known to exist between the elementary particles in the nucleus.

About 1945 evidence from several sources began to accumulate that the well-accepted liquid drop or strongly interacting model of the nucleus was not completely correct. The finding that certain nuclei, containing so-called *magic numbers* of particles—the magic numbers being 50, 82, and 126—behave differently from others, indicated that strong, local interactions did not constitute the whole story. The existence of magic numbers, or *nuclear shells* showed that particles in the nucleus could move in the average field of all the other particles, a behaviour not at all expected on the basis of a strongly interacting liquid drop model.

Definite evidence for shell structure came from neutron cross sections themselves, particularly in the MeV region where the individual resonances are not resolved for most nuclei. Measurements with fast neutrons showed that the cross sections did not always decrease monotonically with energy but that the cross sections sometimes actually increased. The behaviour of the measured total cross sections is more a smooth long-wavelength dependence on energy, superimposed on a monotonic decrease, as shown in Figs. 1–8 and 1–9 for Hg and Au. A wavelike dependence in any physical phenomenon immediately suggests an optical interference effect, and it was soon found that the peaks and valleys in the total cross-section curves correspond to definite optical effects. The maxima and minima of the total cross section occur when the wavelength of the neutron inside the nucleus (given by $1/K$) bears a simple numerical relationship to the size of the nucleus. The effects are extremely closely allied to those observed when light is passed into a crystal sphere, in other words, typical optical diffraction effects are observed in the cross sections in the MeV region.

The work of Weisskopf and his collaborators soon showed what

results were to be expected for neutron cross sections if the nucleus were weakly absorbing instead of black. This model of the nucleus as a partially transparent sphere soon came to be called the *cloudy crystal ball* model of the nucleus. The prediction of the cross section averaged over many resonances, the same procedure we have outlined for the black nucleus, is a straightforward optical calculation. The theoretical results give the wavelike character observed in the MeV region with reasonable success as we shall learn in the next chapter. In the low energy region, where individual resonances are observed, the ratio $\overline{\Gamma_n^0}/D$ again gives the penetrability of the nuclear surface for the cloudy crystal as for the black nucleus. The difference, however, is that instead of this ratio having the constant value of about 10^{-4}, it varies about the 10^{-4} figure with increasing atomic mass. The theoretical $\overline{\Gamma_n^0}/D$ ratio, or strength function, varies slowly with atomic mass, i.e. with nuclear radius, and has peaks at atomic mass about 60 and 160. The correlation between the theoretical prediction and the actual experimental values will be discussed in Chapter 4, where we shall learn that the variation characteristics of the cloudy crystal ball model is indeed seen in the experimental data, but to a smaller extent than predicted by theory.

The experimental results show that there is a great deal of truth in the basic assumptions of the cloudy crystal ball model. It is certain that the incident neutron enters the nucleus and does not lose its identity for a long time, in spite of the strength of nuclear forces. In other words, it may cross the nucleus several times without passing its energy on to other particles, and in fact even have a good chance of leaving the nucleus before its energy is shared. However, should the neutron be absorbed by the nucleus it then lives a long time and the further development of the compound nucleus, that is, the possibility of emission of gamma radiation or of the incident neutron again, is very similar to the behaviour of the black nucleus model. The essential difference between the two models appears in the period *before* the neutron shares its energy with the other nuclear particles, this time being much greater in the cloudy crystal ball model.

In the theory of the cloudy crystal ball, the nucleus is represented by a potential well with a real and an imaginary component, being expressed in the following way,

$$V = V_0(1 + i\zeta) \ . \tag{2–27}$$

The relationship between the imaginary part of the potential well and the absorption is that the wave number K is now complex:

$$K^2 = \frac{2m \mid V_0 \mid}{\hbar^2} (1 + i\zeta) \ , \tag{2–28}$$

or $$K = K_1 + iK_2 \,. \qquad (2\text{–}29)$$

The component K_2 damps the wave function of the incident neutron and the resulting absorption coefficient of the neutron is $2K_2$, given by

$$2K_2 = \zeta \left(\frac{2mV_0}{\hbar} \right)^{\frac{1}{2}}, \qquad (2\text{–}30)$$

for small ζ. From the magnitude of the imaginary component found necessary to fit the experimental data, namely the value of $\zeta = 0{\cdot}03$ and $V_0 = 42$ MeV (for a rectangular well), it follows that the mean free path before absorption, $1/2K_2$, is surprisingly large, 24×10^{-13} cm, which is actually several times larger than the nuclear radius.

This concept is extremely difficult to understand under the old nuclear model, according to which the neutron should never go a distance as large as the nuclear radius before sharing its energy. At the present time, however, experimental evidence makes it absolutely certain that a neutron can move a considerable distance in nuclear matter before being absorbed. The main reason for this weak interaction is that many of the possible energy states for the neutron in the nucleus are already filled and hence are unavailable to the incoming neutron. As the energy of the incoming neutron is raised, then the chance of its absorption becomes greater, because more energy levels are available to it, and the result is that ζ becomes larger as the neutron energy increases.

Experimentally the increase in ζ is found to be the case with the result that at about 15 MeV the nucleus is almost black to an incoming neutron. Above this energy the nucleus becomes more transparent again because the elementary interactions that absorb the neutron, that is the neutron-neutron and neutron-proton cross sections, become very small. The actual values for these elementary particle cross sections are accurately known because the *n-p* and *p-p* cross sections can be measured, using free particles. There is some uncertainty as to whether the nucleons behave within the nucleus just as they do in free *n-p* and *p-p* collisions, but the differences probably do not cause more than a factor of two in the effective cross sections within the nucleus. Thus, arguing from the experimental evidence as well as the theory it seems reasonable that the incoming neutron does not amalgamate with the rest of the nucleus when its energy is very low, because of the Pauli exclusion principle, nor when it is very high because of the small value of the elementary *n-p* and *n-n* cross sections.

As we shall see in later chapters, it is necessary to refer often both to the properties of the black nucleus and to the cloudy crystal ball model, sometimes in essentially the same phenomenon. It is certainly true that some aspects of both models represent the actual structure

of the nucleus, and it is the present task of theoretical nuclear physics to decide the proper combination of the two models, or perhaps find a third that is superior to both. Of course each model is actually a great simplification of the true structure of the nucleus; the advantage of models is not that they are *true*, but that they are sufficiently *simple* so that calculations are made possible because of their simplifications. The actual nucleus is probably so complicated that calculations, involving all the details of reality, simply could not be carried out. Thus a model is useful just because it is simple, and cross-section predictions can easily and directly be made with it. It is of course always necessary to use the model only in connections where it is justified; in other words, just because the model is not "true" its use must be restricted to those connections in which its predictions correspond well with reality. At the present time much work is proceeding in connection with improving the models by adjusting such parameters as well shape, and also in seeking a firm theoretical basis for the simplified aspects of nuclear behaviour incorporated in the models. In all this theoretical development the twofold relationship of theory and experiment that we have mentioned is evident. The experimental cross sections furnish clues for the refinement of the theoretical models and the improved theory is of ever-increasing value in predicting as yet unmeasured cross sections.

REFERENCES FOR ADDITIONAL INFORMATION

1. J. M. BLATT and V. F. WEISSKOPF, *Theoretical Nuclear Physics*, (Wiley, 1952). Chapter I, a review of the general properties of nuclei; Chapter VIII, pp. 311–358, a thorough treatment of general principles of nuclear reactions.
2. H. FESHBACH and V. F. WEISSKOPF, *Phys. Rev.*, **76**, 1550 (1949). Gives the theory of the "black nucleus" just before nuclear transparency was becoming evident.
3. H. FESHBACH, C. E. PORTER and V. F. WEISSKOPF, *Phys. Rev.*, **96**, 448 (1954). The theory of the "cloudy crystal ball" model is presented in its original form as a sharp-edged potential well.
4. M. G. MAYER, *Phys. Rev.*, **74**, 235 (1948). A review of the experimental evidence for "closed shells" in nuclei from a variety of phenomena.
5. E. FERMI, *Nuclear Physics* (University of Chicago Press, 1950), p. 9. A description of nuclear energetics and the details of the semi-empirical mass formula.

CHAPTER 3

FAST NEUTRONS

VARIOUS criteria are in common use for classifying neutrons according to energy, such as the energy range produced by particular neutron sources or the types of cross sections that are characteristically observed at different energies. Concerning the type of neutron source as a criterion, *fast neutrons* are usually considered to be those produced mainly in particle accelerators, such as Van de Graaff or Cockcroft-Walton machines. According to this method of classification, fast neutrons would be those in the range from about 0·1 to 20 MeV, although recently neutrons have been obtained from Van de Graaff's at energies even as low as one keV.

From the standpoint of the type of interaction observed, fast neutrons are usually distinguished from intermediate energy, or *resonance* neutrons, because many resonances are observed for most neutrons of the latter classification. This distinction between fast and resonance neutrons is extremely vague, however, because the energy at which resonances are observed is a function of the particular resolving power used in the measurement and of the atomic weight of the nucleus investigated. Thus individual resonances are hardly seen higher than several hundred eV for a heavy nucleus like U^{235}, Fig. 1–7, whereas with something as light as carbon the resonances do not merge even at energies of 50 MeV. However, if we consider the great majority of nuclei, omitting the lightest, it is true that with presently used resolution, individual resonances are not observed above an energy of about 0·1 MeV. Hence from this standpoint we can consider "fast" neutrons as those above 0·1 MeV, for which individual resonances are not resolved in "typical" nuclei.

With regard to the comparison of cross sections with theory, consideration of the fast neutrons as those for which individual resonances are not seen is an extremely useful concept because we can then concentrate on the aspects of the theory that are related to average cross sections alone. Both on the experimental side and in theoretical developments of nuclear models, this limitation to average cross sections provides a great simplification. Thus we reserve the theory that deals with individual resonances for the next chapter even though some of these resonances may occur at extremely high energy for sufficiently light nuclei.

Another useful method, both with regard to theory and experiment,

for deciding the energy region appropriate to fast neutrons is in terms of the *angular momentum* involved in the collision. For the great bulk of the resonances that we shall discuss in Chapter 4, $l = 0$ is the only angular momentum involved and many of the equations are thereby simplified greatly. However, in the MeV region higher angular momenta occur, and it is useful to consider the higher angular momenta as being particularly associated with the fast neutron cross sections that we shall consider in the present chapter. The restriction to $l = 0$ for slow neutrons is of course a restriction that changes somewhat with atomic weight. From the discussion following Eq. (2–10) we see that $l = 1$ interactions become appreciable when $\lambda\!\!\!^{-}$ is equal to the nuclear radius, R. If we take the latter to be given, Eq. (2–1), by $1{\cdot}35\ A^{\frac{1}{3}} \times 10^{-13}$ cm and λ by Eq. (1–3) we find that $l = 1$ collisions are important at about 2·5 MeV for $A = 10$ but at the much lower energy of 0·33 MeV for atomic weight 200. These energy limits are rough guides only, and individual p resonances are often seen at lower energy.

The various criteria for delineating fast neutrons that we have listed have a rough consistency in setting a lower limit in the neighbourhood of 100 keV. In the present chapter then we shall be concerned mainly with reactions in the energy region above 0·1 MeV and for sufficiently heavy nuclei so that individual resonances are not observed. The upper energy limit for our present purposes is about 20 MeV, fixed by the availability of neutron sources, the complications of theory above that point (many partial waves, relativistic effects), and the practical importance of the fission neutron spectrum, which extends to about 20 MeV. For the light elements for which individual resonances are seen in the MeV energy region, discussion will be deferred until the next chapter, which deals exclusively with resonance behaviour.

SOURCES OF FAST NEUTRONS

In the early days of neutron cross-section measurements, when no monoenergetic sources were available, it was necessary to measure fast neutron cross sections utilizing sources that would hardly find application at the present time. A good example of this kind of source is Ra–α–Be, which emits an extremely widespread and complicated neutron spectrum. Whereas it is true that important cross sections were measured with Ra–Be sources in the 1930s, at present such excellent results are available from accelerators that the old cross sections are of little value now. The emphasis in BNL 325 is on cross sections measured with monoenergetic sources, and for this reason as well as the superiority of monoenergetic measurements for comparison with theory, we shall concern ourselves almost

exclusively with those fast neutron cross sections that are measured at specific energies. However, at the end of this chapter we shall refer briefly to cross sections measured with sources of wide energy spread. Such measurements have importance because they can sometimes give results that are available in no other way, and in addition they may have a great practical importance because the results are often directly applicable to a desired phenomenon. The prime example of this type of measurement for a wide-spread energy source is of course the use of the fission spectrum itself. Measurements made with the entire fission spectrum may be extremely useful in a direct practical way but are not usually of much use for comparison with theory. Results of these "integral" types of measurements are not in general listed in BNL 325.

The accelerators that are commonly used for neutron cross section measurements are the Van de Graaff, the Cockcroft-Walton or cascade generator, the cyclotron, and the synchrocyclotron. The Van de Graaff generator is the most widely used accelerator; it can supply up to tens of microamperes current of accelerated protons or deuterons, whose energy can be varied continuously from a few hundred keV to the maximum energy of the machine, which is about 10 MeV in recent designs. The charged particle current is well focused, being a few millimeters in diameter, with a spread in energy of only about 2 keV. By employing either a magnetic or an electrostatic analyser, focused beams of a few microamperes with less than one keV energy spread can be obtained.

Cockcroft-Walton accelerators range from 50 to 500 keV in output energy, with currents of several hundred microamperes with only a few keV spread in energy. Cyclotrons range from a few MeV to about 20 MeV, but the external beams in practically all cyclotrons are of fixed energy. External beam currents of approximately 100 microamperes spread over a few square centimetres with a few per cent energy spread have been obtained. In contrast to Van de Graaff and Cockcroft-Walton generators, which are continuous current machines, cyclotrons give a pulsed output of the order of millimicrosecond duration at a repetition rate of 10 to 20 megacycles. Lower energy accelerated particles can be obtained in a cyclotron by inserting the target at smaller radius inside the acceleration chamber.

Neutrons are produced from the charged particle beams of accelerators by a variety of (p,n) and (d,n) nuclear reactions. The most useful reactions are those on lithium and tritium for (p,n), and those on deuterium and tritium for (d,n). The neutron energies available from these four reactions as functions of the bombarding energy are shown in Fig. 3–1, which is a revised version of a figure

from the article of Hanson, Taschek, and Williams, reference 5. The neutron energy is shown for emission at angles of 0° and 180° to the direction of the incident particle; results for other angles can be readily obtained from nomographs in the article cited. From Fig. 3–1 it is

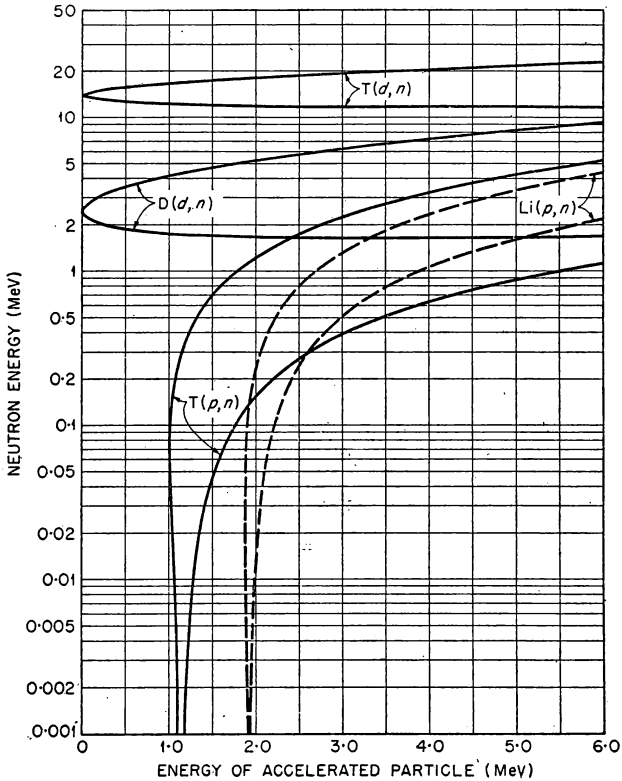

FIG. 3–1. Curves giving the neutron energies for emission at 0° (upper curve and 180° (lower curve) in the most important (p,n) and (d,n) reactions used as neutron sources.

obvious that with incident particles up to 6 MeV, neutrons of all energies up to 23 MeV, except the small range from 9·5 to 11·5 MeV, can be obtained from these sources.

Both (p,n) reactions we are considering have negative Q values, hence thresholds for neutron production. For lithium the threshold energy is 1·882 MeV, with the neutron yield rising very rapidly in about 30 keV and varying only slightly for higher energies. At threshold the neutrons are all forward and have an energy of 29 keV, but above the threshold energy, and extending to 1·92 MeV proton

energy, two neutron energy groups are emitted at each angle in the forward direction. (These details of the near-threshold behaviour cannot be shown clearly in Fig. 3–1 because of the scale used.) For example, with 1·90 MeV incident protons, 80 and 3 keV neutrons are present at 0°. To obtain monoenergetic neutrons below 120 keV it is necessary to utilize those neutrons emitted at back angles, such as 120°. An advantage of back angles is that the spread in neutron energy, at 120° for example, is only one half the spread in proton energy, whereas at 0° they are nearly equal. At 0° the yield is approximately constant for neutrons greater than 100 keV and is about 2×10^5 neutrons per sec per unit solid angle per microampere of protons for a target of 2 keV thickness.* Unfortunately, for neutron energies greater than 600 keV the Li^7 (p,n) reaction is not a monoenergetic source, since the Be^7 nucleus is left in the 435 keV excited state with a 10 per cent probability at these higher energies. However, the detector may be biased so as not to count this lower energy group and the Li source may then be used for neutrons above 600 keV.

The $T(p,n)He^3$ threshold is 1·019 MeV, at which point the neutrons are all forward and have an energy of about 60 keV. Two energy groups of neutrons are present in the forward hemisphere up to a neutron energy of about 300 keV at 0°, thus monoenergetic neutrons with energies greater than 300 keV can be obtained at 0°. Since there are no known excited states of He^3 up to many MeV these neutrons are truly monoenergetic. The yields from a tritium target are generally better than from a lithium target, although preparation of the former is more difficult and usable beam currents are lower. Two types of tritium targets have been developed, however, tritium adsorbed in a thin film of zirconium metal and a tritium gas target. In the adsorbed target about one atom of tritium is present per atom of zirconium. The gas targets are several centimetres in length and require windows (about 10^{-3} cm thick) to hold the tritium gas, which is used at pressures as high as one atmosphere. For a given target thickness, the gas target, if it can be used, has the advantage over the adsorbed target because of the larger number of tritium atoms present and the resultant higher neutron yield.

As the $D(d,n)He^3$ and $T(d,n)He^4$ sources have positive Q values, relatively high energy neutrons can be obtained from low energy machines, Fig. 3–1. For the $D(d,n)He^3$ reaction and for incident deuteron energies up to 400 keV the neutron spectrum at 90° is approximately monoenergetic with an energy of about 2·5 MeV for a thick target, whereas the neutrons in the forward direction have a finite spread in energy. For a thick D_2O ice target the total neutron

* That is, one in which the incident protons lose 2 keV energy.

yield varies approximately as the square of the deuteron energy and is about 3×10^7 neutrons per sec per microampere for 200 keV deuterons. The angular distribution is not isotropic, the yield at 90° being about 40 per cent of that in the forward direction. With deuteron energies greater than 500 keV it is necessary to use thin targets to get monoenergetic neutrons. These thin targets are usually deuterium gas targets a few centimetres in length contained by thin aluminium or nickel windows. At the higher energies the angular distribution is peaked somewhat in a forward direction and neutrons are usually used at 0°. The total cross section rises up to a broad maximum at a deuteron energy of about 2 MeV and falls slowly for higher energies. It is difficult to make accurate measurements with a thin deuterium target at the higher energies since there are large numbers of neutrons produced by deuterons striking various collimating apertures and the foils containing the gas. Since there are no excited states of He^3 the D(*d*,*n*)He^3 source can supply monoenergetic neutrons up to 7 MeV. Above 7 MeV the neutron beam is contaminated with low energy neutrons from the D(*d*,*np*) reaction, which has a threshold at 4·6 MeV deuteron energy.

The T (*d*,*n*)He^4 reaction can produce neutrons from 12 to 20 MeV for incident deuterons of 3 MeV, Fig. 3–1. It is an extremely useful source of high energy neutrons for use with low energy accelerators since the reaction has a very high, broad resonance at 100 keV deuteron energy. For a thick tritium gas target and 600 keV bombarding deuterons the yield is 5×10^8 neutrons per sec per microampere; for tritium adsorbed in a thick zirconium target and 200 keV deuterons the yield is about 10^8 neutrons per sec per microampere. For these low deuteron energies the neutrons emitted at 90° are usually used since their energy, 14·1 MeV, is rather insensitive to the incident deuteron energy. By using thin gas targets and higher deuteron energies neutrons from 12 to 20 MeV can be obtained by observing neutrons at various angles. The thin gas targets used have a thickness of about 100 keV and the neutron yield is only a few per cent that of the thick targets for 600 keV deuterons.

TOTAL CROSS SECTIONS — EXPERIMENTAL

We have already considered briefly the general principles that are applicable to the measurement of total cross sections and have learned, for example, that the attainable accuracy is far greater for a total cross-section measurement than it is for any partial cross section. In addition to the general principles, there are several specific matters applicable to the measurement of cross sections in the fast neutron region, and we shall examine these before proceeding to the experimental results. Because of the basic simplicity of total

cross section techniques, and the availability of monoenergetic sources, almost all elements have been measured in the MeV energy region. However, only for the lightest nuclei has the energy resolution been sufficiently good to resolve all the resonances up to a few MeV. For intermediate atomic weight nuclei, although some structure is observed in the total cross section below 1 MeV, many resonances are not resolved even with the best available resolution. For heavy nuclei ($A > 100$), which have level spacings of the order of a few eV, the total cross section observed for fast neutrons is the average over many resonances and no *fine-structure* is observed.

The measurement of a total cross section consists of a simple transmission experiment, Fig. 1–2, in good geometry, with the sample inserted between the neutron source and the detector. "Good geometry" means simply that very few of the neutrons scattered by the sample reach the detector (one is shown doing this in Fig. 1–2), because of the small angle subtended by the latter. The sample thicknesses are usually such that they have transmissions ranging from 0·3 to 0·7; if the cross section varies strongly with energy, samples of different thicknesses must be used at different energies to assure reasonable values of transmission throughout. In most measurements no shielding is used around the source, sample, or detector, in order to reduce complications caused by scattering of neutrons from extraneous material. For the same reason, the walls and floor of the room and other neutron scattering material are kept as far away as possible. The diameter of the sample must be sufficiently large to shadow the detector completely, but no larger because neutrons could otherwise "inscatter" and be detected.

Whenever available, samples of the element in the solid form are used. If the element is not available in elemental form, chemical compounds are used. However, these "chemically pure" compounds frequently contain water, which affects the accuracy of the measurements greatly, because of the large hydrogen cross section. Measurements on gases are difficult but may be made using the gas at high pressures or with liquefied gases at low temperatures. For typical total cross section work with fast neutrons, the samples are about 1 inch in diameter and thus require tens to hundreds of grams of material. Although some work has been done with separated isotopes, the measurements are difficult, for the isotopes are usually available in amounts of several grams only.

In general two corrections have to be made to the measured transmission before computing the cross sections from Eq. (1–5). The first arises because some neutrons scattered by the sample will reach the detector. This correction for "geometry" is kept as small as possible by using samples and detectors of small area at large

distances, since there is always some uncertainty involved in the correction. For low energies, where the angular distribution is isotropic, the correction for geometry is calculated simply from the solid angle subtended by the detector at the source, and is generally of the order of 0·1 per cent. At high energies, such as the frequently used 14 MeV neutrons from the T(*d*,*n*)He^4 source, the angular distribution of the scattered neutrons is strongly forward and inscattering increases by an order of magnitude, in some cases reaching several per cent. Measured angular distributions, when available, together with optical diffraction theory, are used to make the correction.

The second correction that must be applied to the observed transmission is for background neutrons that are scattered into the detector from the floor and other objects in the environment. This "room background" is determined by inserting a long *shadow cone*, typically 50 cm of copper, between the source and the detector, Fig. 3–2. The background measured in this way is generally less than

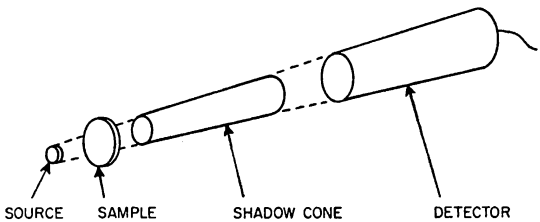

FIG. 3–2. The method of use of a *shadow cone* in a total cross section measurement by transmission.

a few per cent. For the low energy measurements, which as we have seen are made in the backward direction, the background is relatively much higher and necessitates use of a highly directional counter that detects neutrons from the source only. Since there is always some uncertainty in the determination of both the inscattering and the background, thick samples, with transmissions of less than 30 per cent, are seldom used, because the corrections would then be much more important relative to the transmitted neutron intensity.

As some fast neutron cross sections, even for light nuclei, exhibit resonances only a few keV wide, it is necessary to have monoenergetic neutrons with a very narrow energy spread in order to study resonance structure. The energy spread of a neutron beam depends on three factors: (1) the spread in energy of the charged particles incident on the target; (2) the energy loss of the charged particles in the target, and (3) the angle subtended by the neutron detector at the source, since the neutron energy varies with angle. In principle, all three factors may be made as small as desired, with a

resulting loss in intensity. Measurements have been made from a few keV up to 1 MeV with energy resolutions as good as 1 keV. From 1 to 8 MeV resolutions used range from 30 to 100 keV, and better resolutions are used only in specific ranges for particular resonances. From 12 to 20 MeV resolutions of about 100 keV are generally used, while above 20 MeV measurements are made with about 10 per cent energy resolution.

The accuracy that has been attained for total cross sections is well shown in the curve for hydrogen, Fig. 3–3. Much effort has gone into

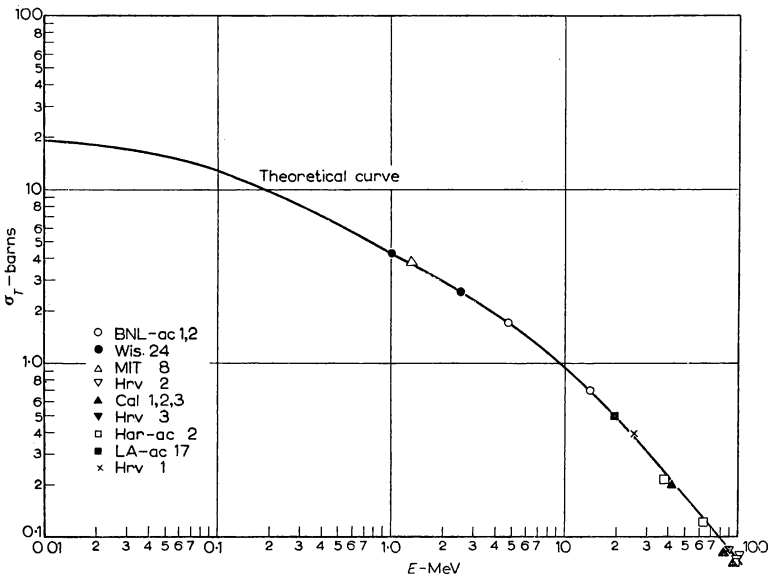

FIG. 3–3. The total cross section for hydrogen in the MeV region, compared with a "theoretical" curve involving several empirical parameters.

the careful determination of this particular total cross section curve because it is of great interest to nuclear theory, representing as it does the interaction between two fundamental particles, the neutron and the proton. The curve labelled "theoretical" in Fig. 3–3 is based on the fundamental theory of scattering from a potential, some of whose principles we have covered briefly in Chapter 2. The curve is not completely "theoretical", that is, computed from the basic theory of nuclear forces, for it involves some parameters that are empirical results of other measurement involving the fundamental neutron-proton interaction, such as the total cross section at zero neutron energy, and the fraction of the scattering that is coherent (in the

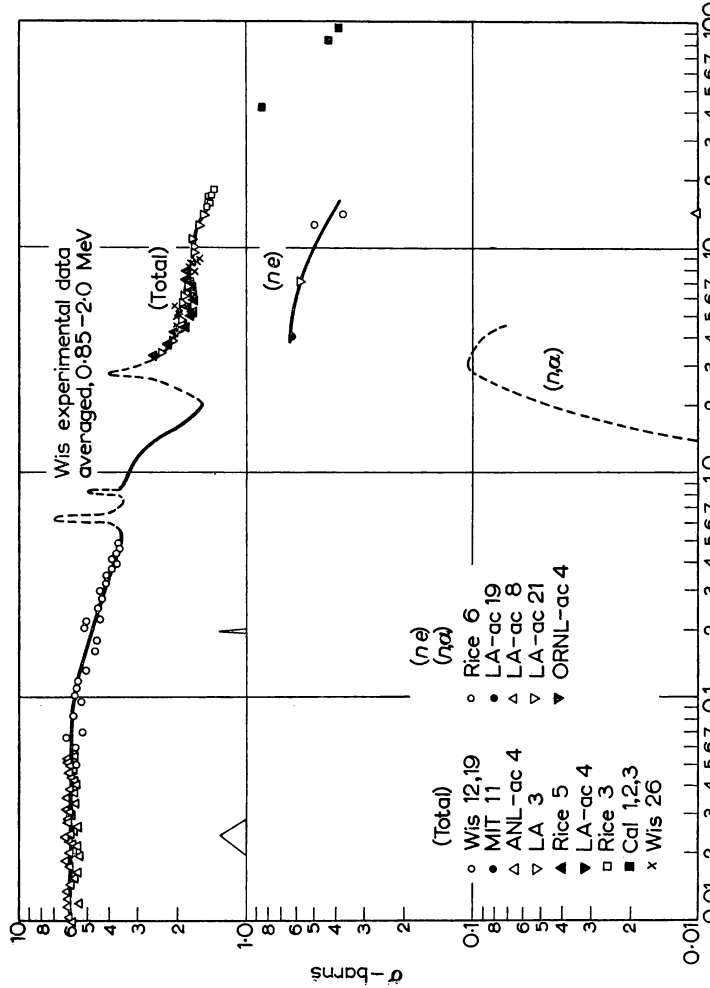

FIG. 3–4. The total cross section of beryllium in the MeV region; several resonances are observed, in contrast to the curve for hydrogen, Fig. 3–3.

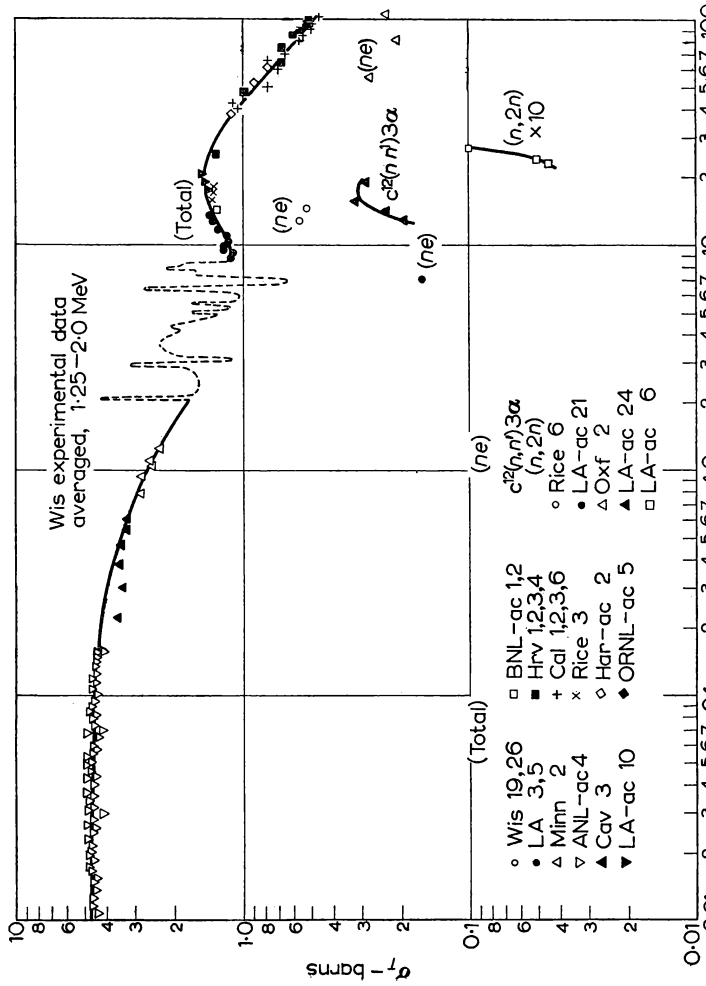

FIG. 3-5. The total cross section of carbon in the MeV region; the agreement among the results of various laboratories is particularly striking in the region above 10 MeV.

sense of Chapter 6). Nevertheless, the fundamental reality of the theory and the excellence of the various total cross-section measurements are shown by the exceptionally good agreement of the theoretical curve with experimental points.

For such a "simple" interaction as the *n-p* scattering, which is treated as the interaction of a particle with a potential well, it is not at all surprising that resonances are not seen, even in the large energy region shown in Fig. 3–3. Of course, the reason for the absence of resonances here is just the opposite of the reason for their absence in heavy elements. Resonances are not seen in Fig. 3–3 because they are not present, whereas for heavy elements they are so numerous that they cannot be resolved. Even for an element as light as beryllium, Fig. 3–4, the number of resonances is already seen to be much greater than for hydrogen. Carbon, Fig. 3–5, is of course a very important element for use in reactors, and is extremely important to nuclear theory as well, because of its particularly simple structure, being made up of the equivalent of three alpha particles. The list of references in Fig. 3–5 shows how many laboratories have contributed to the composite curve for carbon and the accuracy of the measurements is demonstrated by the excellent agreement, which is particularly good in the region above 10 MeV. Figure 3–5 constitutes striking evidence that the entire region from 10 kilovolts to 100 million volts is adequately covered with present-day instruments and that accurate cross-section measurements are available for the entire energy range. Even though the resonance structure for carbon is quite simple in one sense because of the light nucleus, it is still interesting that high resolution in the region from 2 to 8 MeV is necessary because the resonance structure is highly complex in spite of the simple nature of the C^{12} nucleus.

The total cross section of cobalt is a very good illustration of the way in which resonances are unresolved with presently available resolution for medium weight nuclei above an energy of about 0·5 MeV. The results shown in Fig. 3–6 reveal a prominent resonance at about 30 kilovolts, but at higher energies a resonance structure so complex that at several hundred kilovolts the resonances are almost completely merged even with the best available resolution. Above 1 MeV sharp resonances have disappeared, and are replaced by a gentle wavelike behaviour of the average cross section with energy. This slow variation is related closely to the predictions of the cloudy crystal ball model of the nucleus, which we shall discuss in the next section. The good agreement of the results from Wisconsin and Los Alamos where they join at 3 MeV is noteworthy, indicating again the high attainable accuracy in total cross-section measurements.

For heavier elements in general no resonances are seen in the fast

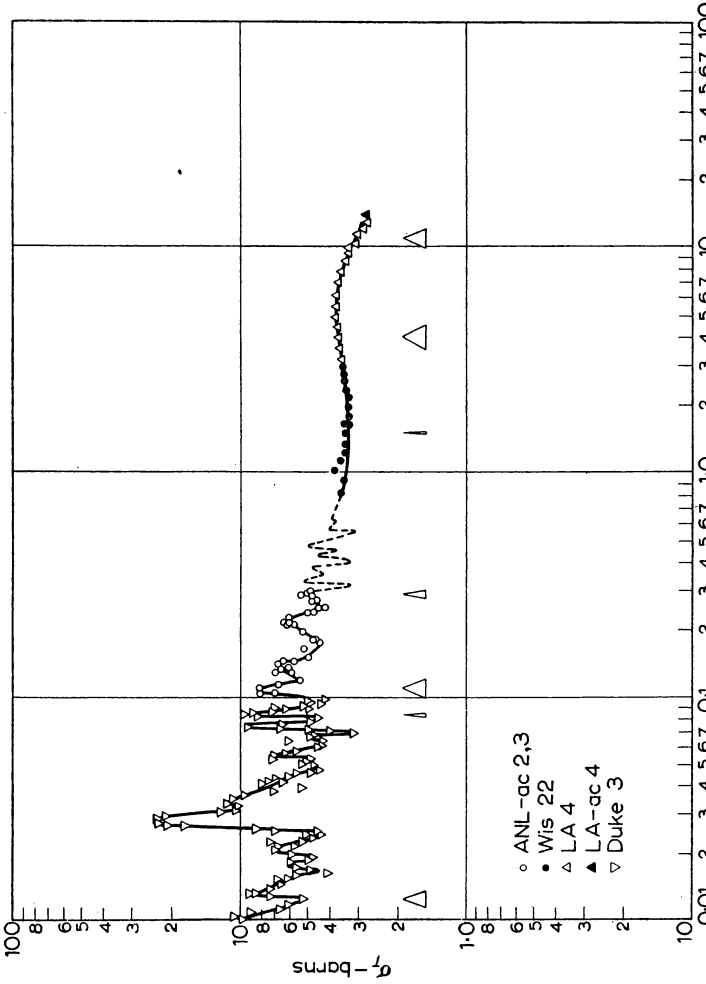

FIG. 3–6. The total cross section of cobalt in the MeV region; presently available resolution is not sufficient to resolve levels above several hundred kilovolts.

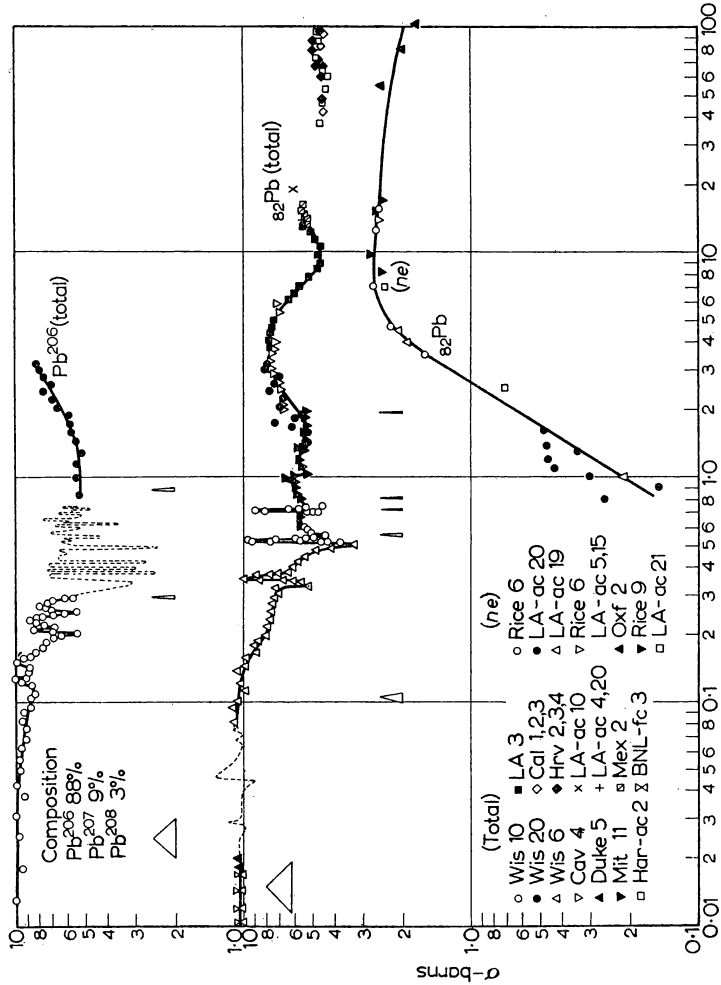

FIG. 3–7. The cross sections of lead in the MeV region; levels are observed at several hundred kilovolts in contrast to other heavy elements because of the closed shells of this nucleus.

neutron region and the smooth average cross sections that are measured are typified by curves we have already considered, namely those for mercury and gold, Figs. 1–8 and 1–9. Exceptions to the general trend for heavy elements are furnished by lead and bismuth, which, because of a peculiar stability related to closed shells of nucleons ("magic numbers"), in some ways resemble light elements. Thus lead, Fig. 3–7, shows individual resonances at several hundred kilovolts, but above one MeV even this "light element" exhibits only an average, merged cross section even with the best resolution. Further examination of the many curves in BNL 325 for fast cross sections demonstrates how many more results are available than for partial cross sections, and the high accuracy of total cross sections in the region of fast neutrons. We shall now turn to a discussion of the way in which these carefully measured cross sections give convincing support for the concept of nuclear transparency, at first so extremely difficult to reconcile with existing theory, but which now, primarily because of the cross-section results, seems to be well founded.

TOTAL CROSS SECTIONS AND THE CLOUDY CRYSTAL BALL

We have already seen that one simple consequence of the black nucleus model is that the total cross section, averaged over resonances, should decrease monotonically with increasing neutron energy, Eq. (2–20). Doubt was first cast on this result of the black nucleus, which had seemed so logical before, by the fact that total neutron cross sections did not decrease monotonically but had a slow wave-like variation with energy. This behaviour immediately brings to mind an optical analogy and the likelihood of an optical phenomena is supported by a simple consideration of the orders of magnitude involved.

The wavelength of the neutron inside the potential well representing the nucleus is about 10^{-13} cm, and as this is of the order of magnitude of the size of the nucleus itself, it would be expected that diffraction effects would be appreciable, from the standpoint of dimensions alone. Reasonable as this consideration is concerning orders of magnitude, diffraction is nevertheless a bit difficult to believe, especially in the light of the previous success of the black nucleus, for the diffraction effects observed necessitate a transparent diffracting particle. It would be necessary for the neutron, after entering the nucleus, to move freely in a potential well without loss of identity, for it is only in this way that the neutron wave can be reinforced, and the cross section augmented, when its wavelength bears a simple relationship to the size of the nucleus. An opaque object of course displays diffraction effects, but only if it is at least partially transparent

can it produce a non-monotonic variation of cross section with energy.

Once one is willing to accept the assumption that the neutron can move freely about in the nucleus without amalgamation and, with a high probability, re-emerge, it is a straightforward task to compute the variation of total cross section with energy. The simplest calculations, assuming the nucleus to be a completely transparent sphere with no absorption, give a total cross section that has the wavelike characteristics observed experimentally, with a "wavelength" about right but an amplitude much too large. In other words, a completely transparent sphere, which is the opposite extreme to the black nucleus, gives exaggerated diffraction effects, and the truth must be represented by some intermediate position.

A nuclear model that involves characteristics of a transparent sphere as well as the black nucleus is the so-called *cloudy crystal ball* model developed by Weisskopf and his collaborators. We have already examined some of the simple properties of this model, especially the average value of the cross section for the formation of the compound nucleus at low energy. One of the basic principles of the theory of the cloudy crystal ball is that this simple nuclear model correctly gives the cross section averaged over the actual resonances that are present in a real nucleus. It can be shown that actual resonances, of the form to be described in the next chapter, when averaged over an extended energy range give a cross section that is the same as would result from the very simple model of a transparent sphere, containing a slight degree of cloudiness or absorption, with no mechanism leading to sharp resonances. The fact that the cloudiness is rather slight means that a neutron moves on the average a distance much greater than the size of the nucleus before it is absorbed; after absorption, however, the nucleus is then in a situation very similar to that of the compound nucleus model, living a very long time before its energy of excitation is lost in some process or other.

If cross sections were measured in all their wealth of resonance detail, utilizing resolving powers not as yet achieved, analysis of the cross-section curves measured with such high resolution would be rather simple, for actually the cross-section curve is made up only of the actual sharp resonances plus the cross section between resonances, which is usually rather constant, called the *potential scattering*. Theoretical prediction of all the details of sharp resonances, while possible in the remote future perhaps, is not at all a feasible procedure at present. Even if one considers only the cross sections averaged over resonances in the theoretical treatment, great care is necessary to classify correctly the various components of the slowly varying

average cross section. The difficulty in the theoretical computation of the average cross section in terms of the cloudy crystal ball model comes because it is rather difficult to specify the phenomenological difference between the potential scattering and that part of a resonance that is scattering, as contrasted to the part of the resonance that is absorption. With high resolution the scattering associated with a resonance is identified by its shape but, averaged over energy, this clue is of no use.

For *elastic resonance scattering* the neutron emerges from the nucleus with exactly the same energy as that with which it entered, hence from an energy measurement it would be impossible to distinguish the elastic resonance scattering from the potential scattering. However, from the standpoint of actual behaviour within the nucleus there is a great difference between potential scattering, in which the neutron is scattered by the nuclear potential well, leaving immediately, and the resonance scattering, in which the neutron amalgamates with the nucleus to form a long-lived compound nucleus, and finally *some* neutron emerges with the same energy as the incident neutron. Averaged over energy, thus giving a smooth cross-section curve, Fig. 3–8, it is extremely difficult to distinguish the two types of

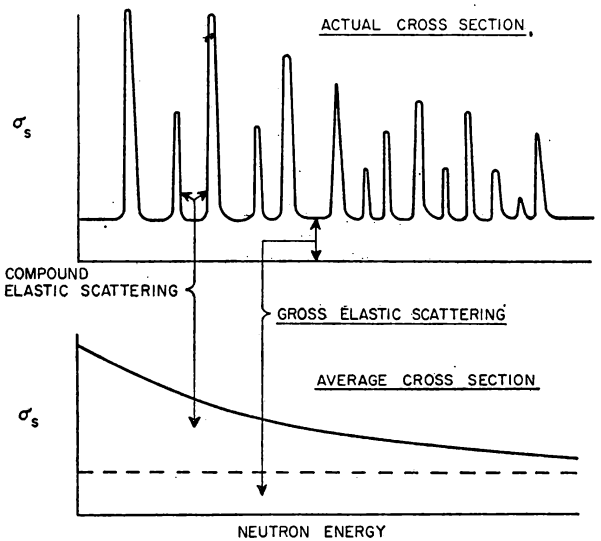

FIG. 3–8. The division of elastic scattering into resonance scattering, in which the compound nucleus is formed, and potential scattering, which is scattering from a potential well. For the average cross section the two types cannot be distinguished experimentally; theoretically, however, they are considered as "compound elastic scattering" and "gross elastic scattering".

scattering experimentally but it is essential to do so in the theoretical computations, where they are specified as *gross elastic scattering* and *compound elastic scattering.*

In fixing the few parameters available in the theory in order to obtain the best agreement with observations, one of the principal adjustments is that for the amount of "cloudiness" of the crystal, given by the constant ζ in Eq. (2–27), which fixes the imaginary component of the nuclear potential well.

We have already considered, Eq. (2–30), how ζ determines the probability for "absorption", that is, *compound nucleus formation*, as the neutron moves through the nucleus. For the usual constants of the model, a ζ of 0·03 and a well depth of 42 MeV, the mean free path is 24×10^{-13} cm, much larger than the size of a nucleus. The radius of course enters into the calculations but other types of work, such as the scattering of protons, fix the nuclear radius rather well, as given by Eq. (2–1) and there is actually little chance for adjustment of this parameter in the cloudy crystal model. The *well depth*, V_0, and ζ can be separately adjusted somewhat in obtaining a fit to the experimental data, but the position on the atomic mass scale of the peaks and valleys of the cross-section curves, together with the amplitude of the oscillations, fix these constants rather well.

In most of the calculations that have been carried out until recently with the cloudy crystal ball, the potential well was that given by Eq. (2–27), which is a simple rectangular well with a sharp nuclear surface. Comparison of the computed results with experiment, however, showed discrepancies that could not be removed by simple adjustments of the parameters. As a result, it was found necessary to take into account the fact that the nucleus does not have a sharp, but a *diffuse surface*, the nuclear density dropping from its central value to zero in about 10^{-13} cm. As the computations of average cross sections for the diffuse surface are much more involved than for the rectangular well, it was not until the summer of 1956 that the results, obtained by Feshbach, Porter and Weisskopf, reference 8, became available.

Because of the lengthy nature of the computations it is essentially impossible to investigate wide ranges in value of the various parameters. Fortunately, however, some of the parameters are fixed reasonably well by certain items of experimental data independently of other parameters. As a result, the remaining parameters could be limited to a narrow range without the complete calculations being carried out for a great range of parameters. The parameters actually settled on as the most likely set for the final calculations were as follows:

$$R = 1{\cdot}35\, A^{\frac{1}{3}} \times 10^{-13} \text{ cm}, \tag{3-1}$$

$$V = V_0(1 + i\zeta)\,\frac{1}{2}\left(1 - \tanh\frac{r - R}{d}\right), \tag{3-2}$$

$$V_0 = -42 \text{ MeV},$$

$$\zeta = 0{\cdot}08,$$

$$d = 1{\cdot}16 \times 10^{-13} \text{ cm}.$$

The potential of Eq. (3–2), with the constants shown, is sketched in Fig. 3–9, where it is clear that R is the distance to the half-way point of the potential. The well depth is about the same as was used for the rectangular well but, in order to counteract the effect of rounding the edge, which increases the penetrability and thus the diffraction effects, the absorption, hence ζ, had to be increased greatly.

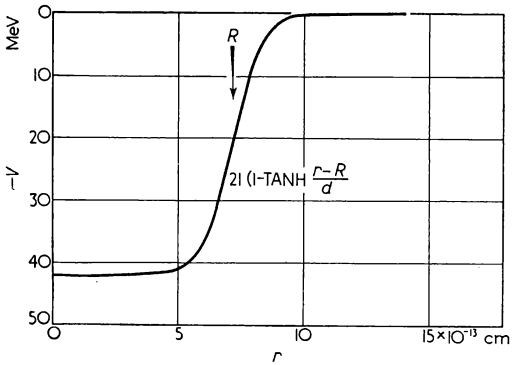

FIG. 3–9. The form of the potential well used in computations for the cloudy crystal ball model; the real component of the well is shown and in addition there is an 8 per cent imaginary component of the same shape.

Results of the calculation for the total cross section, from reference 8, are shown in Fig. 3–10, while the experimental results, given as smooth curves with no individual points, also from reference 8, are shown in Fig. 3–11. The agreement between experiment and theory is really quite striking and seems to prove beyond a doubt that the transparency of the nucleus is an established fact. Contributions of the various angular momenta to the total cross section are clearly seen, the S-contributions being distinguished by the monotonic rise of the cross section at very low energy, whereas the P- and D-contributions have peaks at particular values of the neutron energy.

The one particular class of experimental data considered here, the total cross section, fits rather well with the predictions of the cloudy crystal ball, especially in light of the fact that very few parameters are

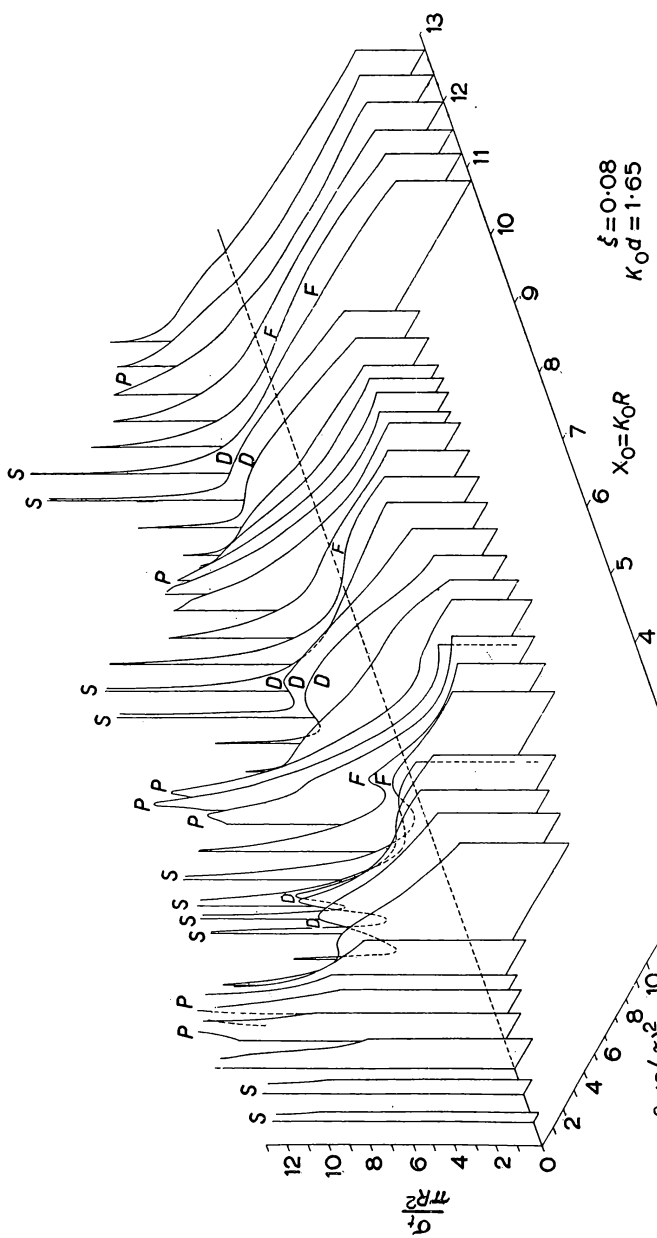

FIG. 3–10. The theoretical total cross sections as functions of energy and atomic weight as calculated from the potential well shown in Fig. 3–9.

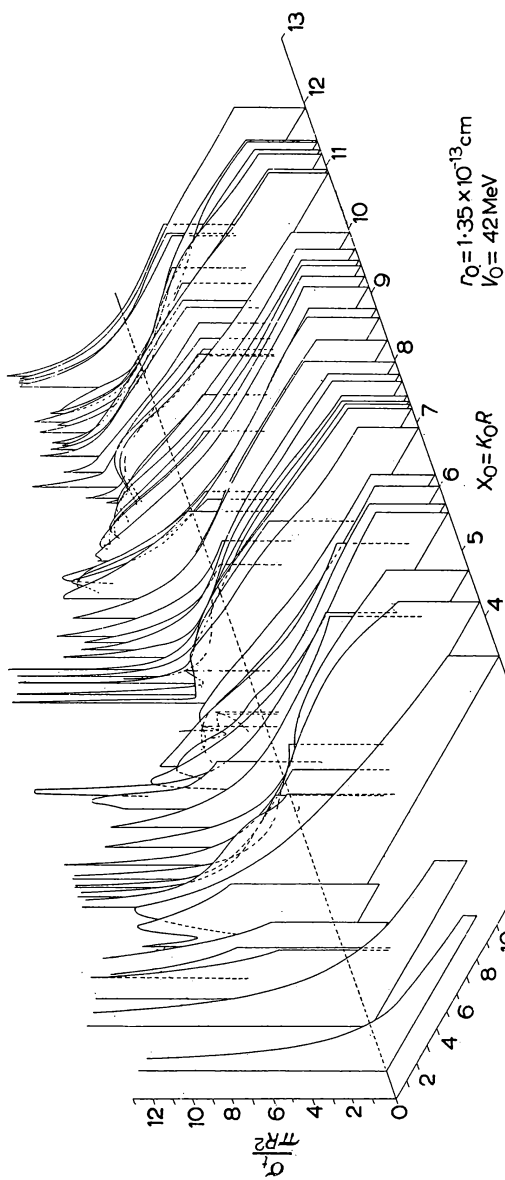

FIG. 3–11. The experimental total cross sections plotted in the same manner as Fig. 3–10 for comparison with the theoretical predictions.

available for producing the fit. Other types of information, such as angular distributions and the Γ_n^0/D ratio, which we shall consider later, do not fit the computations nearly as well. It is hardly likely that significant improvement in the fit for these data can be made by simple adjustment of the existing parameters of the model. It may very well be that the crude nature of the assumed model limits its agreement essentially to that already attained. However, the fact that the model does not fit exactly does not limit its tremendous usefulness in correlating and predicting cross sections. Rather than criticizing the model for its crude nature, we should point out that it is indeed fortunate that the simple model gives such a good prediction of the way in which actual cross sections vary with energy and from element to element.

One obvious refinement of the model has to do with the energy variation of the absorption parameter ζ. The value of 0·08 fits very well for low neutron energies but it is certain that as the neutron energy gets higher ζ increases, becoming particularly high around 15 to 20 MeV. The high value results because the measured compound nucleus formation cross section, primarily nonelastic scattering, becomes equal to the actual geometrical size of the nucleus at about 15 MeV. At much higher energies ζ decreases again, primarily because the elementary interaction of the neutron with the individual nuclear particles becomes so small. The decrease in ζ as the neutron energy is lowered from about 15 MeV to the energies of Fig. 3-11 at first seemed very surprising, but is almost certainly a result of the Pauli *exclusion principle*. The application of the principle to energy states in nuclei implies that, for a low energy neutron moving through the nucleus, most of the energy states into which it can fall are already occupied. As a result its mean free path is extremely great in nuclear matter, and ζ is low.

At higher energies, above 100 MeV, a rather crude *optical model* had been used for a number of years before the advent of the cloudy crystal ball at low energy. The optical model at higher energy was admittedly approximate but did have the essential principles of the cloudy crystal ball, that is, a potential well containing an imaginary component. The optical model at high energy, however, did not have nearly the transparency of the model at low energy, for the mean free path of a particle in the nucleus, computed from the known *n-p* and *p-p* cross sections, was of the order of 4×10^{-13} cm. This value of the mean free path was much smaller than that found necessary in the cloudy crystal ball, and certainly did not seem out of line with the then-prevalent black nucleus at low energy because the elementary *n-p* and *p-p* interactions were known to be quite small at high, but large at low, energy. It is for this reason that even though the optical

model was used for some years at high energy it was not thought to apply at low energy where the known large *n-p* and *p-p* cross sections, applied in a straightforward way, indicated a completely black nucleus.

NONELASTIC CROSS SECTIONS

Some of the cross sections that we have defined and discussed were necessitated by the nature of the theoretical models, an example being the compound nucleus formation cross section. However, we are now to consider the *nonelastic cross section*, which term arises primarily because it is a quantity particularly amenable to experimental study. It is, by definition, the total cross section minus the elastic scattering, that is, the inelastic scattering plus all other reactions. In many cases it is the same as the cross section for inelastic scattering but should be carefully distinguished from the latter because of the experimental methods involved and the possibility that in some cases they may be markedly different.

Several experimental methods have been developed in which the cross section is measured for all but elastic scattering processes, with no distinction between neutrons that lose most of their energy by inelastic scattering and those that are absorbed by other processes, such as (n,p), (n,α), (n,γ), $(n,2n)$, (n,F), etc. Of these methods, which give the nonelastic cross section directly, perhaps the most-used is the *sphere technique*, illustrated in Fig. 3–12. The principle of the method consists of measurement of the counting rate of a threshold detector, D, with and without a thin spherical shell of the material in question surrounding the source, S. If only elastic collisions take place in the shell the counting rate will not be changed by the shell. If the detector has a sufficiently sharp threshold near the primary neutron energy so that inelastically scattered neutrons will not be detected, and if the neutron source is isotropic, then the measured transmission gives the nonelastic cross section only. The elastic scattering cancels out from an isotropic source since the neutrons scattered into the detector will compensate those scattered out of the direct path.

A small correction must be made in the case of light nuclei, for which the neutron loses some energy even in an elastic collision. It is also necessary to correct for multiple scattering but this correction can be computed accurately if the shell is kept so thin that the transmission is above 0·70. When the nonelastic cross section is small compared to the total cross section, the transmission of the sphere is nearly unity and it is difficult to obtain an accurate value for the nonelastic cross section. By making measurements at a given incident

neutron energy with several different *threshold detectors* an approximate measure of the spectrum of the inelastically scattered neutrons is obtained.

Since neutron sources are not isotropic and, in addition, the neutron energy often varies with angle, an *inverted sphere technique* has been developed to overcome these difficulties. In this variation, the roles of the source and the detector are interchanged so that the sphere surrounds the detector. From Fig. 3–12 it is obvious that for each

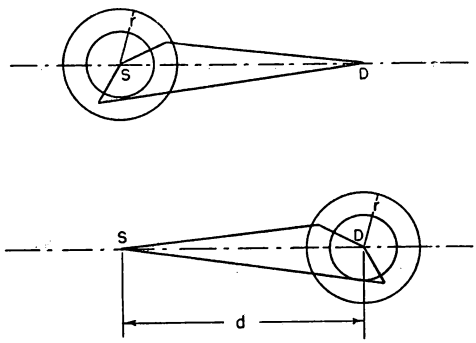

FIG. 3–12. The geometrical arrangement used for nonelastic cross-section measurements by means of the sphere technique, upper figure, and the inverted sphere technique, in which the sphere surrounds the detector *D*.

possible neutron path with the sphere around the source there is an equivalent one when the sphere is around the detector. The sphere radius must be small compared to the distance, d, between source and detector ($d > 3r$) to minimize energy and intensity changes across the sphere from non-isotropic sources. It is also necessary that the detector have the same efficiency regardless of the direction of neutrons relative to the source-detector axis.

Several types of neutron detectors have been used for these sphere experiments. There are *threshold detectors*, such as fission counters, using those nuclides that have thresholds in their fast fission cross sections, as well as hydrogen or helium gas proportional counters. Fission counters have very sharp thresholds but have inadequate sensitivities for accurate measurements with the presently available neutron fluxes. Also, the threshold for a particular fissionable nuclide is fixed, which is generally undesirable if one wishes to make measurements as a function of incident neutron energy. The *fission thresholds* of the various available nuclides extend only to a little over 1 MeV, constituting a severe limit to the range of measurement. Other threshold reactions, such as the $Cu^{63}(n,2n)Cu^{62}$ reaction, which has a threshold at 11·5 MeV, have been used but their

efficiencies are quite low. Gas-filled hydrogen or helium recoil proportional counters have recently been developed, which have sharp thresholds that can be readily changed by varying the bias, and in addition have reasonably high efficiency.

With all corrections carefully made, one can determine the nonelastic cross section, if large, to an accuracy of about five per cent. To illustrate the results obtained, the total and nonelastic cross sections for bismuth are given in Fig. 3–13. For low energy neutrons the nonelastic scattering is very small; below 0·9 MeV the inelastic scattering is zero, the capture cross section at 0·9 MeV is only 0·1 b, and other cross sections are negligible. For neutrons above 0·9 MeV the inelastic scattering cross section rises, and for energies above 6 MeV the nonelastic cross section is about half the total cross section, which is shown by the dashed line in Fig. 3–13. At the higher energies the nonelastic cross section also includes $(n,2n)$, $(n,3n)$, etc. reactions. A brief survey of the cross section curves in BNL 325 shows that, relative to the total cross sections measured, there are few results for nonelastic cross sections. The reason for this scarcity of nonelastic results is of course their much greater difficulty relative to the simplicity and rapidity of total cross-section measurements. In addition to bismuth, Fig. 3–13, another typical result is that for gold, already shown as Fig. 1–9. In this case the nonelastic cross section is almost completely inelastic scattering, for the radiative capture cross section, shown in the same figure, is extremely small and the probability of (n,p) and (n,α) reactions for such a heavy element is extremely low because of the small penetrability of the nuclear potential barrier.

It is obvious that the cross section for production of the 250 keV gamma ray by inelastic scattering shown in Fig. 1–9 is higher at 1·8 MeV neutron energy than the nonelastic cross section, which implies some error in measurement for the production of a single gamma ray can hardly be larger than the nonelastic cross section which includes *all* reactions. Another example is furnished by the cross section of bismuth in Fig. 3–13 in which the nonelastic scattering is again primarily inelastic scattering. Here in contrast to the gold results, however, the nonelastic cross section is definitely larger than the specific inelastic scattering that results in production of particular gamma rays. The main trend noticed in gold, however, seems to be present in bismuth also, for the two gamma rays shown can barely be encompassed by the nonelastic cross section shown. Thus the nonelastic cross section at 2·5 MeV is one barn whereas the production cross section for the two gamma rays shown is slightly over one barn.

For the few nonelastic cross sections that are available it is noticeable that they level off after an initial rise and that the value

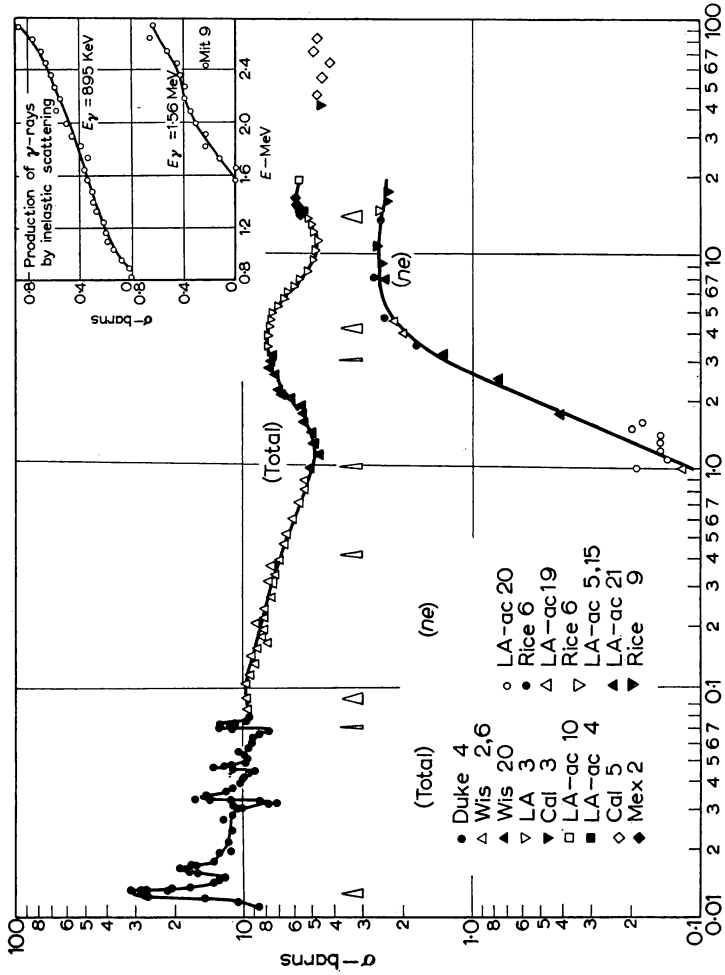

FIG. 3–13. The cross sections of bismuth in the MeV region, showing that the nonelastic cross section is approximately half the total cross section. The inelastic scattering is about equal to the nonelastic scattering, indicating that the nonelastic scattering is principally inelastic scattering, other reactions being negligible.

then reached is roughly of the order of half the total cross section. This behaviour is about what is to be expected from a strongly absorbing nucleus, because at high energy, where the wavelength is smaller than the size of the nucleus, scattering is partly diffraction around the opaque nucleus and in magnitude is equal to the absorption of the neutrons that hit the nucleus directly. This result, which follows from any simple optical model of the nucleus, would lead us to expect an elastic scattering cross section, or *diffraction scattering*, approximately πR^2, together with an equal cross section for all processes in which the neutron is absorbed, that is, the nonelastic cross section. A more exact view is represented by the calculations of the cloudy crystal ball, but nevertheless the simple prediction just mentioned is reasonably well borne out by the curves in BNL 325, which show that the measured nonelastic cross section is of the order of half the total cross section, although the latter shows the distinct wavelike behaviour characteristic of the cloudy crystal ball.

INELASTIC SCATTERING

A very important type of neutron interaction is that in which a neutron is emitted from the compound nucleus with less energy than the incident neutron, the decrease in energy representing the excitation of the final nucleus, an energy that is then lost as gamma radiation. This type of scattering is of course impossible for very low energy neutrons because the neutron must have sufficient energy so that it can leave the nucleus excited to at least its first energy level. This energy level, being near ground, will have an excitation energy not of a few volts but usually of the order of 100 kilovolts, hence the threshold for inelastic scattering will be the same. Whereas the energy levels represented by capture or elastic scattering of slow neutrons are at an excitation of about 5 to 7 MeV, where the level spacing can be as small as several eV, for inelastic scattering the levels excited in the residual nucleus, being just above ground, have a much greater spacing, about 100 kilovolts.

The inelastic scattering is important not only in nuclear theory but for many practical applications as well. The close relationship to nuclear theory arises partly because the study of inelastic scattering gives properties of the levels near ground, but also because it has a direct bearing on the manner in which the excitation energy is present in a nucleus. For high energy neutrons, say of 14 MeV, entering a nucleus, the energy distribution of the emergent inelastically scattered neutrons gives information on the distribution of energy among the nuclear particles in the compound nucleus.

Thus the study of inelastic scattering provides a test for the *statistical assumption*, that a thermodynamic equilibrium is established

in the "hot" nucleus. It is possible to check this theory of a statistical nuclear excitation, as it leads to a distribution of inelastically scattered neutrons that is predicted from a thermodynamical view of the nucleus possessing a true temperature. As far as applications are concerned, inelastic scattering is extremely important because of its effect in determining the energy distribution of the neutrons within reactors, as well as playing a vital role in the processes by which neutrons are stopped in shields. In the latter application, the inelastic scattering can be very important in reducing neutrons to energies at which they are more easily stopped by capture; in the process gamma rays are produced, of course, and these must also be taken into account in the shielding calculation.

As mentioned earlier, direct study of inelastically scattered neutrons is very difficult. A few measurements have been made on the energy distribution of scattered neutrons using the proton-recoil *photographic plate technique*. In this technique, large amounts of shielding

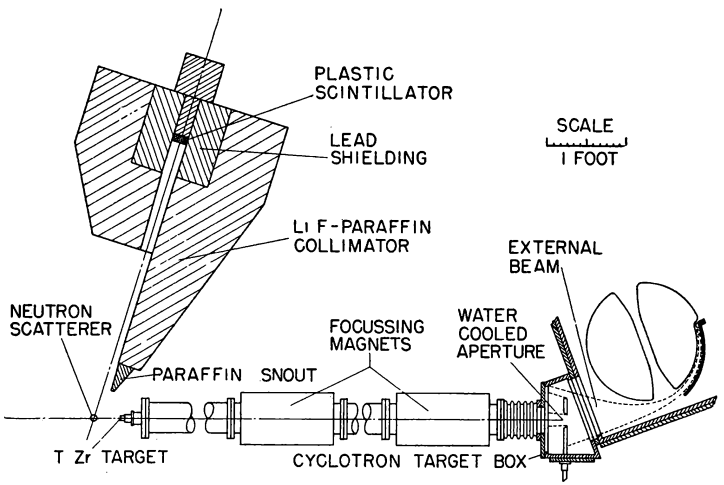

FIG. 3–14. Diagram of the equipment used at Brookhaven for the time-of-flight technique for measuring inelastic scattering of neutrons.

must be used to reduce background in the plates. Since the exposure times are long and the scanning of the plates very tedious, the method is severely limited.

Recently successful measurements have been made on the energy distribution of inelastically scattered neutrons by the *time-of-flight technique*, as illustrated in Fig. 3–14. The efficiency is quite high and the entire energy spectrum of scattered neutrons is recorded

simultaneously on a multichannel time analyser. This technique is being pursued at several laboratories and has already yielded some valuable results. It seems possible that the time-of-flight method may render the other inelastic scattering techniques obsolete within the next few years because of its directness of interpretation and possibility of rapid, accurate data collection. Some recent results obtained at Brookhaven by the time of flight method for iron, shown in Fig. 3–15, illustrate the clarity and directness of interpretation

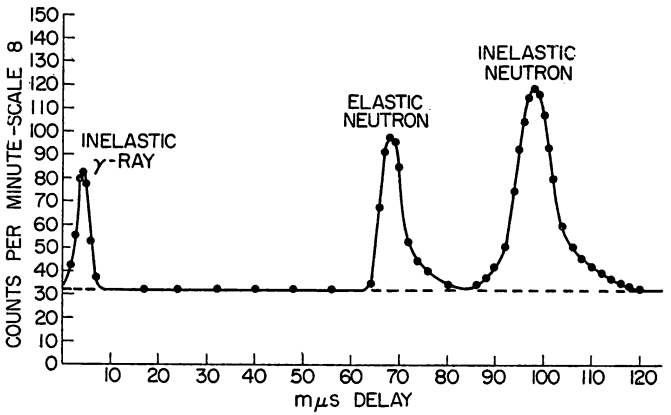

FIG. 3–15. The results obtained for scattering of 1·66 MeV neutrons from iron using the time-of-flight technique. The counting rate as a function of delay time shows first the arrival of the inelastic gamma rays, of 0·845 MeV energy, then the elastically scattered neutrons and finally a single group of inelastically scattered neutrons.

characteristic of the method. Further details of this, as well as the other techniques for inelastic and nonelastic cross sections are given in reference 3.

Whenever inelastic scattering takes place the bombarded nucleus is left in an excited state and will return to its ground state with emission of one or more gamma rays. Thus observation of the gamma rays emitted from inelastic scattering yields information on inelastic scattering cross sections. In a few cases the gamma ray is not emitted instantaneously but decays at a measurable time later, i.e. from one second to several hours. The special techniques that can be used for these *metastable states* will be described later.

The technique of observing the *prompt gamma rays* has been feasible only because of the recent development of sensitive, high resolution, scintillation counters. The experimental arrangement is similar to that illustrated in Fig. 1–3, with the neutron detector

replaced by a NaI (Tl activated) gamma-ray detector. The yield of a particular gamma ray from inelastic scattering is measured at a given angle as a function of neutron energy. Correction must be made to allow for the multiple scattering of the neutrons in the sample and also for the self-absorption of the gamma ray in getting out of the sample. Absolute cross sections are obtained by measuring the efficiency of the detector and geometry, using a calibrated source of gamma rays, and from a determination of the absolute neutron flux. Because of the difficulty of these absolute calibrations, present results are good only to about 15 per cent.

The cross section for the production of the 900 keV gamma ray in bismuth is shown in Fig. 3–13. Since the first excited level in bismuth is at 900 keV, no inelastic scattering is possible until neutrons have energies greater than 900 keV. From 900 keV to 1·56 MeV (the second level) the inelastic scattering cross section consists only of this gamma-ray production. As the 1·56 MeV level decays independently of the 900 keV level, the entire inelastic scattering cross section, above 1·56 MeV and up to the next excited level, is simply the sum of the two cross sections for the gammas. If, as is often the case, the second excited level all decays to the first level, the yield of the gamma ray from the first level is a measure of the inelastic scattering. As already observed, the gamma-ray-production cross section is in rough agreement with the nonelastic cross section, hence the latter seems certain to contain no appreciable contributions other than inelastic scattering of the gamma rays cited.

In a few cases the excited state is metastable, for example the 7·5 sec state at 410 keV in Au^{197m}. Here an activation method is used to advantage. The sample is irradiated with monoenergetic neutrons for several half lives and then the induced activity is counted. An advantage here is that the background is considerably lower with the neutron source off than in the prompt gamma measurements. The cross section is generally lower than the total inelastic scattering since only transitions to the isomeric state are observed. In some cases, for example Au^{197m}, about half the nonelastic cross section for neutrons from 1 to 5 MeV arises from transitions to the 410 keV metastable level. Absolute cross sections are again obtained from a measurement of the absolute neutron flux, and the absolute activity produced, using the simple activation formula, Eq. (1–17).

REACTION CROSS SECTIONS

Reaction cross sections are measured by a variety of techniques; for fission the fission fragments are detected, for (n,p), (n,α) reactions in light nuclei the protons or alphas are detected, many (n,p), (n,α), $(n,2n)$, and (n,γ) reactions can be measured in terms of the activity

produced, and a few $(n,2n)$ cross sections can be measured by a modified sphere technique. Although the variation of the reaction cross section with energy can often be measured accurately, an absolute measurement of the cross section is usually very difficult.

For most of the reaction cross sections, as we have seen for inelastic scattering, it is necessary to make a neutron flux measurement in order to determine the absolute cross section. There are several methods for absolute flux measurement but only the two most useful and accurate will be mentioned here. The first is the *associated particle method*, in which the charged particles from the source, having a one-to-one correspondence with the produced neutrons, are counted. As an example, for the $T(d,n)He^4$ source, the number of neutrons emitted in a small solid angle can be determined from the number of He^4 particles emitted in the corresponding solid angle. Absolute flux determinations have been made by this method to about five per cent accuracy. Secondly, we have the *recoil particle method*, in which the proton recoils produced by the neutrons from a thin radiator are counted in an ionization chamber. Corrections must be made for these small recoil pulses lost in background noise and for several other small effects. The best results of the recoil proton technique have an accuracy of three per cent. Detailed methods for measurement of fast neutron flux are described in reference 2.

Relative fission cross-section measurements have been made in two ways, first by measuring fission counts in an ionization chamber relative to a *long counter* flux monitor and second by measuring the ratio of the fission cross section to a standard fissionable nuclide. A long counter is an arrangement of a BF_3 counter located in a large paraffin block such that it has almost a constant efficiency for neutrons from a few hundred keV to 8 MeV. For measurements utilizing the long counter flux monitor, the thickness of the fissionable foil need not be known since only a relative cross section measurement can be made. When measuring the ratio of a fission cross section to a standard material, the fissionable foils are mounted back-to-back in a parallel-plate ionization chamber. In this arrangement the actual ratio, not only the energy variation, of the two fission cross sections can be measured if the thickness of the two foils are known, as they are in the same neutron flux. After correcting for small effects, such as non-uniformities of the foils, inelastic scattering, and room background, the ratio of two fission cross sections can be determined to an accuracy of two per cent. The measurements relative to the long counter, which give only the energy variation of the fission cross section, can be performed with the same accuracy.

The absolute fission cross section of U^{235} has been measured to an accuracy of four per cent at 1·25 MeV, using the recoil proton method to determine the neutron flux. This result is then used to obtain the U^{235} fission cross section from 100 keV to 8 MeV, by means of the energy variation of the fission cross section measured with the long counter. This U^{235} cross section then serves as the standard for measurements of other nuclides by the ratio method.

Reactions producing charged particles, protons or alphas, usually from light nuclei, may be observed in the same manner described for fission. However, the low energy of the particles makes their observation more difficult. The targets to be investigated may be used in the form of thin foils in an ionization chamber or, if possible, as gaseous compounds. When thin foils on heavy backings are used the foil is placed perpendicular to the neutron beam and the detector is generally biased to count only the light particle, i.e. the proton or alpha, and not the recoil nucleus. Since nitrogen and neon have appreciable disintegration cross sections they cannot be used as the gas in the chamber. In addition, disintegrations produced in the counter walls or recoil protons from water or organic materials absorbed in the walls can give prohibitive background. Most of the difficulties encountered with thin foils can be avoided if the element to be investigated is a gas or forms a gaseous compound. All reactions of the same reaction energy will release the same amount of energy in the gas. For both the foils and gas samples the absolute neutron flux must be measured, as is true for fission and inelastic scattering, in order to obtain absolute reaction cross sections.

Frequently a radioactive nucleus is formed as a product of a nuclear reaction. Observation of the activity, if it has a convenient half-life, may be used for the determination of the reaction cross section. In addition to (n,p) and (n,α) reactions, (n,γ) and $n,2n)$ cross sections can also be measured by this *activation method.* In order to obtain absolute cross sections the absolute beta-activity of the radioactive nucleus as well as the absolute neutron flux must be determined. For nuclei involving *K*-capture, beta-counting can still be used if a known fraction of the disintegrations involve beta-particle emission. With considerable care absolute activity measurements can be made to an accuracy of six per cent. However, when errors arising from the neutron flux and the source thickness are included, even the best activation measurements still have an error of ten per cent. Relative measurements as a function of energy, since they do not involve absolute beta-counting, can be as accurate as a few per cent.

The difficulties involved in the measurement of reaction cross sections are reflected in the small number of results that are to be found in BNL 325. The light elements, in which exothermic (n,p)

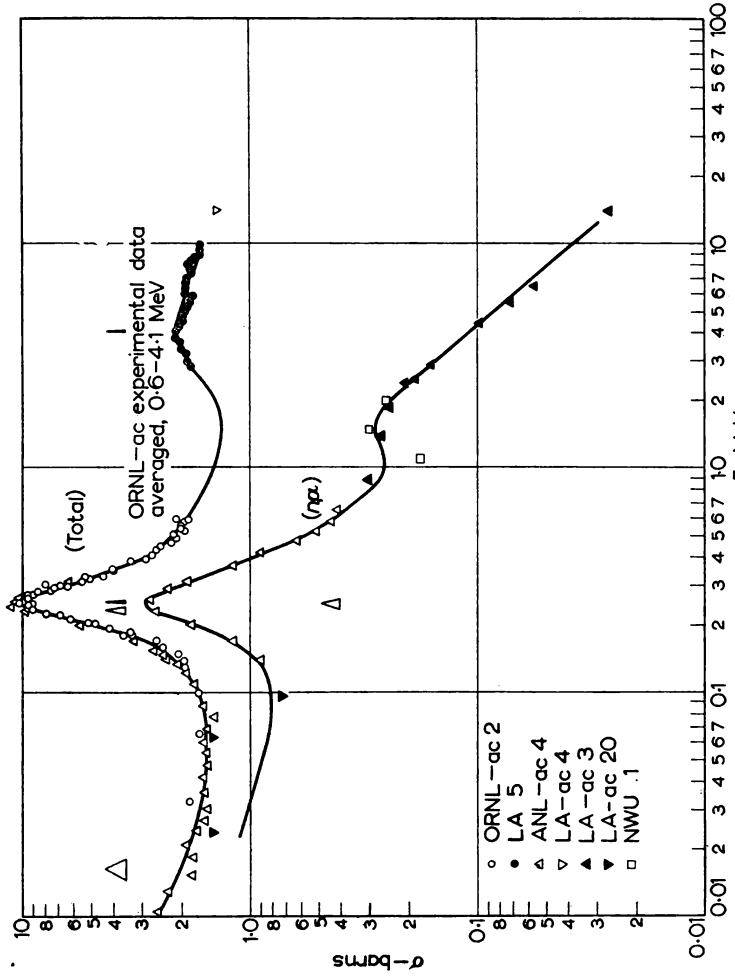

FIG. 3-16. The (n,α) reaction cross section of Li^6, measured with a pulse ionization chamber as detector, compared with the total cross section.

and (n,α) reactions are sometimes to be found, provide some of the cases where measurements are possible. An example is the (n,α) reaction in Li^6, whose cross section is shown in Fig. 3–16. The energetic alpha particle emitted in this reaction can be detected without undue difficulty in a proportional counter or ion chamber, hence the cross section can be measured more accurately than most reaction cross sections. The comparison of the (n,α) and the total cross section in Fig. 3–16 is interesting in that the resonance at 0·26 MeV appears in both, whereas the apparent small resonance in the (n,α) cross section at 1·5 MeV does not seem to be present in the more accurate total cross section, thus casting some doubt on its reality. For heavy nuclei, the (n,α) and (n,p) reactions are much less likely because of the outgoing charged particle's small penetrability of the nuclear potential barrier. As a result the cross sections are extremely small and difficult to measure. In addition, for an endothermic reaction, the energy of the outgoing particle is less, hence its detection more difficult.

There are very few measurements of the (n,γ) cross section as a function of energy; one of the best of these, however, is that for aluminium, shown in Fig. 3–17. These results were obtained by activation and represent a task of much greater magnitude than that of the total cross section shown for the same element. A comparison of the curve in Fig. 3–17 with the total cross section of aluminium, Fig. 3–18, reveals the rather surprising fact that, while there is a rough correlation between the resonances found in the capture and the total cross section, there are definite cases where a resonance appears in one cross section and not in the other. Fig. 3–17 also gives the (n,p) cross section for aluminium, which exhibits resonances superimposed on the typically rapidly rising cross section, which represents the threshold behaviour of an endothermic reaction.

With the exception of a few (n,γ) cross sections measured by activation and even fewer $(n,2n)$ reactions, also measured by activation, the region of intermediate weight nuclei have very few reported results for reaction cross sections. For very heavy nuclei, which undergo fission, the fission cross section has been measured with care, especially for the important nuclides, as U^{235}, Pu^{239}, etc.

In glancing through the curves of BNL 325 it must be remembered that some reaction cross sections have been measured that do not appear on the curves, e.g. for cases in which only a few isolated points have been measured. These additional isolated values are presented in tabular form, following the curves in BNL 325. This page of additional data shows that many reaction cross sections, for (n,p), (n,α) and $(n,2n)$ reactions, have been measured at 14 MeV. In addition a number of capture cross sections have been measured at

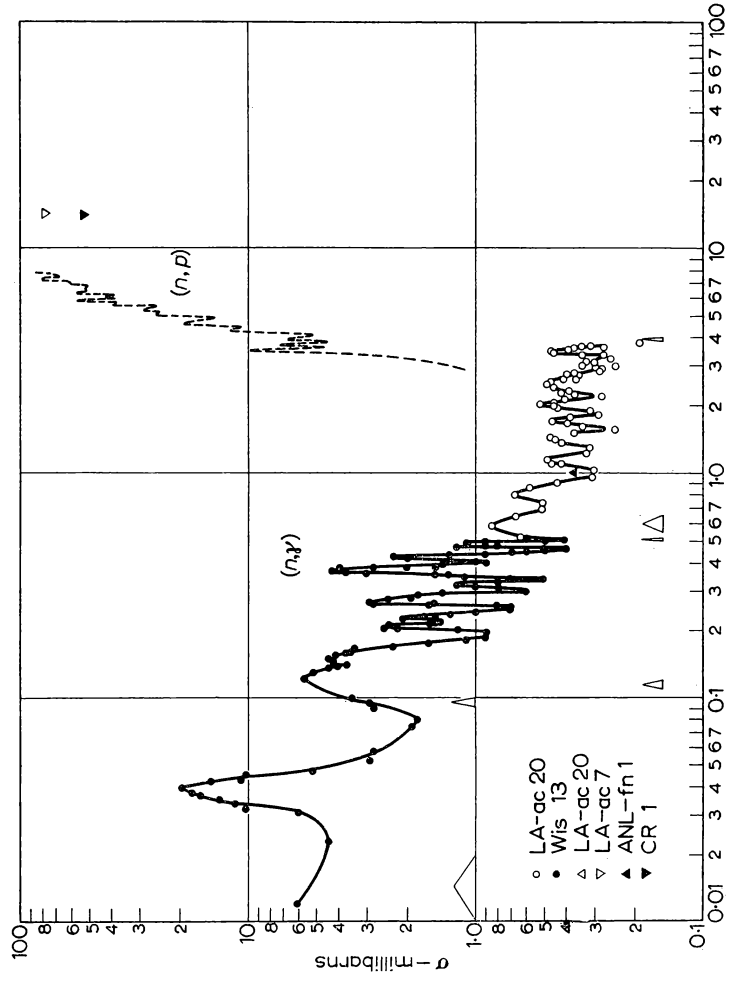

FIG. 3–17. The radiative capture cross section as a function of energy in the MeV region for aluminium. The capture cross section was here measured by activation.

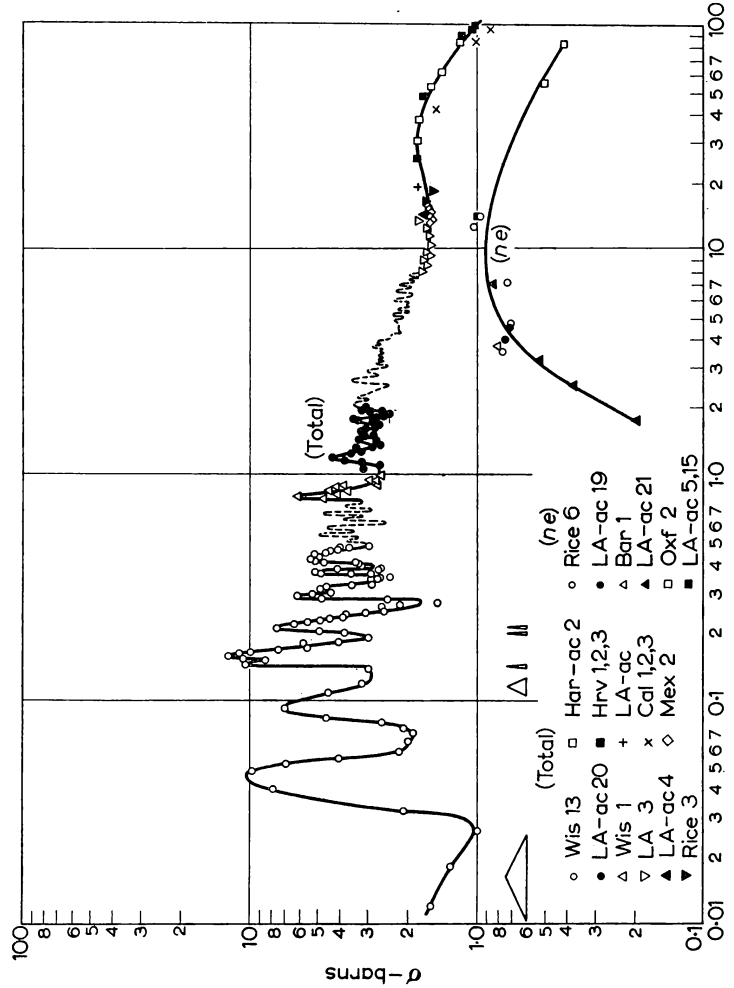

FIG. 3–18. The total cross section of aluminium in the MeV region, for comparison with the activation cross section of Fig. 3–17.

1 MeV. Actually the entire fission spectrum was used as a neutron source but, as we shall see later in this chapter, the measured cross sections can be plotted as monoenergetic values at 1 MeV.

ANGULAR DISTRIBUTIONS

The *angular distribution* of elastically scattered neutrons is of considerable interest for reactor calculations and nuclear theory. At low energies neutrons are scattered isotropically; hence there is no need to measure angular distributions until they depart from isotropy as higher angular momenta become significant, Eq. (2–1). Intermediate and heavy nuclei exhibit a strong forward peaking for high energy incident neutrons, but for light nuclei, for which the scattering is due to individual resonances, the distribution depends on the angular momentum of the particular level of the compound nucleus corresponding to the resonance.

In the experimental technique, Fig. 1–3, it is thus necessary to use good energy resolution ($\sim$ 10 keV) for light nuclei; a resolution of 100 keV is sufficient for heavy nuclei. The samples must be thin, scattering less than 30 per cent of the incident neutrons, so that multiple scattering in the sample can be corrected for with reasonable accuracy. Since the detector usually subtends less than a one per cent solid angle at the source the scattered intensity is typically very low. The basic problem is to optimize the ratio of scattered neutrons from the sample to those unwanted neutrons arriving in some way at the detector without scattering at the sample. Neutron sources usually emit neutrons in all directions, hence the detector must be well shielded from the source.

It is desirable that the detector have a step-function sensitivity near the primary neutron energy, to discriminate against lower energy background neutrons scattered by the shield, the walls of the room, or even the air. This sharp *threshold detector* will also be quite insensitive to those neutrons inelastically scattered from the sample and thus will detect only the elastically scattered neutrons. In addition to its other characteristics, the detector must also be insensitive to gamma rays so that it does not detect the gamma rays resulting from inelastic scattering. Various detectors with suitable characteristics have been used, such as hydrogen or helium recoil gas counters or hydrogen recoil scintillation counters. They are biased at a high level, about 90 per cent of the energy of the elastically scattered neutrons. Very recently the neutron time-of-flight to the detector, using a pulsed source, has been used as a means to distinguish neutron energy.

The obvious way to measure the angular distribution is simply to scatter neutrons from a small cylindrical sample and measure the

counting rate as a function of angle. Typically, the sample is about 50 cm from the source, with the detector about 5 cm in diameter and 10 cm long. Angular resolutions of about 5° are used and the distribution can be measured in this way from 15° to 150°. A suitable paraffin or polyethylene slab to shield the detector is used at each angle. The background, determined by removing the scattering sample, varies with angle but averages 40 per cent of the scattered neutrons. The absolute differential elastic scattering cross section $\sigma_n(E;\theta)$, as given by Eq. (1–7), can be computed from the angular distribution, the distance from scatterer to detector, and the counting rate of the detector when placed at the scattering sample position. This latter result gives the product of the unknown counter sensitivity and the primary neutron flux at the scatterer.

Another arrangement for measuring angular distribution, which increases the scattered neutron intensity greatly, involves a *ring geometry*, as shown in Fig. 3–19. The scatterer is in the form of a

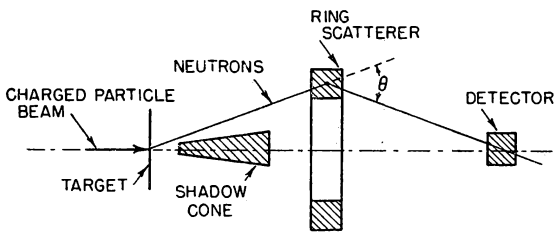

FIG. 3–19. The ring geometry method for angular distribution measurements; the shadow cone is used to shield the detector from the source and θ is varied by moving the ring or varying its radius.

ring on whose axis lie the source and detector, with a *shadow cone* to shield the detector from the source. The scattering angle, θ, may be varied either by moving the detector or by moving the rings and varying the size of the ring. Ring diameters average about 15 cm, and the average source to detector distance is about 50 cm. However, the angular range is limited in the backward direction since the detector must be moved closer to the source than the scatterer, thus making the shielding problem very difficult.

For light nuclei, for which inelastic scattering is not important and the *recoil nuclei* have appreciable energy, the angular distribution of the scattered neutrons can be determined indirectly, in terms of the angular or energy distribution of the recoil nuclei. The properties of the recoil nuclei can be determined in principle more accurately than the neutrons, because the recoil nuclei are charged. The angular distribution of the recoils from a thin foil or a gas can

be measured directly by means of a counter telescope, photographic emulsion, or a cloud chamber filled with the gas under investigation. The neutron angular distribution can also be obtained from the energy distribution of the recoiling nuclei, for the former is readily computed from this energy distribution. High energy recoils correspond to neutrons scattered in the backward direction, whereas neutrons scattered through small angles produce low energy recoils. This method is limited to gases and measurements have been made by its use for hydrogen, deuterium, helium, nitrogen, oxygen, and neon. The energy of recoil nuclei is determined from the pulse height in a proportional counter filled with the gas being investigated. Small pulses, corresponding to neutrons scattered through small angles, are difficult to detect because they may be lost in pulses produced by electrons, recoils from other heavy nuclei, or possible inelastic scattering.

A small amount of angular distribution data is found in BNL 325 but the amount of such data has increased rapidly and a new compilation has been prepared to handle angular distribution data alone. This compilation, BNL 400, is dated June 1, 1956.* Angular distributions are given in this compilation for elastically and inelastically scattered neutrons and the gamma rays associated with the latter. Results are also included for reactions in which the exit particle is a proton, deuteron, or alpha particle. An example of the way the data are presented is shown in Fig. 3–20, for the differential elastic scattering of oxygen. Only the data for incident energy distributions from 0·4 to 2·9 MeV are included, the other energies being given on a separate sheet to prevent confusion of points. An interesting set of curves is found in BNL 400 for the elastically and inelastically scattered neutrons from iron, and for the gamma rays produced in inelastic scattering, for which space does not allow reproduction here. The differences in angular distributions among the elastically scattered neutrons, a typical diffraction pattern, the slight anisotropy of the gamma ray, and the almost isotropic inelastically scattered neutrons, are very striking. These results have been obtained by use of the recent time-of-flight techniques, described in more detail in reference 3.

CROSS SECTIONS FOR FISSION NEUTRONS

Although cross sections measured with neutron sources of rather wide energy spread have been important in the past, at the present time almost all measurements are made with nearly monoenergetic

* *Neutron Cross Sections—Angular Distributions*, D. J. Hughes and R. S. Carter, available from Office of Technical Services, U. S. Department of Commerce, Washington 25, D. C. ($.50).

neutrons. In a few cases, cross sections measured with sources other than accelerators are useful enough so that they can be plotted on cross section curves, even though the sources are hardly monoenergetic. One example of this type of measurement is the use of *photoneutron sources*, which, although having about a 20 per cent spread in energy, are readily adaptable to the measurement of capture cross sections by activation because of their small size and ease of preparation. A number of the results of activation cross sections with photoneutron sources are to be found in the curves of BNL 325.

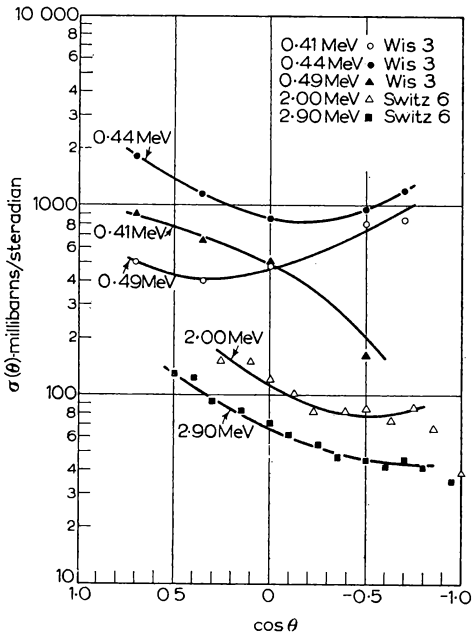

FIG. 3–20. The differential elastic scattering of oxygen for several incident neutron energies; from the compilation BNL 400.

Another type of neutron source, far from monoenergetic, can nevertheless be used to give cross sections that have significance at a particular energy. This source is the *fission spectrum* itself, which is particularly useful because fission neutrons can readily be attained in high intensity by placing a fissionable material, usually U^{235}, in a flux of thermal neutrons. In this way it is rather simple to obtain a high intensity source of unmoderated fission neutrons, very free of resonance neutrons. The total emission rate or source strength, Q, can be as high as 10^{11} neutrons per sec, as discussed in reference 6.

The thermal neutrons can be eliminated by simple interposition of a sheet of cadmium. Because the behaviour of the capture cross section as a function of energy is well known, the capture cross sections measured with unmoderated fission neutrons can be interpreted in terms of a monoenergetic value, which turns out by chance to be almost exactly 1 MeV. Measurements made in this way are to be found for a number of elements in the curves of BNL 325, and in the tabular section of reaction data following the curves.

Other types of measurements can be made with fission neutrons that are extremely useful in the sense of practical applications. Examples are threshold reaction cross sections, inelastic cross sections, etc.; in short almost all cross sections can be measured using as a source the entire fission distribution. In general, measurements made with fission neutrons have little value as far as comparison with theory is concerned simply because the results represent an average over a very wide spectrum. However, the practical utility of the results is extremely great because of the widespread use of the fission neutrons in reactors as high intensity sources for neutron reactions.

One example is the use of the fission neutrons in the pile to make high specific activity *radioisotopes* by threshold reactions. Here what is needed to guide the manufacturer of radioisotopes is the average cross section for the particular threshold reaction over the fission spectrum. These average reaction cross sections can easily be measured and the results directly applied to the manufacture of radioisotopes. The actual cross section of the reaction, of course, for the neutrons really effective, those above the threshold energy, may be far different from the average value because of the possible high threshold energy. Thus for $O^{16}(n,p)N^{16}$, for example, only those neutrons at the extreme upper end of the fission spectrum, actually over 12 MeV, are effective in making the reaction take place, and their cross section is 90 mb at 14 MeV (BNL 325). However, the cross section averaged over the fission spectrum is what is needed to predict the rate of production of N^{16} and it is this cross section, which averaged over the fission spectrum is only a few microbarns, that is the useful quantity. The lack of significance to theory or to monoenergetic cross sections results in the omission of these average cross sections from BNL 325; the methods and results are given in reference 6.

Many measurements have been made of such significant quantities as the total cross section, the inelastic scattering cross section, and the nonelastic cross section for fission neutrons on very many important materials. However, these results are not considered in BNL 325, cannot be utilized for comparison with theory, and we shall

not concern ourselves with them. They belong to that category of *integral experiments*, which can have very great practical utility, but cannot be compared with theory nor even used for other applications than those very similar to the conditions of each particular measurement itself. Thus they are very practical measurements, but without a wide range of applicability.

Measurements at the present time using the fission neutrons as a source, which represent a very large amount of work, but can hardly be considered even as a cross section averaged over the distribution, are the investigations of a variety of *shielding* problems. Here, of great importance in determining the penetration through shield are the cross sections for the various processes that affect the fission neutrons. However, the shielding arrangements themselves can hardly be interpreted in terms of cross sections at specific energies although the understanding of the results is heightened by use of somewhat artificial cross sections, such as the *removal cross section*, which are used in cataloguing the results. These shielding measurements*, while important, and having a direct intimate relation to neutron cross sections, usually cannot be considered as sources of cross section information and hence are not found in BNL 325.

REFERENCES FOR ADDITIONAL INFORMATION

1. H. H. BARSCHALL, *Rev. Mod. Phys.* **24**, 120 (1952). A discussion of the neutron cross-section techniques particularly applicable to the fast neutron region.
2. BARSCHALL, ROSEN, TASCHEK and WILLIAMS, *Rev. Mod. Phys.* **24**, 1 (1952). Description of the principles and techniques of neutron flux standardizations in the fast neutron region.
3. CRANBERG, DAY, ROSEN, TASCHEK and WALT, *Physics and Mathematics*, Vol. I, *Progress in Nuclear Energy Series*, (Pergamon Press, 1956). Comprehensive discussion of all techniques now in use for elastic and nonelastic cross sections for fast neutrons.
4. FESHBACH, PORTER and WEISSKOPF, *Phys. Rev.* **76**, 1550 (1949). The theory of the cloudy crystal ball nuclear model and its use in predicting neutron cross sections.
5. HANSON, TASCHEK and WILLIAMS, *Rev. Mod. Phys.* **21**, 635 (1949). Properties of the neutron sources involving charged particle accelerators.
6. D. J. HUGHES, *Pile Neutron Research* (Addison-Wesley Press, 1953), pp. 93–117. The use of unmoderated fission neutrons as a source for cross section measurements.
7. D. J. HUGHES and R. S. CARTER, *Neutron Cross Sections—Angular Distributions* (Office of Technical Services, U.S. Department of Commerce, Washington, D.C., 1956, $0.50). Graphical presentation of angular distributions of various exit particles for many neutron-induced reactions.
8. V. F. WEISSKOPF, *Physica* **22**, 952 (1956). The fundamentals underlying the cloudy crystal ball nuclear model as well as the results of the recent computations including a diffuse nuclear surface.

* Discussed in *Radiation Shielding*, by Price, Horton, and Spinney (Pergamon Press, 1957).

CHAPTER 4

NEUTRON RESONANCES

EVEN though the cross-section curves look much more complicated in the region of neutron resonances than they do for fast neutrons, the situation in one sense is much simpler for the resonance neutrons. The reason for the greater simplicity is that each individual neutron resonance is determined by a few *parameters*,, which are properties of the nuclear excitation level represented by the neutron resonance. Usually the only constants needed to describe the resonance level completely are the neutron and radiation widths and the spin of the compound nucleus. There are fewer types of cross sections than in the fast neutron region, which is reflected in the small number of level parameters, because in practically all cases the only reactions are elastic scattering and capture. Furthermore, most neutron resonances are investigated for sufficiently low neutron energy so that only $l = 0$ interactions occur, hence all angular distributions for these cases are isotropic.

The resonance region is more complex than the fast neutron region as far as the amount of data is concerned, simply as a result of the great number of energy levels that have been investigated. Thus, even though the analysis of each level involves a small number of types of cross sections, usually only σ_T, the number of levels analysed is so great that a large amount of information on level parameters is now available for analysis and comparison with theory. Various regularities have been observed in the parameters and their distribution laws are now being analysed in detail. These empirical laws are useful both as raw material for suggesting theoretical developments and for testing existing theory.

A field of application of the parameter information that shows great promise at present is the application of the systematics of level parameters to the computation of cross sections at energy regions or for nuclides for which measurements are extremely difficult, such as short-lived fission products. In the present chapter we shall consider resonances for only the non-fissionable nuclei, deferring the additional complication of fission until the next chapter.

THE BREIT-WIGNER FORMULA

The analytical form of a neutron resonance is given by the *dispersion formula*, which is analogous to the formula for anomalous

optical dispersion or the formula for a resonating electrical circuit. The dispersion, or *Breit-Wigner*, formula, when written in its most general form gives the cross section as a function of energy, taking into account the contributions of many levels at the same time. The formula in this general case, however, contains so many parameters that it is extremely difficult to use in actual practice. The experimental analysis is usually performed in the immediate vicinity of a level, to investigate the properties of that level, and the simplified form or the *single level formula* is almost always sufficiently accurate for such cases. We shall concentrate our attention on this formula, then cover briefly those cases where it is not applicable.

The single level formula applies at an energy where a single level is the principal contributor, and processes other than those resulting from compound nucleus formation, for example the potential scattering, are negligible. Under these assumptions the formulae for the elastic scattering and the reaction cross section for a particular interaction of angular momentum l are:

$$\sigma_n^l = \pi\lambda\!\!\!^{-2}_0 g \frac{(\Gamma_n^l)^2}{(E - E_0)^2 + (\Gamma/2)^2} , \tag{4–1}$$

$$\sigma_x^l = \pi\lambda\!\!\!^{-2}_0 g \left(\frac{E_0}{E}\right)^{\frac{1}{2}} \frac{\Gamma_n^l \, \Gamma_x}{(E - E_0)^2 + (\Gamma/2)^2} , \tag{4–2}$$

$$g = \frac{2J + 1}{2(2I + 1)} , \tag{4–3}$$

Here x denotes a "particle" such as a proton, alpha particle or gamma ray, and Γ_x is the corresponding *width*, giving the probability of emission of particle x from the compound nucleus, the emission probability being $\Gamma_x/\hbar$ per sec. The *total width* Γ is given by the sum of all possible partial widths. The *statistical factor* g gives the probability of the neutron and nucleus adding their angular momenta in such a way as to produce the compound nucleus with the correct spin J of the particular level, with I the spin of the target nucleus.

The widths appearing in the formulae are the values at the *resonance energy*, E_0, hence are constants, as is the wavelength $\lambda\!\!\!^{-}_0$. This method of using the values at the energy E_0 in the formulae helps to eliminate confusion; the actual variation of widths and wavelength with E is taken into account in the way the formulae are written. For example, the change in Γ_n with neutron energy is as $E^{\frac{1}{2}}$, but Γ_n in the formulae is a constant, the value for $E = E_0$. The widths could be written as Γ_n^0 etc., to signify values at resonance, as is done for $\lambda\!\!\!^{-}$, but the width might then be confused with the *reduced neutron width*, usually written as Γ_n^0 ($\Gamma_n^0 = \Gamma_n/E_0^{\frac{1}{2}}$). This usage is consistent with BNL 325 in which Γ_n is the value at resonance and Γ_n^0 is the reduced width.

The formulae in the simple way in which we give them refer to the formation of a state of a certain J via only one particular combination of the incoming neutron's spin 1/2, angular momentum l, and target nucleus spin I. In some cases, even for a single l, the two possible combinations of l with the neutron spin ($l \pm 1/2$, the two incident *channel spins*) can *both* give the same J; g can then be twice the value given by Eq. (4–3) but cannot be predicted *a priori*. Additional complications arise because a single resonance level may have contributions from various incident angular momenta. The combination of the various l contributions as expressed in a general formula produces a very complex result, even though only one level is being considered. However, in the analysis of actual data, the angular momenta involved are usually known or can be identified by the magnitude of the peak cross section observed or from angular distribution measurements. The angular distributions of scattered neutrons for various l's were discussed in connection with Eq. (2–9). The completely general formula, which includes contributions of all l values is considered in detail in reference 1.

Examples of the way in which the angular momenta are involved in the formation of levels are furnished by the table of "Parameters of Light Nuclei" in BNL 325, p. 35. Thus for the one level shown for Li^6, at a neutron energy of 248 keV, the l value of 1, the neutron spin of 1/2 and the target nucleus spin of 1 combine to give an excited state of spin, J, of 5/2. This result can be obtained via only one channel spin, $l + 1/2$, or 3/2, which adds to the I of 1 to give the J of 5/2. Similarly, the 258 keV level in Li^7 also necessitates $l + 1/2$ to give $J = 3$ from $I = 3/2$ and $l = 1$. For Be^9, the formation of the 620 keV level is unambiguous for the spins are identical with the Li^7 level just discussed. However, the 810 keV level formation is much more complicated; it is not known whether $l = 1$ or 2 is responsible, furthermore, for each l, the two channel spins $l \pm 1/2$ can both produce the J of 2 by addition to the I of 3/2. It is just these ambiguities of formation that make the identification of J and l difficult in many cases at energies sufficiently high so that $l > 0$ is possible.

Actually, relative to heavy nuclei, there are not many levels in the light nuclei whose parameters have been measured, and most of our attention will be paid to the heavier elements. For them, resonances are found at such low energy that only $l = 0$ is important, and under these conditions, the formulae simplify greatly and analysis of the experimental curves to obtain actual parameters is very direct. In the case of $l = 0$, the Breit-Wigner formula is sufficiently simple so that it is possible to include the effect of *potential scattering* in the analysis with little complication. The formulae for $l = 0$, but including

potential as well as resonance scattering are the following, where we write γ for x, because in practically all resonances only capture and scattering occur:

$$\sigma_n = 4\pi\lambda\!\!\!^{-2}_0 g \left| \frac{\Gamma_n/2}{E - E_0 + i\Gamma/2} + \frac{R'}{\lambda\!\!\!^{-}_0} \right|^2 + 4\pi(1-g)\,(R')^2 \,, \quad (4\text{–}4)$$

$$\sigma_\gamma = \pi\lambda\!\!\!^{-2}_0 \left(\frac{E_0}{E}\right)^{\frac{1}{2}} \frac{\Gamma_n\,\Gamma_\gamma}{(E-E_0)^2 + (\Gamma/2)^2} \,, \quad (4\text{–}5)$$

$$g = \frac{1}{2}\left(1 \pm \frac{1}{2I+1}\right) . \quad (4\text{–}6)$$

Here all the symbols have their previous significance, and R' is a quantity approximately equal to the nuclear radius, R. Its evaluation on the basis of the cloudy crystal ball nuclear model will be considered later in the present chapter.

The form of Eq. (4–4), in which the *amplitudes* are added before squaring, is an example of the interference of one resonance with other components of cross section, here with the potential scattering amplitude. This equation is appropriate for the *coherent* addition of amplitudes in which the intensity is obtained from the square of the absolute value of the combined amplitudes. The interference between resonance scattering and potential scattering is a marked effect that has been verified in many cases; it establishes the reality of the interference between the potentially scattered neutron wave and that resulting from formation of the compound nucleus. The type of interference in which the amplitude from one resonance interfers with that from another is much harder to detect experimentally, because it has an appreciable effect only if two levels are a distance apart of the order of magnitude of Γ. As this is a very small spacing it is not surprising that there are few cases of resonance-resonance interference.

The energy level parameters are obtained from experimental cross-section curves in a variety of ways, all based on the formulae just presented. The methods vary, depending on the relative magnitude of scattering and capture as well as the resolution available. Before considering the analysis techniques and their results, however, we shall first examine briefly the experimental methods used in the resonance neutron region.

RESONANCE NEUTRON SOURCES

For the lightest elements, individual neutron resonances are observed at rather high neutron energies, hence these resonances are studied with the neutron sources we have already described in the

preceding chapter. However, the great majority of neutron resonances, i.e. for all but the lightest nuclei, are seen at low neutron energies and instruments designed specifically for use at these energies, with the highest possible resolving power, are used. Because of the nature of the instruments used in the two regions, the relative energy spread, $\Delta E/E$, decreases with increasing energy at high energy, and increases with energy in the resonance region. As a result, the attainable energy resolution is the poorest ($\Delta E/E$ the largest) in a region between those appropriate for the two types of measurements. A few years ago the resolution was so poor ($\Delta E/E > 1$) in this intermediate region, which extended from about 1 to 20 keV, that a definite gap existed in the data on resonance as a function of energy. Recent improvements in techniques at both high and low energy, however, have now closed the gap in the sense that at the energy of poorest resolution, about 5 keV, $\Delta E/E$ is now of the order of 0·05.

For both high and low energy neutrons, the instrumental task is one of producing neutrons of a narrow spread in energy at an adjustable energy, or selecting narrow energy bands from a source of wide initial energy spread. High neutron source intensity is essential because of the severe reduction in intensity resulting from monochromatization. For all but the lowest energy regions the improvement of neutron detectors is an important phase of the problem, for their efficiencies, usually discouragingly low, must be increased as much as possible to obtain practicable counting rates. Although the techniques mentioned in the preceding chapter can demonstrate the existence of resonances even below 1 keV, the superiority of the time-of-flight instruments in the low energy region implies that the Van de Graaff is more suitable for use at higher energy, above say 5 keV. In the 5–50 keV region, these "fast neutron" techniques can be used to isolate resonances for atomic weights ranging up to about 60. For heavier nuclei, however, with the exception of a few magic-number anomalies, the spacing is too close to allow resolution of individual resonances.

Below 10 keV there are at the present time two methods of neutron spectroscopy in general use, one based on Bragg reflection of neutrons by single crystals and the other on time-of-flight measurements. The instruments used in these methods, *crystal monochromators* and *time-of-flight velocity selectors* respectively, have in common a neutron source produced by moderation of fast neutrons, which results in a neutron flux inversely proportional to energy, the "dE/E" spectrum. In other respects there are important differences; these determine the specific energy regions and cross sections most appropriate to instruments of the two types.

The crystal monochromator, Fig. 4–1, or "spectrometer" as it is usually described, requires a well-collimated high intensity neutron beam; thus a chain-reacting pile is necessary for its successful operation. The beam of neutrons for a crystal spectrometer is formed by opening a hole through the shield of the pile and into the "lattice" (uranium fuel plus moderator), usually to a point as near the centre of the pile as possible. At this point a high flux of neutrons in the resonance energy region, 1 eV to 100 keV, is found. The flux is distributed in energy according to the dE/E spectrum, thus with a

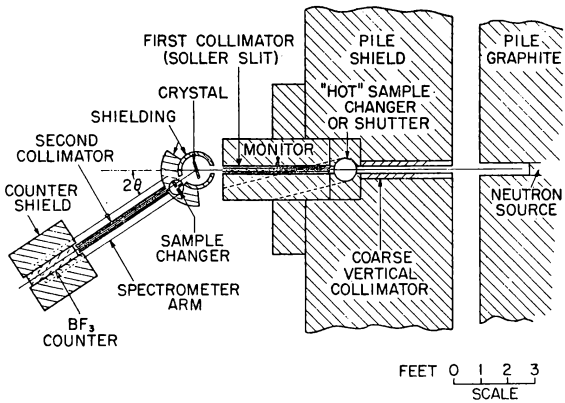

FIG. 4–1. Diagram of the crystal monochromator, used to obtain monoenergetic neutrons by Bragg reflection of reactor neutrons at a single crystal.

magnitude that is the same in each energy decade (1 to 10 eV, 10 to 100 eV, etc.), this magnitude being 7×10^{11} cm^{-2} sec^{-1} in the Brookhaven pile, for example. The flux incident on the monochromating crystal, placed just outside the pile shield, is of course much less, being reduced enormously (a factor of 10^5 to 10^6) by the small solid angle subtended at the crystal by the source area (the base of the hole). The crystal is set at a small, adjustable angle to the incident collimated beam and the diffracted neutrons are detected by a counter, usually an enriched BF_3 proportional counter.

The neutron wavelength, λ, diffracted for a particular incident glancing angle, θ, is given by the *Bragg formula*,

$$n\lambda = 2d \sin \theta \ , \qquad (4\text{–}7)$$

with n the *order* of reflection, usually unity. For a typical crystal LiF, the value of d for the (111) planes is 2·32 A hence for neutrons of 1 eV energy the glancing angle will be 3·5°. Whereas this value of θ is a practicable one, although small, it becomes 0·35° for 100 eV neutrons, of the same order of magnitude as the angular collimation

of many monochromators in use today. Even for a collimation of 0·1° the conditions just described would imply an energy resolution $\Delta E/E$ ($\sim 2\Delta\lambda/\lambda$) of about 50 per cent at 100 eV. The angular requirements just mentioned are important factors in reducing the range of utility of present crystal monochromators to energies well below 100 eV, in practice below about 20 eV. Another effect that restricts the instruments to low energy is the rapid decrease in reflected intensity with increasing energy. This decrease is a result not only of the decreasing incident flux ($1/E$) but of the reflectivity of the crystal itself, which varies as $1/E$. The resulting flux at the neutron detector drops off rapidly with energy, as $1/E^2$, and counting rates are prohibitively low for the high collimation associated with good resolution.

The second general method in use for low energy neutron spectroscopy involves the production of neutrons in sharp bursts, of the highest possible intensity, together with the measurement of their time of arrival at a detector some 5 to 60 metres distant. The underlying principles of the time-of-flight techniques are the same whether the burst is produced by modulation of the output of a charged particle accelerator (cyclotron, betatron, or linear electron accelerator) or by mechanical interruption of a pile neutron beam. For all of the time-of-flight instruments the neutron energy (E,eV), velocity (v, m/sec) and flight time per metre (t, μsec/m) are related as follows:

$$v = 10^6/t \tag{4–8}$$

$$E = 52{\cdot}3 \times 10^2/t^2 \tag{4–9}$$

$$t = 72{\cdot}3/(E)^{\frac{1}{2}} . \tag{4–10}$$

Thus for a typical path of 10 metres, the flight times to be measured for 1 keV and 1 eV neutrons are 22·9 and 723 μsec, respectively, easily accomplished electronically. The spread in energy actually existing for a "single" flight time, i.e. for a single time channel of the electronic recording circuits, is the result of a number of contributions to the uncertainty in timing. The most important of these are the length of the electronic time channel itself, the neutron path length in the detector, the time delay in the action of the detector, the length of the neutron burst, and the moderation time of the fast neutrons (the last not occurring for the pile choppers).

The timing uncertainties just enumerated combine to give a *resolution function*, whose full width at half-maximum, divided by the path length, is the *resolution*, Δt, in μsec/m. In the past few years resolutions have been improved about fivefold with the advent of the recent instruments, and at the present time the best available is about 0·02 μsec/m, giving an energy spread of 0·02 eV at 10 eV (0·2 per cent), rising to 18 eV at 1 keV (2 per cent). Although the variation of resolution with energy is the same as for the crystal

monochromator, the counting rate will be constant with energy, assuming a dE/E flux. As a result, while the crystal has a very good intensity in the 0·1 to 10 eV region, it rapidly becomes inferior to the time-of-flight instruments as the energy is increased and is thus most useful in the lower energy range specified.

For the time-of-flight methods in which the neutron source is pulsed, the accelerator itself (cyclotron, betatron, or linear accelerator) is not specifically designed for the purpose, and only the sharp pulsing of the ion source represents a special technique. At the present time the highest resolution of the pulsed source technique is attained with the Columbia synchro-cyclotron, in which the intrinsic bunching of the accelerated protons produces a very short burst. The resolution of the order of magnitude 0·02 μsec/m already mentioned has been attained with this apparatus.

Very recently, pulsed Van de Graaff neutron sources, combined with mμsec timing techniques and short flight paths, have been used in the 5 to 30 keV region. Here no moderation is necessary because the neutrons are emitted from the the target in the backward direction in the desired energy range. Resolutions are comparable with the best of the other time-of-flight instruments, as shown by the curve for selenium in BNL 325—Supplement 1, p. 44.

Whereas the charged particle accelerators used as time-of-flight sources are of conventional construction, the pile *fast choppers* are designed uniquely for neutron spectroscopy and hence merit a brief description. In order to produce sharp bursts of neutrons, a shutter necessarily heavy to stop neutrons of all energies, must open and close quickly. The large size and high speed of the "fast" chopper (i.e. a chopper for fast neutrons) make it a much more complicated device than the "slow" chopper for which thin cadmium sheets suffice to stop the slow neutron beam. Because of the limited energy range of the slow chopper (0 to 0·4 eV), very few neutron resonances can be studied with it. The requirement of short burst length for the fast chopper—about one μsec—leads to neutron beams of small area, hence low intensity; this latter tendency must be counteracted as much as possible to obtain a finite counting rate at the distant detector. These conflicting requirements result in a rather heavy, rapidly rotating shutter, containing shaped slits for the passage of neutrons, slits whose cross-sectional area is of the order of 0·01 in. by 1 in. As the slits in the moving shutter pass similar slits in a stationary collimator, neutron bursts of duration of about 1 to 5 μsec, depending on the particular chopper, are produced.

A typical high resolution chopper design is that of the Brookhaven machine, which has been in operation for about four years. The rotor is a horizontal disc, Fig. 4–2, 30 inches in diameter, suspended by

a thin flexible shaft in an evacuated chamber. The narrow slits for the burst formation are machined in plastic pieces, which are held in the rotor between aluminium forgings. The present rotor has been in operation for several years at 10,000 rpm with a burst length slightly less than 1 μsec, the shortest burst yet attained in operating

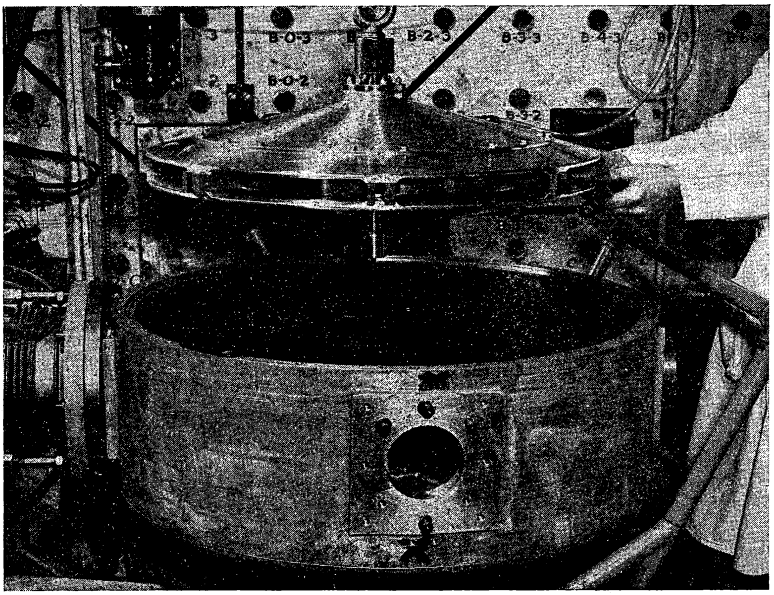

FIG. 4–2. The rotor of the Brookhaven fast chopper, photographed at the face of the reactor. The plastic arms in which the slits for passage of neutrons are cut may be seen, as well as the vacuum chamber in which the rotor is mounted.

choppers. With a scintillation neutron detector and a flight path of 20 metres, the measured resolution function (including all timing uncertainties) has a width of 1·0 μsec, hence the resolution is 0·05 μsec/m under these conditions.

Although the usual enriched BF_3 proportional counters or ion chambers have been used as detectors for time-of-flight work, their low efficiency (arising from the $1/v$ boron cross section), finite neutron path length, and long pulse collection time make it clear that better detectors are needed. The detectors mentioned can of course be improved to some extent. Scintillation counters, however, seem to hold the most promise. At the present time a boron-containing liquid scintillation counter is being used at Argonne in which neutrons are moderated somewhat to increase the efficiency, although a time uncertainty of about 2 μsec is thereby introduced. The Brookhaven

chopper presents a more difficult detector problem than other designs, because of the larger beam area at the detector position and the higher gamma ray content of the beam.

Although fast choppers and the recent pulsed accelerators have approximately equal resolutions, there are several respects in which they differ, the principal differences pertaining to sample and counter sizes. The sample size is much less in the case of the fast chopper because of the inherently small slits. As a result, samples as small as 10 mg have been used, and available supplies of separated isotopes are sufficient for investigation. On the other hand, the counter area is usually smaller for the pulsed source machines and they are more suitable for measurements utilizing complex detection instruments, such as those appropriate for scattering and capture cross sections. However, we shall see that, as for the high energy region, by far the majority of the results pertain to total cross sections resulting from relatively simple transmission measurements. It is noteworthy that none of the time-of-flight methods can be used for activation cross sections, as can be done with the crystal monochromator; neutrons of all energies would activate the target, while in the latter instrument a monoenergetic beam is actually produced.

DETERMINATION OF RESONANCE PARAMETERS

Although the particular problems encountered in the conversion of a measured transmission curve to a neutron cross-section resonance vary somewhat with the type of instrument, there are some principles, which we now consider, that are common to all methods. As before, we shall be concerned primarily with total cross sections; the others have been measured to a much smaller extent and analysis methods to obtain absolute cross sections, as well as the measurements themselves, are much more complex. We cannot go into all the complexities of resonance analysis, but must content ourselves with the broad outlines; the details may be found in the listed references in Appendix 3.

A brief inspection of the Breit-Wigner formulae reveals that the total cross section alone, if accurately measured, gives much information concerning the parameters of the level involved. Considering $l = 0$ interactions only, the ones for which individual resonances are resolved in most nuclei, we see that measurement of σ_0, the peak height of the total cross section, and Γ, gives $g\Gamma_n$ as well. This peak height of the *resonance* in the *total* cross section, i.e. capture plus resonance scattering, but no potential scattering, is seen to be, from Eqs. (4–4) and (4–5),

$$\sigma_0 = 4\pi\lambda\!\!\!^{-2}_0 g \frac{\Gamma_n}{\Gamma} . \qquad (4\text{–}11)$$

If the statistical weight factor, g, is known, Γ_n and Γ_γ (given by $\Gamma - \Gamma_n$) are also obtained.

Thus from a sufficiently accurate total cross-section measurement alone all the level parameters can be obtained if g is known. For a zero-spin target nucleus g is unity and for high spin it is close to 1/2, hence for these cases the total cross section alone gives all the parameters. The largest uncertainty in g occurs for a target spin of 1/2 in which case it is either 1/4 or 3/4. Here a subsidiary measurement of the ratio of scattering or capture to total cross section (usually easier than an absolute determination) is useful as it gives Γ_n/Γ or Γ_γ/Γ and thus resolves the g uncertainty. In the present state of neutron spectroscopy in which precise values of Γ_n are usually not required, the uncertainty of g is not a serious drawback to the utility of total cross-section work. Of course, auxiliary measurements of Γ_n/Γ or Γ_γ/Γ are of intrinsic interest because they determine which of the two possible J values, $I \pm 1/2$, actually applies to the level.

The difficulty of obtaining σ_0 and Γ from an experimental transmission curve varies enormously with experimental conditions, from the exceedingly few cases where Eq. (4–11) may be directly applied to those where only certain combinations of parameters, rather than σ_0 and Γ, can be determined accurately. For a resolution width negligible compared with Γ, the cross-section curve obtained by simple substitution in Eq. (4–11) is a true representation of the resonance, but as the resolution width becomes comparable to, then larger than Γ, increasingly serious complications ensue. We shall briefly describe the methods of analysis that are applicable in these various circumstances starting with the good resolution region.

Because so few resonances are measured with negligible resolution width, we shall consider the "good" resolution to be that in which the resolution width is no larger than Γ, rather than negligible. Under these conditions the observed transmission can be corrected, before conversion to a cross-section curve, for the distorting effect of the resolution function. The width and peak height of the cross-section resonance obtained from the transmission curve, corrected for resolution, do not represent the true Γ and σ_0, however. Rather they refer to a modified resonance in which the cross section at each neutron energy actually corresponds to a spread of energies, caused by the temperature motion of the atoms of the sample. This spreading of the energies, the *Doppler broadening*, lowers the peak height and increases the resonance width. The Doppler broadening is approximately a Gaussian with a width given by

$$\Delta = 2(kTE_0 m/M)^{\frac{1}{2}} \tag{4–12}$$

where m/M is the mass ratio of neutron to nucleus. For a gas T

would be the actual temperature, but for a solid the effective temperature is taken as a few degrees greater.

For heavy elements ($\Gamma_\gamma \gg \Gamma_n$) at energies where straightforward correction for resolution is almost impossible, measurements of combinations of parameters can still be made that give σ_0 and Γ_n indirectly. These measurements relate to the area of the "dip" in a transmission curve corresponding to the resonance, and if obtained for samples of widely different thicknesses give the desired parameters.

In the limiting cases of "thick" and "thin" samples, the areas, A (in eV), are given by

$$A^2 = \pi n \sigma_0 \Gamma^2 \ , \tag{4–13}$$

$$A = \frac{\pi n}{2} \sigma_0 \Gamma \ , \tag{4–14}$$

from which it is clear that a combination of results for the two extremes gives σ_0 and Γ, the same parameters obtainable in the good resolution region. Actual samples never correspond to the extremes for which Eqs. (4–13) and (4–14) apply and in practice more complicated analysis must be made. For these intermediate samples, the accuracy in obtaining σ_0 and Γ is increased by using samples with as large a spread in thickness as possible and the actual determination is most easily accomplished from calculated curves.

Various techniques of analysis have been developed in recent years as part of the fast chopper programme at Brookhaven, in which several hundred resonances have been studied. The method now in use is rapid, accurate, and involves no assumption of parameters in analysing a thick-thin sample combination. It involves only the single set of curves shown in Fig. 4–3, in which A/Δ is plotted against $n\sigma_0(\Gamma/\Delta)$, for various values of Δ/Γ. All these quantities are dimensionless, and the input data, A/Δ, do not involve unknown parameters. The Doppler width, Δ, is given by Eq. (4–12).

The use of the curves for the "thick-thin" sample case is very direct. Points are plotted for each sample at the correct ordinates, A/Δ, and a distance apart horizontally corresponding to the ratio of the sample thicknesses (n). If these two points are moved horizontally, they will fit only one of the curves, whose Δ/Γ value then gives Γ directly, and the abscissa gives σ_0, hence $g\Gamma_n$.* If the experimental errors in A are also plotted it is very simple to obtain the resultant errors in Γ and $g\Gamma_n$ by slight shifts of the sheet carrying the plotted points.

Another type of analysis is involved when only one sample thickness is available. For this situation, which occurs frequently, the usual procedure is to assume a value of Γ_γ for the resonance and thus

* The abscissa, $n\sigma_0 \Gamma/\Delta$, is just $(4\pi\lambda_0^2 n/\Delta) g\Gamma_n$.

obtain $g\Gamma_n$ from the single sample area. The Γ_γ is usually known to about 20 per cent accuracy from other considerations and this uncertainty produces an error in $g\Gamma_n$ that varies with sample thickness in a complicated manner. The curves of Fig. 4–3, however, give a simple solution to this problem also. The measured area and the assumed Γ_γ give an A/Δ and a Δ/Γ value (assuming at first that $\Gamma = \Gamma_\gamma$, i.e., that Γ_n is small), from which $n\sigma_0(\Gamma/\Delta)$, hence $g\Gamma_n$, is

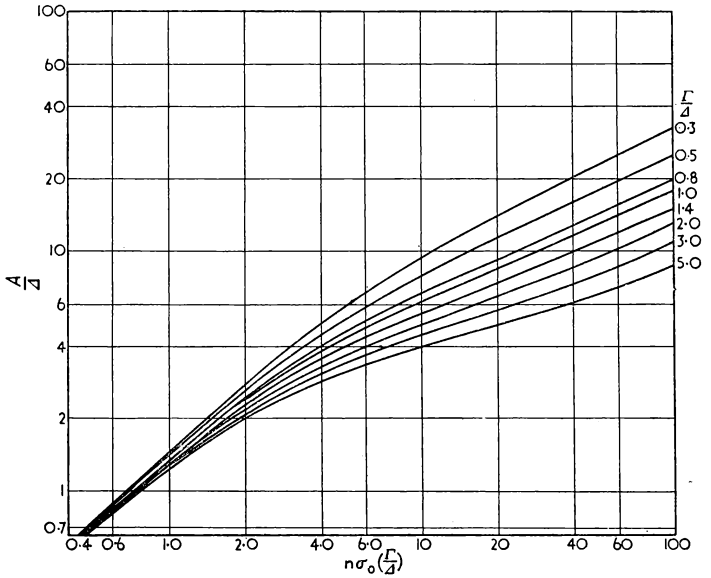

FIG. 4–3. Curves used for analysis of neutron resonances, by means of which the level paramenters are obtained from the areas of dips in transmission curves for samples of various thicknesses.

obtained. If the Γ_n obtained is not small compared with Γ_γ, the Δ/Γ value used can be changed and a revised g/Γ_n obtained. Again, as for the multiple-sample method, no lengthy computations or use of tables are necessary, the conversion of the $n\sigma_0(\Gamma/\Delta)$ value to $g\Gamma_n$ being done by slide-rule. The error in the final $g\Gamma_n$ resulting from the experimental error in A, and that arising from the uncertainty in the assumed Γ_γ, are easily determined by simple geometrical considerations.

RESULTS OF RESONANCE ANALYSIS

The many instruments now in use throughout the world are rapidly giving information on resonance parameters for many nuclides—at present results are available in sufficient number to justify

statistical analysis of various distributions and comparison with current theory. One of the most obvious characteristics of neutron resonances is the manner in which they are spaced, that is whether they occur at random within a single nuclide and how their average spacing varies from one nuclide to another. It is well worth our while to examine briefly the findings that are rapidly emerging from the present programme of resonance analysis concerning level spacings and widths, as reported in BNL 325 and its first supplement.

TABLE 4–1

Resonance parameters of Cd^{113}. *The radiation width is taken as* 110 ± 20 *mV, for levels where it is not measured, and* g *is assumed to be* 1/2 *except for the* 0·178 *eV level, for which it is taken as* 3/4.

E_0 (eV)	Γ_γ (mV)	Γ_n (mV)	Γ_n^0 (mV)
0·178 ± 0·002	113 ± 5	0·65 ($J = 1$)	1·50 ± 0·05 ($J = 1$)
18·5 ± 0·2		0·28	0·064 ± 0·006
64·0 ± 0·7	80 ± 40	3·4	0·84 ± 0·07
85 ± 2		32	3·5 ± 0·5
109 ± 2		14	2·6 ± 0·3
192 ± 5		132	9·6 ± 1·0

As an example of the data now available we list in Table 4–1 the resonance parameters for the isotope Cd^{113} as given in Supplement I of BNL 325, where the references to the data used in the evaluation may be found. The radiation width listed for the isotope, 110 ± 20 mV (milli-eV), is the value assumed to apply to every level, its "error" being larger than the measured value for the 0·178 eV level to allow for some possible variation in Γ_γ from level to level. As the neutron widths can be obtained from total cross sections even when the total width Γ cannot, Γ_n's (and Γ_n^0, there duced width, $\Gamma_n^0 = \Gamma_n/E_0^{\frac{1}{2}}$) appear for all levels, but Γ_γ's for two only. The radiation width is easily obtained when Γ is known by subtraction of Γ_n, which is usually small relative to Γ_γ. Actually $g\Gamma_n$, not Γ_n, is obtained from the total cross section, but g is assumed to be 1/2 (for Cd^{113} it is actually 1/4 or 3/4 for $I = 1/2$) unless J happens to be known as it is here for the first level. For this level g is taken to be its true value of 3/4 in getting Γ_n and Γ_γ, rather than 1/2.

Level Spacings

The question of the distribution of *level spacings* within a single nuclide is unfortunately one that is still not completely answered. The levels formed by slow neutrons represent two separate spin

systems of J's given by $I + 1/2$ and $I - 1/2$, and these, being distributed at random with respect to each other, complicate any regularity that might be present within a single spin system. In order to avoid the complication of two spin systems it is possible to work with even-even nuclei, which of course have only one possible spin state for the compound nucleus, all the levels having $J = 1/2$. The results for even-even nuclei seem to indicate that for all but the smallest spacings the distribution of spacings is approximately random. If the number of levels is plotted as a function of spacing, Fig. 4–4, the result is exponential, corresponding to a random distribution, for all but the smallest spacings, for which there are fewer

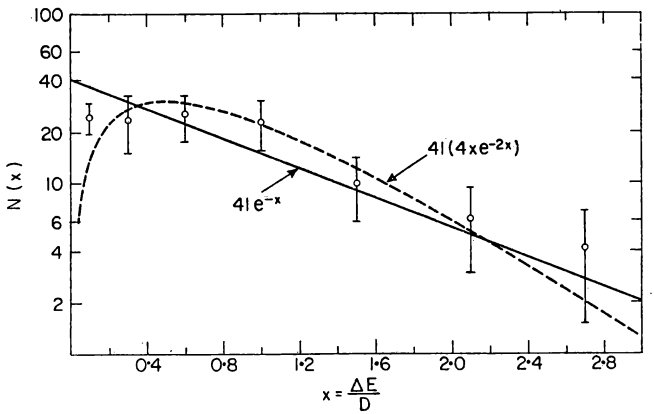

FIG. 4–4. The observed differential distribution of spacings between levels for several even-even nuclei, relative to the mean spacing for each nucleus. Only one spin system is here present in the compound nucleus and a random distribution of levels would exhibit an exponential behaviour.

than would be expected on a random basis. The evidence is strong at the present time that there are too few small spacings, an effect that is usually referred to as the "repulsion" of levels. The reality of the repulsion effect is of course difficult to establish because there is always the experimental difficulty in resolving two levels when they are extremely close together. However, careful examination of even-even nuclei, as shown in Fig. 4–4, seems to indicate that there is a real effect of repulsion of levels. The same effect seems to occur for the odd nuclei, Fig. 4–5, though here the presence of two systems of spin states complicates the experimental results.

The *average level spacing* D refers to an excitation energy just above the neutron binding energy, which energy is in the range 5 to 8 MeV for the heavy nuclides for which D is well known. Because of the rapid change of D with excitation energy, it is useful to convert

the observed spacings to a specific value of the excitation energy for comparison purposes. If very accurate spacings could be obtained for many isotopes, it might be possible, by comparing spacings for different isotopes, to get information on the variation of spacing with excitation energy. However, because of the fact that the results at the present time are limited in number and statistical accuracy, the most

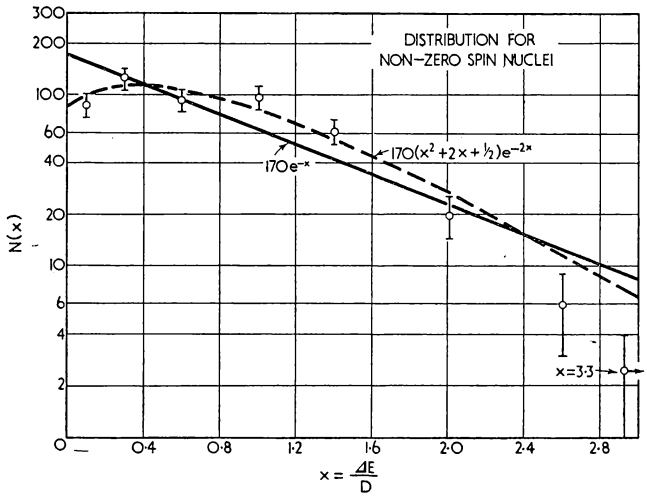

FIG. 4–5. The observed distribution of level spacings for a series of odd nuclei, in which two level systems are present, of spin I $\pm$ 1/2.

profitable procedure seems to be to convert the spacings to a single excitation energy, using the usual *empirical level density formula*,

$$w = 10^6/D = a \exp(b\sqrt{E^*}). \qquad (4\text{–}15)$$

Here w is the number of levels per MeV, E^* is the excitation energy, and a and b are parameters that vary slowly with atomic weight, as described in reference 1. The level spacings obtained by counting the resonance levels in given energy regions, and correcting to 6 MeV by means of Eq. (4–15), are shown in Fig. 2–2. It is seen that the level spacings at a given excitation energy are not a smooth function of atomic weight as would be expected from the statistical model of the nucleus. Instead, a discontinuity of the order of 100 occurs at the 82 neutron shell.

Discontinuities in level spacing near ground at magic numbers is well known and the present results show definitely that the shell structure exerts a large effect on level spacings at 6-MeV excitation as well. It would be very interesting to establish other level-density

variations but unfortunately sufficiently many nuclei have not been investigated to establish definite trends. Although some even-odd effects seem to be present in Fig. 2–2, the data are not extensive enough to establish them definitely. However, one effect that seems definite is the higher D for even-Z nuclei (solid dots in Fig. 2–2). It would be of great interest to investigate the dependance of D on level spin J; the presently available data, while not extensive, do not seem to show an effect at high J as large as the $1/(2J + 1)$ factor expected theoretically. This factor seems to hold at low J in one case, Ag, as shown in BNL 325, Supplement 1, p. xiii.

Radiation Widths

As we have seen, the radiation widths can be obtained from the total cross section alone, in the good resolution region, with little uncertainty arising from the usual lack of knowledge of g. The values of Γ_γ thus obtained are of value for comparison with nuclear radiation theory for they represent the *electric dipole transition probability* averaged over the many possible final states available in the case of gamma emission. A practical use of the results is that they aid greatly in the analysis of neutron resonances in the poor resolution region, and for fissionable isotopes as discussed in the next chapter.

The first noteworthy fact concerning the radiation widths is the small variation among levels in a single nuclide and as a function of atomic mass. This near-constancy is evident in the resonance parameter table of BNL 325 and is also shown in Fig. 4–6, which reveals a slight decrease of the radiation width with increasing A, and a peak at A slightly above 200, corresponding to the 126 neutron–82 proton shell. The excitation energies of the levels whose widths are given in Fig. 4–6 range from 6 to 9 MeV, and represent levels in target nuclei of odd Z-odd N (N, number of neutrons), odd Z-even N, even Z-odd N, and even Z-even N. None of these variables, nor the wide range in level spacing, however, results in large differences in radiation width. The level spacings for the isotopes considered vary greatly, yet this difference in spacing apparently is not reflected in a change in radiation width. An extreme example is furnished by Hf^{177} with a level spacing of 8 eV and Hf^{178} with 100 eV, both having similar Γ_γ's. The peak at $A \approx 208$ is well explained by the unusually large discontinuities in D and excitation energy at that point on the basis of electric dipole radiation.

As the levels studied represent a wide range of angular momenta, J, it is possible to investigate the dependence of Γ_γ on J, the spin of the compound nucleus. The result is that there is little or no dependence of the radiation width on J, in conformity with radiation theory. It is a well-known fact that theoretical estimates of the

electric dipole radiation width of highly excited levels are much larger than experimental results. For example, the widths calculated in reference 1 are about 300-fold larger than those of Fig. 4–6, using the single particle model. It is evident that a large depression of the theoretical electric dipole transition probability takes place for these highly excited states.

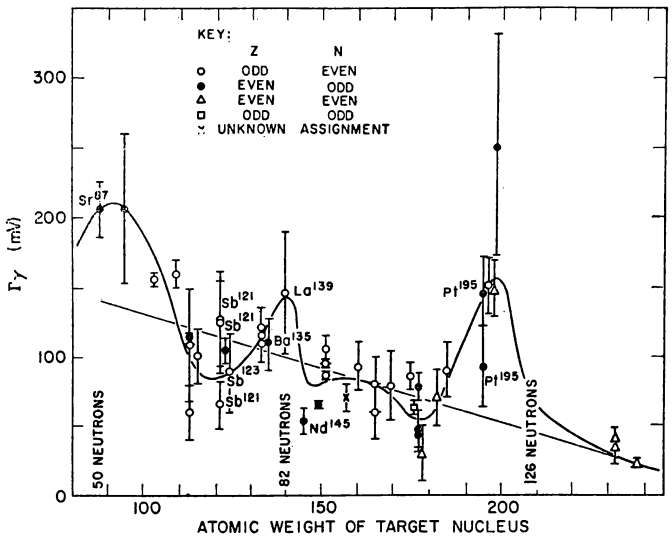

FIG. 4–6. Measured radiation widths plotted against atomic weight, revealing the slow decrease of radiation width with atomic weight as well as a sharp discontinuity at the closed nuclear shells near $A = 200$.

The near-constancy of Γ_γ is of great value in the analysis of neutron resonances in the region of poor resolution, e.g. 20 to 200 eV. Here the variation of Γ_n from level to level is much greater than that of Γ_γ, hence in studying the former in the 20 to 200 eV region it is safe to use values of Γ_γ obtained at lower energy to obtain Γ_n from the poor-resolution measurements.

The information that has so far been obtained from the total radiation widths of highly excited levels in medium and heavy nuclides is not by itself sufficient to enable one to determine which mode of decay is most important in these transitions. However, when taken with other experimental data, it seems almost certain that most of the radiation emitted by these levels is electric dipole.

Neutron Widths and $\overline{\Gamma_n^0}/D$ *Ratio*

We now turn from the radiation width, a property of the nucleus

that is independent of the method of excitation to the "external" properties, which are of particular interest to recent nuclear models. Here the matters of interest are the neutron widths of levels and the *strength function*, or $\overline{\Gamma_n^0}/D$ ratio. The neutron width of a level seems at first to be an internal nuclear property for it gives the probability of disintegration of a state of the compound nucleus by neutron emission. However, after division by the average level

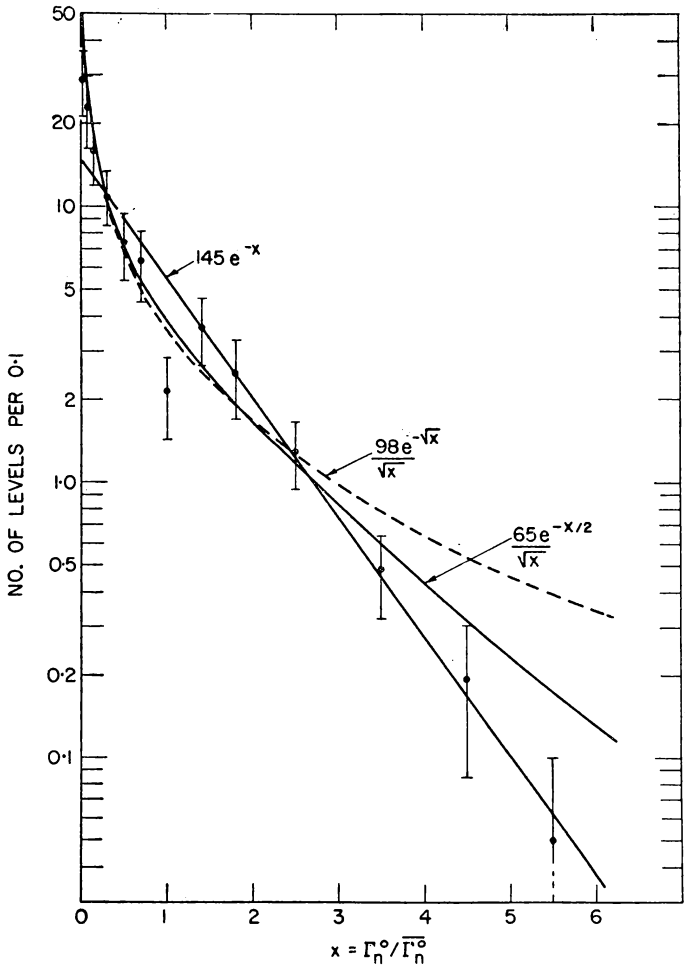

FIG. 4–7. The differential distribution of neutron widths observed in a series of nuclides, plotted relative to the average neutron width for each nuclide; the significance of the curves is discussed in the text.

spacing D the ratio is a property primarily of the penetrability of the nuclear surface, as we have already considered in Chapter 2.

The disintegration probability for the nuclear state per second by neutron emission is of course just $\Gamma_n/\hbar$. The time required for the excitation energy to be concentrated on a single neutron so that the neutron has a chance to emerge from the nucleus, or in other words, the time between collisions with the surface, is given by h/D. The product of these quantities, or the probability of emergence per collision, is the *penetrability* of the nuclear surface, $p = 2\pi\Gamma_n/D$, Eq. (2–25.) Thus the strength function is simply $p/2\pi$ and is not a property of the nuclear energy level system, but of the nuclear surface itself. It is for this reason that the strength function is of particular importance to the cloudy crystal ball nuclear model and is used to fix some of the parameters in the theory. It is usually evaluated as $\overline{\Gamma_n^0}/D$ where $\overline{\Gamma_n^0}$ is the average value of Γ_n^0, the neutron widths converted to their values at 1 eV.

Before considering the $\overline{\Gamma_n^0}/D$ ratio, however, it is interesting to examine the *size distribution* of neutron widths that exists within single nuclides. The neutron width is related to the magnitude of the nuclear wave function at the nuclear surface, and the distribution in size of the widths gives information on the variation of the wave function from level to level. The neutron widths, in marked contrast to the radiation widths, show an extremely large variation, as seen in Fig. 4–7, which gives the distribution for many nuclides plotted together in terms of the average value for each nuclide. The distribution is roughly exponential (the straight line in the figure) but closer examination reveals an excess of small widths. A distribution law with more physical significance than the empirical exponential has been suggested by Porter and Thomas, reference 5, and it is shown by the curved line in the figure. In Fig. 4–8 the same distributions are given as functions of $(\Gamma_n^0)^{\frac{1}{2}}$, which is more meaningful physically in terms of the nuclear wave function. In this figure the Porter-Thomas distribution is Gaussian, corresponding to their fundamental assumption for the magnitudes of the reduced amplitudes of these authors. Although not obvious in the figure, a statistical analysis of Porter and Thomas shows that their distribution is more likely than the exponential.

The ratio $\overline{\Gamma_n^0}/D$ can be obtained by averaging the parameters observed for individual resonances, which average is the integral of the observed neutron width as a function of neutron energy. The slope of this quantity gives the strength function but fluctuations limit the accuracy severely. It is also possible to get the strength function by cross-section measurements at higher energy because it is proportional to the average of that part of the cross-section curve

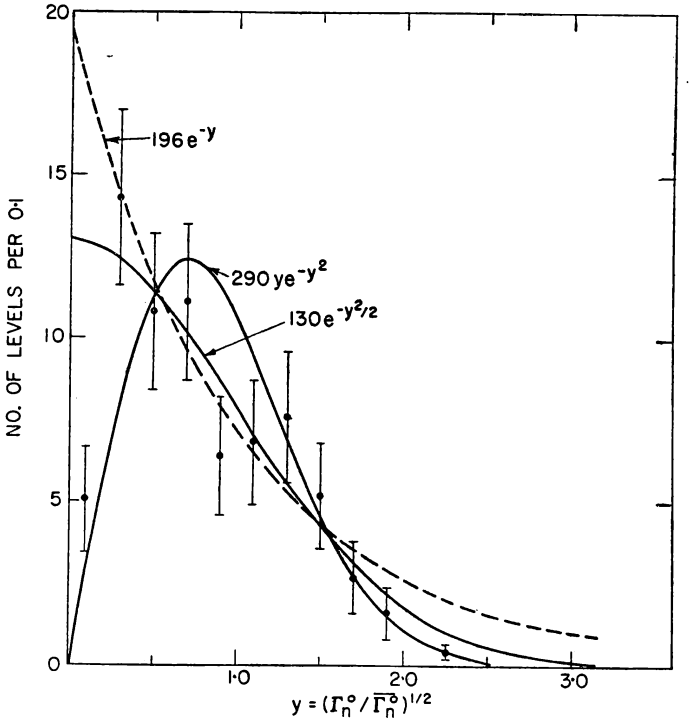

FIG. 4–8. The size distribution of neutron widths as a function of Γ_n, plotted relative to the average values for each nuclide.

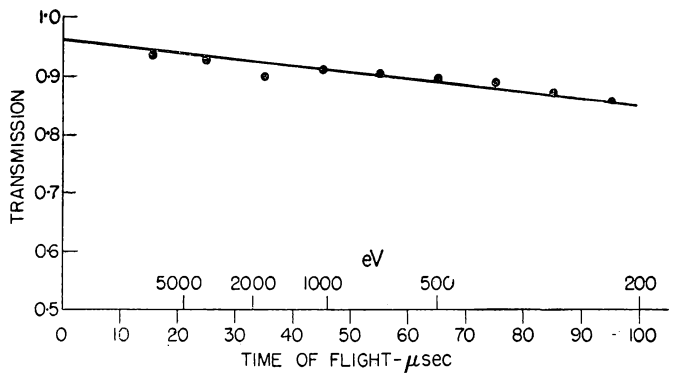

FIG. 4–9. The method of obtaining the strength function by means of the average transmission in the kilovolt region: the results shown are for U^{235}.

corresponding to resonances. Even though individual resonances cannot usually be observed at 1 keV it is still possible to separate that part of the *average cross section* representing resonances from that representing potential scattering. The separation is possible because the resonance contribution is proportional to $1/v$ or to time of flight for a velocity selector measurement, while potential scattering is constant in the region of several keV.

This recent method is illustrated in Fig. 4–9 for U^{235}. The slope of the straight line on the transmission plot gives the strength function directly, and the intercept gives the value of the potential scattering, although the latter is not obtained with great accuracy. The method is extremely simple as illustrated by the fact that the cross section averaged over resonances at 1 keV is simply $13{\cdot}0(\overline{\Gamma_n^0}/D) \times 10^4$ barns. A summary of the strength function results is given in Fig. 4–10, as

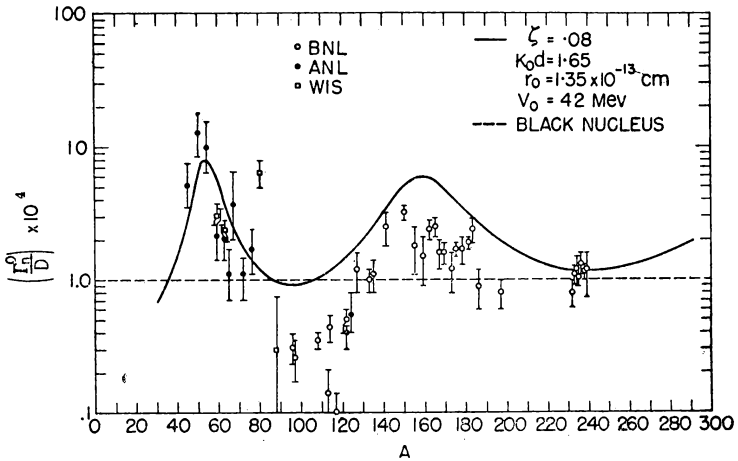

FIG. 4–10. The experimental values of the strength function, $\overline{\Gamma_n^0}/D$, as a function atomic mass, compared with calculations based on the cloudy crystal ball nuclear model, including the diffuse edge.

determined both from individual resonances and from the average cross section. The theoretical curves are based on the diffuse edge potential of Eq. (3–2); the agreement of experiment with theory is good but certainly not striking.

Nuclear Radii

The *potential scattering* which is the other item that can be determined accurately with slow neutrons, is of direct interest for nuclear models because it is intimately related to the size, shape and transparency of nuclei. Like the strength function, the potential

scattering can be measured not only in the region of a few volts but at higher energies also, where resonances cannot be resolved. At low energies, as shown in Fig. 4–11 for U^{238}, the potential scattering

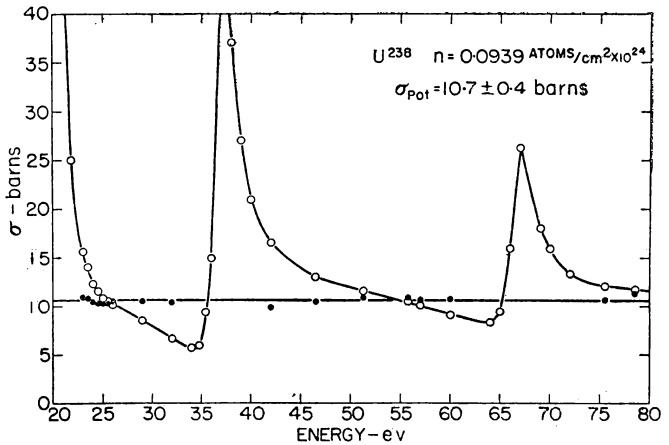

FIG. 4–11. Determination of the potential scattering, here for U^{238}, by correcting the measured cross section between resonances (open points) for the interference effects of nearby resonances; the curve obtained after correction is shown by the solid points.

is observed between resonances but is affected by the *interference* of the potential scattering with the resonance scattering, their amplitudes being added coherently. In the figure the cross section is shown as measured (open points) and as corrected by subtraction of the interference effects (solid points) by a computation involving the measured parameters of the nearby levels. The corrected curve is remarkably constant and represents accurately the potential scattering of 10·7 b for U^{238}.

At higher energy, measurement of the cross section for a thick sample gives a value that is almost the same as potential scattering because neutrons of the resonance energies are removed in the first part of the sample and do not affect the results. Small corrections for the residual resonance effects can be made, however. The calculated correction for U^{238}, for example, involves consideration of an average level in U^{238} at 1 keV and the total cross section as affected by Doppler broadening. The *computed* transmission curve, based on a potential scattering cross section of 10·7 barns, is given in Fig. 4–12, compared with the experimental results. The very close correspondence of calculated and measured values shows that the potential scattering in the energy region of several keV agrees within a few per cent of that obtained at low energy.

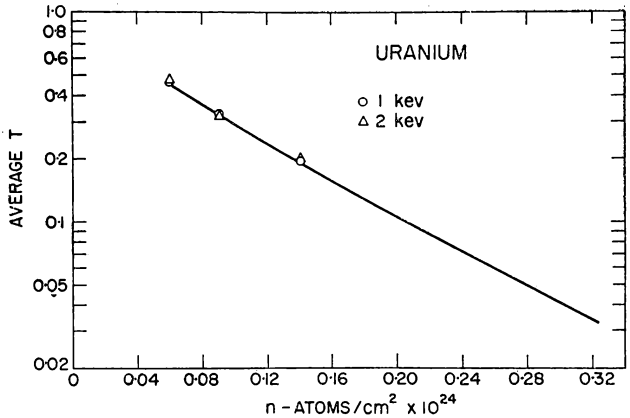

FIG. 4–12. The measured transmission of U^{238} for several neutron energies as a function of sample thickness, compared with the calculated curve based on resonance parameters and a potential scattering cross section of 10·7 barns.

The question of the relationship of the potential scattering thus determined to the *nuclear radius* is best discussed in terms of a specific nuclear model. This comparison is shown for the cloudy crystal ball model in Fig. 4–13, which gives the recent calculations including

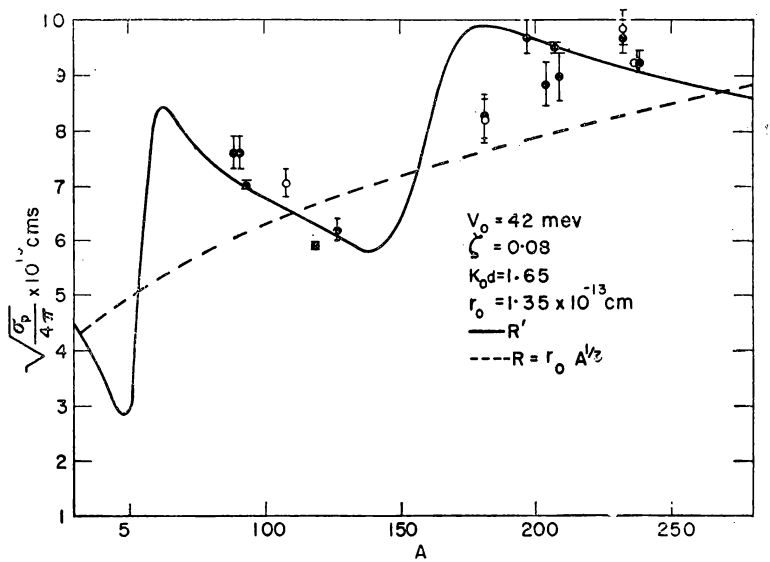

FIG. 4–13. Theoretical values of the nuclear radius, R, and R', the quantity that gives the potential scattering, as $4\pi(R')^2$, compared with experimental values of R'.

the diffuse edge modification, reference 7. The figure gives R', which is the "effective nuclear radius" for potential scattering, as well as the actual nuclear radius R, where R is the distance to the half-way point of the nuclear potential well (Fig. 3–9). The potential scattering is given in terms of R' by $\sigma_p = 4\pi(R')^2$.

The experimental values of Fig. 4–13, measured at Brookhaven, agree reasonably well with the theoretical curve, and thus not only justify the model but show that R is close to the value used in the calculation, namely $1{\cdot}35A^{\frac{1}{3}} \times 10^{-13}$. It is evident that further refinements of the model are necessary to fit all the points. In addition, it will be valuable to measure potential scattering for other nuclei, for which R' is appreciably different from R, in order to test the nuclear model in more detail. The ratio of R' to R is not greatly sensitive to the parameters of the model, however, hence the measurement of potential scattering can be considered to give good values of R, basing the conversion of the measured R' to R on the model. Interpreted in this way, the experimental points of Fig. 4–13 give a nuclear radius R, i.e., the distance to the half-way point of the potential, slightly larger than that used in the calculations, or about $1{\cdot}38 \times A^{\frac{1}{3}} \times 10^{-13}$ cm. This nuclear radius, which is the so-called nuclear reaction radius, is definitely larger than the electro-magnetic radius, as mentioned in Chapter 2, an effect that is usually interpreted as a manifestation of the finite range of nuclear forces.

APPLICATIONS OF RESONANCE PARAMETER DATA

In addition to their use in supplying raw material for the development of nuclear theory and for testing the results of theoretical predictions, neutron resonance parameters are finding an increasingly important role in practical applications. These applications are concerned with computations of reactor temperature coefficients, neutron reaction yields, self-protection effects, and related matters, for which measurements are not easily accessible. Because detailed information on resonance parameters has not been available until recently, these applications of properties of individual levels and the statistics of level parameters have not been pushed very far as yet. However, a rapidly increasing amount of theoretical work concerned with the parameters is becoming evident and practical results are being reached rapidly.

In some cases, particularly in reactor design, the effects of individual resonances can be very important. In this type of application the best possible parameters for one or a few resonances are of vital concern. An example of this application is the first resonance in plutonium, at 0·29 eV. As plutonium is built up rapidly in a uranium reactor operating at high specific power, the effect of this increasing amount

of plutonium on the *reactivity* can be quite important. For the plutonium level in question, for instance, the matter of the ratio of fission to capture is of great importance. If this level should have an unusually large fission width then a detrimental effect on the temperature stability of the reactor would result. For if the temperature of the reactor should accidentally rise appreciably the neutron energy will also increase and more neutrons will be found in the region of the 0·29 eV resonance. Under these conditions, if this resonance has an unusually large fission component, the rate of fission in the reactor will increase as well, which will in turn raise the temperature still more, this situation leading to temperature instability. On the other hand, if the level should have a large amount of capture relative to fission, just the reverse process would take place and the reactivity would decrease as the neutron "temperature" moved toward the 0·29 eV level. Thus the variation of the *temperature coefficient* of the reactor with its operating history depends very directly on the parameters of this one particular level in plutonium.

The parameters of other levels are also important to the understanding of the reactivity temperature coefficient, primarily because the Doppler effect causes the absorption to be a function of temperature. Long term changes in reactivity, which are of extreme importance to the successful design of a power reactor, also require resonance parameters for theoretical computation. A particular effect of resonances in a reactor, most important in a large reactor in which a dE/E spectrum obtains, is the so-called *resonance absorption integral*, where the integral extends from thermal energies to the highest energies found in the reactor. The resonance integral is important because it determines, for example, how many neutrons will be captured as they slow down from fission neutron energy to thermal, this absorption being very important in determining the reactivity of large reactors. Heretofor, resonance absorption integrals have been measured by experiments simulating the actual behaviour of the material in a reactor. However, these measurements have a weakness in that they do not at the same time give information on how the integral will change as the shape of the sample changes, as a result of self-protection effects. Thus a more complete understanding of the situation would be available if the resonance absorption integrals could be computed on first principles, from the parameters of individual resonances.

An example of the way in which the resonance parameters can give the integral with good accuracy is that of U^{238}. Here the resonance absorption integral can be calculated very simply from the parameters of individual references,

$$\int \sigma_\gamma dE/E = \Sigma \pi \sigma_0 \Gamma_\gamma / 2E_0 \ . \qquad (4\text{–}16)$$

For U^{238} the value calculated from the resonances up to 420 eV, those given in BNL 325, is 265 $\pm$ 12 barns. The additional contribution for the resonances above 420 eV can be calculated from the average resonance parameters, that is, the averages of the neutron widths, radiation widths, and spacings observed below this energy. This addition amounts to only 11 $\pm$ 3 barns, and the entire resonance integral is thus 276 $\pm$ 12 b. This resonance absorption integral is actually known somewhat better by this method than it is from direct measurements; furthermore the value computed from resonance parameters and the directly measured value agree within their errors. The advantage, of course, of the calculation using the resonance parameters is that it is possible to compute other quantities as well, such as the *effective value* of the integral for various physical conditions, as the shapes of uranium metal fuel, which are always sufficiently thick so that self-protection reduces the resonance absorption.

Another example of the application of measured resonance parameters is to the prediction of *capture cross sections* in the region of several kilovolts, where direct measurement is extremely difficult. Here the calculation can be made if the distribution of neutron widths, the average radiation width, and the level spacing are known. There is some difficulty in the calculation of course because the exact law for the spacing of the energy levels is not as yet known. However, an example of the accuracy with which the computation can be made is furnished by U^{238}, which is one of the few nuclides for which capture cross sections can be measured in the region of several kilovolts. The reason that the measurement can be made is that the final

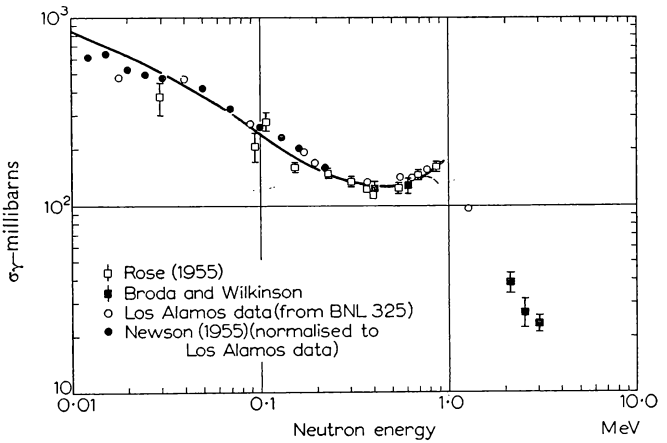

FIG. 4–14. The measured activation cross section of U^{238} compared with the value computed from the resonance parameters of this nuclide.

nuclide, U^{239}, has a beta activity of convenient half-life (23 min) and the cross section can be measured by activation, using Van de Graaff neutrons in the backward direction as source. For U^{238} the capture cross section computed by the resonance parameters agrees extremely well with that directly measured with Van de Graaff neutrons, Fig. 4–14, thus justifying the use of parameters in this way. It is necessary of course to assume that the parameters measured in the region of a few hundred volts will be the same as those in a few kilovolts but there seems to be no reason to suspect that any change should occur in this small energy region. It is of course necessary to estimate the contributions of higher l's with increasing energy.

These examples, although few and simple, are sufficient to show the way in which resonance parameters can be used to compute effects at higher energies where measurements are extremely difficult. The examples of practical significance occur for fissionable isotopes, which we shall consider in the next chapter. These are particularly important because the change of the ratio of capture to fission with increasing energy is directly related to the stability of reactors and their possibilities of breeding. Here again, however, if the parameters are well known as well as their distribution laws, from work at low energy, it is a simple matter to compute the cross sections to be expected in the region of several kilovolts. The prediction cannot go much above about 100 kilovolts, however, because higher l interactions become appreciable and it is difficult to compute their effects accurately.

REFERENCES FOR ADDITIONAL INFORMATION

1. J. M. Blatt and V. F. Weisskopf, *Theoretical Nuclear Physics* (Wiley 1952). Chapter VIII, pp. 379–485, extensive treatment of resonance theory; pp. 365–374, the semi-empirical level density formula; Chapter XII, pp. 639–651, theory of radiation widths.
2. L. B. Borst and V. L. Sailor, *Rev. Sci. Instr.* **24**, 141 (1953). Description and operating characteristics of a typical high-resolution crystal monochromator.
3. Feshbach, Porter, and Weisskopf, *Phys. Rev.* **96**, 448 (1954). The theory of the cloudy crystal ball and prediction of neutron cross sections, utilizing the sharp nuclear boundary.
4. J. S. Levin and D. J. Hughes, *Phys. Rev.* **101**, 1328 (1955). A summary of the experimental results on radiation widths of slow neutron resonances and comparison with theory.
5. C. E. Porter and R. G. Thomas, *Phys. Rev.* **104**, 483 (1956). Theory of the distribution laws of level parameters.
6. Seidl, Hughes, Palevsky, Levin, Kato, and Sjöstrand, *Phys. Rev.* **95**, 476 (1954). Description of the construction, operating characteristics, and typical results of the Brookhaven fast chopper.
7. V. F. Weisskopf, *Physica* **22**, 952 (1956). The prediction of various neutron cross sections based on the cloudy crystal ball with the diffuse surface, as well as a discussion of the basic theory of the model.

CHAPTER 5

RESONANCES IN FISSIONABLE NUCLIDES

IN THE previous chapter we have considered measurements of the parameters of neutron resonances and the relationship of the results to nuclear theory, limiting ourselves to the nonfissionable nuclides. We now turn to the heavy nuclides, in which the possibility of *fission* adds complication to the investigation of the properties of the cross-section resonances. In the energy region of fast neutrons there are no radically different problems for the fissionable nuclides as compared with the others, the fission cross section being measured much as any reaction cross section, usually by means of a fission chamber as a detector. As we have seen in Chapter 3, absolute measurement of any reaction cross section requires knowledge of the neutron flux, hence fission cross sections in the high energy region are affected by the same difficulty as any other reaction cross section. However, there are no other distinctly new problems and the fission measurements in the MeV region are similar to those of other reactions. The results as given in BNL 325 show some structure, which is probably related to various modes of fission as discussed later in this chapter, but the energy variations are much less abrupt than those in the eV region, with its complex resonance structure.

In the low energy region, however, where many resonances are observed, the matter of analysis of the fissionable nuclides involves great complexity. This complexity is a result partly of the presence of fission, introducing another parameter, the *fission width*, in the analysis, and partly because the many closely spaced levels makes determination of the parameters of the individual levels difficult. The latter difficulty is accentuated by the possibility that the shape of a level may be appreciably distorted by neighbouring levels because of the presence of *fission interference*.

Various special techniques have been devised for the study of fissionable nuclides in the resonance region and these, together with intensive effort by means of conventional techniques, have produced a large amount of information on the important fissionable nuclides. Although the state of knowledge of the parameters is still far from satisfactory, nevertheless great progress has been made recently and it now seems as if in a few years the parameters of the fissionable nuclides will be accurately known. Knowledge of these parameters is of great significance not only for the obvious applications to reactors

but because of the close relationship to nuclear theory. The importance to reactors is primarily in connection with the neutron interactions in the resonance region of the principal fissionable nuclei and the direct effect on such things as breeding gain and temperature stability. Even though fission has been known for a long time the theory of fission is still in a very unsatisfactory state, and the fission resonance parameters are greatly needed in testing present theory and helping to point the way to improved theoretical models of fission. After examining briefly some of the techniques for measurement of fissionable nuclides, we shall survey the present state of the level parameters and then their relationship to fission theory and various reactor applications.

TECHNIQUES FOR FISSION MEASUREMENTS

As for any reaction cross section, the fission cross section is much harder to determine than the total cross section. Actually most fission cross sections are merely measured relative to some cross section standard, either to some other fissionable nuclide or to a material whose cross section as a function of energy is known. The principle of the measurement relative to another fissionable nuclide is very simple for it involves only a measurement of the rate of fission of a given sample relative to the rate of fission of the standard, in the same neutron beam, as the neutron energy is changed. The most widely used standard for the measurement relative to a known cross section is boron, whose cross section is strictly $1/v$ in the resonance neutron region. The use of boron is somewhat more complicated than a fissionable standard, for the rate of fission in the sample under investigation must be measured relative to the boron (n,α) disintegrations as a function of neutron energy, and care must be taken that the relative efficiency for detection of α's and fission fragments does not change with energy. The relative fission cross section measured as a function of energy by either method can be put on an absolute scale by referring the cross section to the value at 2200 m/sec, which is now known rather well for most fissionable nuclides, as we shall see in Chapter 6. These 2200 m/sec values serve as very useful standards for measurements at other energies.

In measuring fission cross sections, the detector of the fission event is either an ionization chamber or a gas scintillation counter. Until recently, practically all measurements of fission cross sections had been made with *pulse-counting ionization chambers*. In this type of chamber the fissionable material is present as a very thin foil and the ionization produced by the fission fragment in the gas of the chamber is detected by means of fast electronic circuits. Because of the short range of the fission fragments, a few mg/cm^2, only a small amount of

fissionable isotope can be used in the chamber. The result of this limitation in amount is that the absolute efficiency of the fission chamber is very low, hence for the usual neutron velocity selectors the counting rate in the fission chamber is extremely small.

Although it is possible to increase the efficiency of a chamber by building a multi-plate chamber, a limit in the amount of material that can be placed in an ionization chamber is fixed by the alpha activity for many of the fissionable isotopes. The intense emission rate of alpha particles from U^{233} and Pu^{239} is such that only a few milligrams

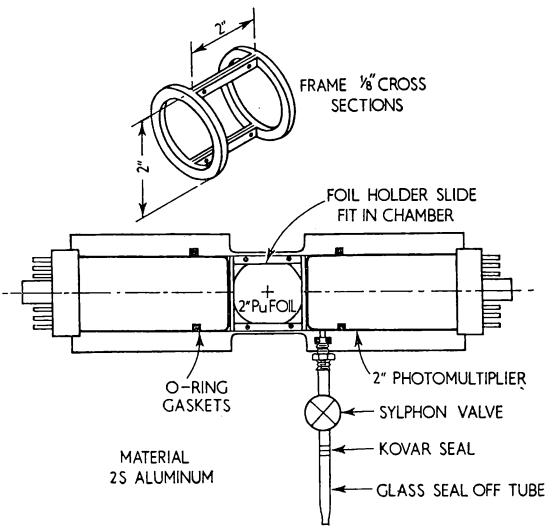

FIG. 5–1. The xenon-filled gas scintillation counter that enables larger amounts of plutonium to be used for fission measurements than is possible with a conventional ion chamber.

of material can be placed in the chamber without providing inordinate background from the pile-up of alpha particles. At the Geneva meeting in 1955 it was reported by the Soviets that they had been able to use as much as 22 milligrams of Pu^{239} in an ionization chamber by depositing the plutonium on thin nylon so that fission fragments would emerge into the gas on both sides of the film. The two fission fragments pulses were then added and better discrimination obtained against alpha pile-up in this manner.

A recent development that is of great value in the measurement of fission cross sections is the use of a gas scintillation chamber in which the ionization of the fission fragments causes a faint scintillation, which is then detected by a photomultiplier tube. Because of the great speed of the scintillation process and the photomultiplier tube,

the alpha pile-up is much less serious than for an ionization chamber and a hundred or so milligrams of Pu^{239} can be used in a typical chamber, Fig. (5–1). This type of detector will certainly be a powerful aid in the analysis of the fissionable nuclides of high specific α activity.

A method for obtaining fission cross sections that has been developed only recently but holds great promise involves the detection of the neutrons produced in fission rather than the fission fragments themselves. If a thin foil of fissionable nuclide is used and the

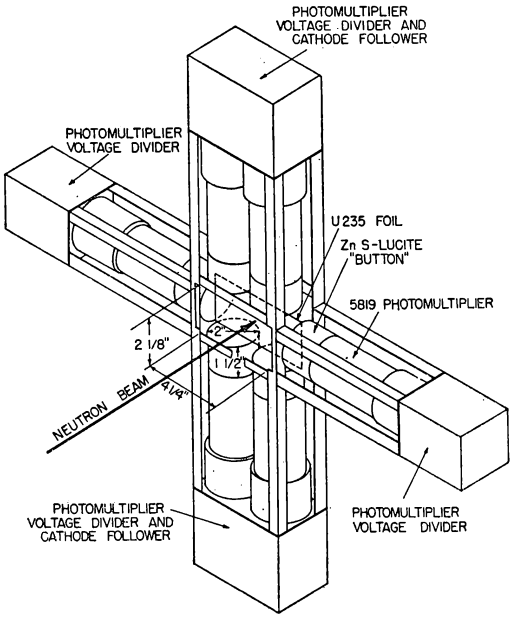

FIG. 5–2. The equipment used for the direct measurement of η by counting fission neutrons from a thick foil.

detector of fast neutrons is placed nearby, the counting rate in the detector will be a measure of the fission cross section. Actually the counting rate will be proportional to $\nu\sigma_F$ but as ν, the *number of neutrons per fission*, is constant with energy in the resonance region, σ_F is obtained. However, in order to get a higher neutron counting rate it is necessary to use a thick foil. In this case, the counting rate is not a measurement of the fission cross section, but rather a measurement of η, the *number of neutrons emitted per neutron absorbed.* In the so-called "direct η experiment" as developed at Brookhaven, Fig. 5–2, a foil is used that is of sufficient thickness so that all the neutrons stop in it. Under this condition, the flux incident on the foil, which can easily be measured with a thin BF_3

counter in the incident beam, gives the absorption rate of neutrons, and the counting rate in the fast neutron detector is then a measure of η:

$$\eta = k \frac{I_F}{\nu I_0} \quad . \tag{5-1}$$

Here k is a constant, for the measurement is a relative one, I_F is the counting rate of the fission neutrons, I_0 of the incident neutrons and ν the neutron velocity (because of the $1/\nu$ counter sensitivity).

The η experiment is particularly useful for very slow neutrons, but becomes more difficult to interpret as the neutron energy increases because a larger fraction of the incident neutrons are scattered from the foil. The simple equation given is based on the assumption that all neutrons hitting the foil are absorbed, an assumption that is quite accurate at low energy, where the scattering cross section is so small relative to absorption. Because it now seems certain that η is constant with energy, the η experiment can be considered a measurement of the ratio of the total cross section to fission, that is a measurement of $1 + \alpha$, where α is the *ratio of capture to fission*,

$$\eta = \frac{\nu}{1 + \alpha} \quad . \tag{5-2}$$

The neutron velocity selectors used for measurements of fissonable nuclides are the same as those described in Chapter 4 for the non-fissionable materials. However, because of the low counting rates of the fission detectors, a premium is placed on neutron flux, and those instruments that give high neutron flux, even though not of the highest resolution, are particularly valuable for the fission measurements. Also, because it is difficult to build fission detectors of a very large area, the type of instrument such as the Brookhaven fast chopper, which uses a small beam at the chopper but a large detector area, is not very appropriate. This velocity selector is particularly good for total cross section measurements of rare materials, but an instrument of smaller target area and larger area at the chopper itself, such as the crystal monochromator, is a better instrument for fission cross section measurements.

In analysis of a fissionable nuclide, measurements are usually made of the total cross section as well as of the fission cross section, or of the fission neutrons as in the η method. Actually, measurements of the three types are redundant, for only two of the three are necessary in order to give Γ_γ, Γ_F, and $g\Gamma_n$, in principle. However, because of the general difficulty of analysis of the fissionable isotopes, and some remaining uncertainties about the details of the methods, it is definitely advisable to measure as many types of cross

sections as is possible for the important fissionable isotopes. As we have seen for the non-fissionable nuclides, the total cross section gives the total width and the peak height of the levels. Analysis of these total cross-section results, as before, gives the values of $g\Gamma_n$ and Γ for the levels. From these total cross-section measurements alone there is no knowledge of the fraction of the total width that is capture and the fraction that is fission. Knowledge of α then gives all the information necessary to obtain the remaining parameters. Thus, in addition to the total cross section all that is actually needed is a measurement of α at each resonance or the fission cross section. The information thus needed, in addition to the total cross section, is supplied either by a measurement of the η type or by a fission cross-section measurement.

PARAMETERS OF FISSIONABLE NUCLIDES

Before considering the present theories of fission, it is well for us to discuss the experimental results in themselves. In this way we can examine the measured parameters alone, without prejudicing the results in terms of any theory. The analysis of fissionable nuclides is difficult not only because of the extra parameter, the fission width, but because of the complexity of the resonance curves. The complexity of the curves is not so much a matter of the absolute value of the spacing, although it is very small for U^{235}, for there are other isotopes that also have extremely small spacing. The difficulty arises because the shapes of the levels are not symmetric, and additional difficulties are thus caused in the analysis of the levels by standard methods. Still another difficulty has resulted from the lack of availability of samples of high isotopic purity. Fortunately this difficulty is becoming less important now, but accurate work has been hindered in the past by the difficulty of getting samples. We shall now examine briefly the results for the measured resonance parameters in the three important fissionable isotopes, U^{233}, U^{235}, and Pu^{239}, as they are reported in the first supplement to BNL 325. These results represent what are considered the "best values" based on all available measurements throughout the world. Unfortunately, in spite of the large amount of effort devoted to the fissionable isotopes, for many resonances results are available for a particular type of measurement from a single laboratory only, and the "best values" therefore do not represent the combined results of a large number of measurements.

U^{233}

Of the three fissionable isotopes that we are to consider, the information is probably the poorest for U^{233}, partly because this

isotope has not been the subject of intensive research, and partly because of the fact that good samples have not been available until recently. In Table 5–1 are given the resonance parameters for those levels in the energy region in which it is reasonably certain that all levels have been located. Levels are given to a somewhat higher energy in Supplement 1, BNL 325, even though it is almost certain that some levels are lost at these higher energies. The shape of the U^{233} cross-section near zero energy shows beyond a doubt that there is

TABLE 5–1

Resonance parameters of U^{233}. *The radiation width is taken as* 42 ± 8 *mV, based on the levels below* 4 *eV, and* g *is assumed to be* 1/2.

E_0 (eV)	Γ_γ (mV)	Γ_F (mV)	Γ_n (mV)	Γ_n^0 (mV)
< -0.5		270		
0.38 ± 0.05		400 ± 200		
1.785 ± 0.005	48 ± 13	260 ± 30	0·46	0.34 ± 0.03
2.290 ± 0.005	38 ± 8	60 ± 15	0·18	0.12 ± 0.01
3.21 ± 0.02			0·011	0.006 ± 0.002
3.29 ± 0.02			0·014	0.008 ± 0.003
3.61 ± 0.02	43 ± 9	155 ± 35	0·10	0.05 ± 0.01
4.43 ± 0.03			0·029	0.014 ± 0.004
4.74 ± 0.03			0·058	0.026 ± 0.007
5.90 ± 0.05			0·17	0.07 ± 0.01
6.80 ± 0.06			1·0	0.38 ± 0.06
8.63 ± 0.08		145 ± 25	0·06	0.021 ± 0.006
9.27 ± 0.05			0·14	0.047 ± 0.009
10.37 ± 0.07		250 ± 50	2·1	0.7 ± 0.2

a level at a nearby negative neutron energy, that is, a *bound state* close enough to zero energy so that it exerts a definite effect on the low energy cross section. A particularly interesting point in connection with U^{233} is the extremely small level present at about 0·3 eV. Even though individual laboratories had observed points slightly above the curve representing the other levels in this region, the finding was usually interpreted as insufficient evidence to prove the existence of a level. However, at the time of the Geneva meeting, when results from many countries were made available for comparison, it became obvious that a level actually was present at this point. The evidence is perhaps best shown in the curve for the fission cross section, Fig. 5–3.

The method used to get the parameters for U^{233} that are shown in Table 5–1 is one in which the total width and $g\Gamma_n$ are obtained from the total cross section curve. Comparison of the total curve with the fission curve then gives α, thus allowing a division of Γ into Γ_γ and

Γ_F. In this calculation the uncertainty in Γ arising from lack of knowledge of g is negligible, because Γ_n is so small compared to the other widths. In this manner Γ_γ is obtained for several levels and the average value, 42 $\pm$ 8 mV, is then assumed to apply to other levels. For these other levels, if both thick and thin sample measurements are made, Γ can be obtained even though the shape of each level cannot be determined. From the value of Γ thus obtained and the average Γ_γ it is then possible to compute Γ_F. The values for Γ_F shown in Table 5–1 were obtained in this manner, on the assumption of a constant Γ_γ of 42 mV for each level for which Γ had been measured.

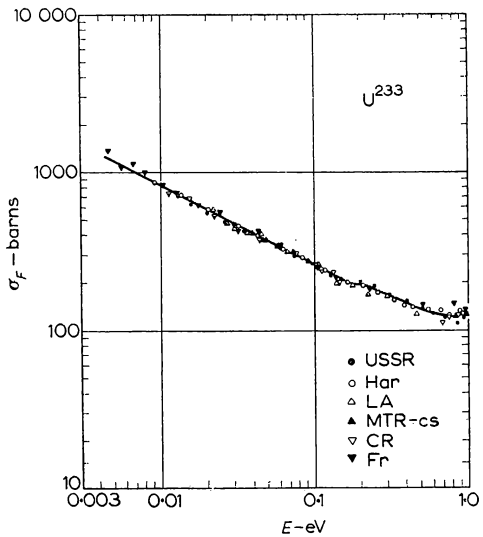

FIG. 5–3. The fission cross section of U^{233} in the low energy region, showing an extremely small resonance at 0·2 eV.

Even though the information thus made available on U^{233} is not very plentiful at present, the main characteristics of fissionable nuclides appear in Table 5–1, although with poor statistics. The neutron widths vary over a wide range, as they do for non-fissionable nuclides, and the fission widths as well show a wide range in size. In contrast, the radiation widths, as for non-fissionable nuclides, are almost constant from level to level. We shall return to the question of the range in size of fission widths in connection with U^{235} where the data are more plentiful, and also in connection with the theory of fission to be discussed shortly. One difficulty in analysis of resonances in fissionable materials is illustrated in U^{233} in connection

with the possible existence of a level at 1·45 eV. The shape of the curve, Fig. 5–3, that gives some evidence for a level at this energy can also be considered an asymmetry of the 1·8 eV level. This interpretation is related to the possibility that the fission component of various levels interfere constructively in contrast to the radiation components of the level, which are incoherent. We shall return to this question of possible *fission interference* shortly. Because of the weak nature of the evidence, no 1·45 eV level is listed in Table 5–1.

TABLE 5–2

Resonance parameters of U^{235}. *The radiation width is taken as* 33 ± 6 *mV, based on the levels below* 5 *eV, and* g *is assumed to be* 1/2.

E_0 (eV)	Γ_γ (mV)	Γ_F (mV)	Γ_n (mV)	Γ_n^0 (mV)
−1·4 ± 0·2	31 ± 4	200 ± 30		2·4 ± 0·3
−0·02 ± 0·1	34 ± 10	85 ± 20		0·002 ± 0·001
0·290 ± 0·005	39 ± 6	98 ± 7	0·0037	0·0069 ± 0·0002
1·13 ± 0·01	35 ± 8	107 ± 10	0·0146	0·0138 ± 0·0006
2·04 ± 0·03	31 ± 5	12 ± 3	0·0066	0·0046 ± 0·0002
2·82 ± 0·05			0·0026	0·0015 ± 0·0004
3·14 ± 0·02		115 ± 44	0·028	0·016 ± 0·001
3·61 ± 0·02		45 ± 24	0·053	0·028 ± 0·002
4·84 ± 0·02	25 ± 9	4 ± 2·5	0·054	0·025 ± 0·002
5·45 ± 0·10			0·022	0·009 ± 0·002
5·8 ± 0·1			0·016	0·0066 ± 0·001
6·1 ± 0·1			0·027	0·011 ± 0·002
6·39 ± 0·03	26 ± 14	27 ± 10	0·29	0·117 ± 0·009
7·10 ± 0·05		23 ± 18	0·11	0·041 ± 0·006
8·82 ± 0·07	38 ± 19	57 ± 11	1·3	0·43 ± 0·04
9·26 ± 0·04			0·12	0·040 ± 0·006
9·73 ± 0·04			0·04	0·013 ± 0·005
10·15 ± 0·04			0·064	0·020 ± 0·002
10·6 ± 0·1			0·033	0·010 ± 0·002
11·1 ± 0·1			0·045	0·014 ± 0·002
11·65 ± 0·07	35 ± 16	6 ± 3	0·7	0·20 ± 0·03
12·40 ± 0·07	39 ± 16	22 ± 6	1·4	0·39 ± 0·02
12·8 ± 0·1			0·050	0·014 ± 0·005
13·35 ± 0·07			0·099	0·027 ± 0·004
13·8 ± 0·1			0·15	0·040 ± 0·008
14·1 ± 0·1			0·20	0·053 ± 0·008
14·65 ± 0·07			0·15	0·040 ± 0·004
15·5 ± 0·1			0·23	0·059 ± 0·005
16·2 ± 0·1			0·34	0·084 ± 0·005
16·8 ± 0·2			0·27	0·067 ± 0·005
18·2 ± 0·2			0·34	0·080 ± 0·003
18·7 ± 0·2			0·20	0·046 ± 0·014
19·4 ± 0·2	45 ± 24	72 ± 11	2·9	0·66 ± 0·04

U^{235}

In contrast to U^{233}, the resonance results on U^{235} are the most complete of all the fissionable nuclides. The parameters given in Table 5–2 again are shown only up to an energy for which it is almost certain all levels have been found; levels at somewhat higher energy are given in the supplement to BNL 325, from which the parameters in Table 5–2 are taken. The neutron widths and total widths are again obtained using the techniques that are well established for non-fissionable nuclei, and the great range in Γ_n^0 is similar to those nuclides.

As for U^{233}, but for many more levels, total cross sections and fission cross sections have both been measured sufficiently well so that a complete analysis of the levels can be made. It is this complete analysis that gives the values of Γ_F, Γ_γ, and Γ_n for most of the levels shown in Table 5–2 for which all parameters are listed. The radiation widths thus obtained are constant within experimental error, and the average value of 33 $\pm$ 6 mV, determined from the lowest levels, can then be assumed to apply to all levels and subtracted from Γ in order to obtain Γ_F for several additional cases, for which Γ is known but for which accurate fission cross section results are not available.

Because of the excellent quality of the total and fission cross sections for U^{235}, as shown in Fig. 1–7 for example, there are sufficient results available that the two methods of obtaining the widths can be checked against each other. As the parameters given in Table 5–2 are the best values, utilizing all possible methods, some of them represent the combination of results of several measurements of the same quantity. It is interesting to compare the fission widths obtained by the method of assuming the constant Γ_γ of 33 $\pm$ 6 mV with the fission widths resulting from the combination of fission with total cross-section measurements. As an example, the fission width obtained for the 8·8 eV level is 60 $\pm$ 19 mV by the first method and 56 $\pm$ 11 by the second. For a small fission width, such as that for the 11·7 eV level, the first method is not accurate because of the subtraction of nearly equal quantities. It gives a Γ_F of 6 $\pm$ 19 mV compared with 6 $\pm$ 3 mV for the second method. The results for these two levels agree within the experimental error and are reassuring in their agreement, even though the two methods used are basically different.

The parameter distributions are similar to U^{233} but of higher statistical accuracy because of the greater number of levels. Again the neutron widths show a wide range in size and the fission widths also show this wide range. The fission width distributions, shown in Fig. 5–4, is of great interest to the theory of the mechanism of fission as we shall see in the next section. U^{235} is unusual in that the first

few levels have remarkably small neutron widths. This seems to be merely a statistical fluctuation in level size but gives an extremely small $\overline{\Gamma_n^0}/D$ ratio if only the first few levels are considered in computing the average ratio. When more levels are included in the average, the $\overline{\Gamma_n^0}/D$ is about normal for similar atomic masses, and as we have seen in the previous chapter, the technique of averaging in the kilovolt region gives about the same value of $\overline{\Gamma_n^0}/D$. This latter finding substantiates the conclusion that the weak levels at low energies in U^{235} represent simply a marked statistical fluctuation.

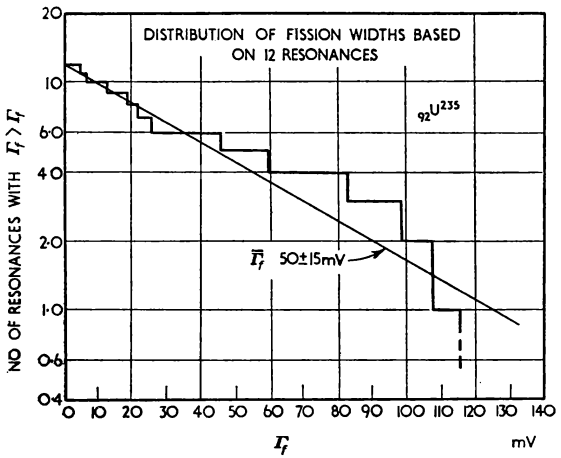

FIG. 5–4. The measured size distribution of fission widths in U^{235}.

The level spacing of U^{235} is extremely small, the value per spin state being only $1{\cdot}3 \pm 0{\cdot}1$ eV, one of the smallest of all observed level spacings. The asymmetry of some of the levels in U^{235} indicates, as it did for U^{233}, the possibility of interference effects in the fission component of the levels. Because of the complicated resonance structure, however, it is very difficult to reach a clear-cut decision on the presence or the amount of interference. This matter makes the analysis of the level structure, particularly for small levels, rather difficult because it is extremely hard to distinguish between an asymmetry of a level and the presence of weak levels near strong levels.

Pu^{239}

The results on this important isotope have been few for some time, primarily because of the difficulty of obtaining good samples. However, in the last few years the number of measurements on plutonium has increased and it now looks as if the information on plutonium will improve rapidly in the near future. The level spacing in Pu^{239} is

much greater than U^{235} so that it is possible to isolate individual resonances up to a rather high energy, about 50 volts. Table 5–3 gives the parameters for Pu^{239}, as they are reported in Supplement 1, BNL 325, and again we list only those levels in the energy range for which essentially all levels are resolved. The complete analysis of the levels of Pu^{239} has been handicapped by the intense alpha activity of the samples, which has made it very difficult to operate fission chambers with more than a few milligrams of Pu^{239}. However, the use of gas scintillation chambers, Fig. 5–1, has now enabled chambers

TABLE 5–3

Resonance parameters of Pu^{239}. *The radiation width is taken as* 40 ± 8 *mV, based on the levels below* 12 *eV, and* g *is assumed to be* 1/2.

E_0 (eV)	Γ_γ (mV)	Γ_F (mV)	Γ_n (mV)	Γ_n^0 (mV)
$0{\cdot}296 \pm 0{\cdot}004$	40 ± 5	58 ± 3	0·122	$0{\cdot}22 \pm 0{\cdot}01$
$7{\cdot}85 \pm 0{\cdot}03$	40 ± 9	32 ± 5	1·8	$0{\cdot}64 \pm 0{\cdot}06$
$10{\cdot}95 \pm 0{\cdot}05$	39 ± 12	116 ± 18	3·1	$0{\cdot}94 \pm 0{\cdot}09$
$11{\cdot}95 \pm 0{\cdot}05$	42 ± 12	20 ± 6	1·7	$0{\cdot}49 \pm 0{\cdot}06$
$14{\cdot}3 \pm 0{\cdot}1$		93 ± 22	0·8	$0{\cdot}21 \pm 0{\cdot}03$
$14{\cdot}7 \pm 0{\cdot}1$		30 ± 6	3·0	$0{\cdot}8 \pm 0{\cdot}1$
$15{\cdot}5 \pm 0{\cdot}2$		400 ± 200	0·8	$0{\cdot}20 \pm 0{\cdot}05$
$17{\cdot}7 \pm 0{\cdot}1$		40 ± 7	2·1	$0{\cdot}50 \pm 0{\cdot}05$
$22{\cdot}3 \pm 0{\cdot}1$	41 ± 15	30 ± 10	4·6	$1{\cdot}0 \pm 0{\cdot}15$
$23{\cdot}8 \pm 0{\cdot}2$		48 ± 15	0·2	$0{\cdot}04 \pm 0{\cdot}02$
$26{\cdot}2 \pm 0{\cdot}2$		30 ± 10	2·9	$0{\cdot}58 \pm 0{\cdot}09$
$27{\cdot}6 \pm 0{\cdot}3$		5 ± 3	0·3	$0{\cdot}06 \pm 0{\cdot}02$
$32{\cdot}3 \pm 0{\cdot}5$		190 ± 60	0·4	$0{\cdot}07 \pm 0{\cdot}02$
$35{\cdot}3 \pm 0{\cdot}6$			0·4	$0{\cdot}07 \pm 0{\cdot}02$

to be built containing sufficient Pu^{239} so that accurate fission cross-section curves can be obtained.

It is also possible to use the η experiment and thus get around the difficulty of the high alpha specific activity, which of course has no detrimental effect in the η experiment because it is not necessary to detect fission fragments. The errors given in Table 5–3, particularly for the fission widths, illustrate that the results of various experimenters on Pu^{239} do not agree as well as would be expected from the accuracy of the measurements themselves, which are primarily of σ_T, σ_F, and η. The poor agreement of results may reflect some unknown sources of error in the measurements, or perhaps uncertainties in the parameter analysis somewhat larger than estimated by the experimenters. It is obvious that more work needs to be done with Pu^{239} to reduce the difference in quoted parameters for the different experimental methods. The $\overline{\Gamma_n^0}/D$ ratio for Pu^{239} is

$1{\cdot}0 \pm 0{\cdot}2 \times 10^{-4}$, in very good agreement with U^{235} and other heavy elements. The general characteristics of the parameters for Pu^{239}, as shown in Table 5–3, are similar to those of the other two fissionable isotopes, with the radiation widths constant from level to level, while the neutron and fission widths show extremely large variations.

THEORY OF FISSION CROSS SECTIONS

The theory of fission constitutes a rather extensive field of research in itself for there are many aspects of the process of fission that require detailed theoretical treatment. Thus there is the analysis of the excitation modes leading to fission, the mechanism that determines the resulting division of mass and charge found in the fission fragments, the emission of neutrons from the fragments while still in motion, and the radioactive decay of the fragments by alpha, beta and gamma rays, and in some cases, delayed neutrons. We are not directly concerned with the theoretical treatment of these matters, but only with cross sections of fissionable materials, and the part of the theoretical picture that determines these cross sections. We are interested in the predictions concerning the parameters of resonances on the basis of current theory and how well the experimental results verify that theory.

Before considering the present theory, it is useful to recall what was predicted from existing fission theory before detailed results of resonance analysis were available. In the '30s, when fission was first being discussed theoretically, the extreme compound nucleus model of nuclear reactions was the basis of the development. It was expected that fission would take place in a compound nucleus much faster than gamma emission, hence that the fission width would be much larger than the radiation width. As a result, it was something of a surprise when it was discovered that the fission width was not significantly larger than the radiation width, that is, that radiation could effectively compete with fission. According to the early theoretical views it was also thought that the fission width would be about the same from neutron resonance to resonance. Experiments performed at Los Alamos during the war, however, showed not only that radiation could compete with fission but that the *ratio of radiation to fission*, usually denoted α, varied markedly from level to level, reference 5.

The experimental results now available give sufficient detail about radiation, neutron, and fission widths, particularly for U^{235}, Table 5–2, to allow a reasonably detailed comparison with theoretical predictions. Fortunately there has been sufficient work on radiation widths for many non-fissionable nuclei so that the general properties

of radiation from the highly excited states formed by neutron capture are well known. As we have seen in Chapter 4, the radiation widths for various levels of a single nucleus are remarkably constant from level to level, the differences being only of the order of magnitude of experimental error.

The constancy of radiation widths from level to level is not surprising when considered in the light of the usual interpretation of gamma emission. At excitation energies in the region corresponding to neutron binding, the level density is high enough so that many levels are available as final states for gamma emission, probably of the order of hundreds of states. With so many final states available, the most rapid type of emission, *electric dipole*, will almost certainly take place and the observed Γ_γ will be the sum over the *partial radiation widths* to the individual final states. Because of this averaging over hundreds of final states it is not at all surprising that the observed radiation width is so nearly constant for each level. Thus for emission of radiation the single value of the radiation width observed is associated with the many possible final states, hence many *exit channels* in the usual terminology. The existence of many exit channels of course implies that the cross section will not be coherent, that is, that the contributions from different resonance levels at a given point in the cross-section curve will add *incoherently*. In other words, for neutron capture the cross sections will add rather than their amplitudes.

The observations on neutron widths for many nuclides, on the other hand, show that within a single nuclide the neutron widths of various levels differ by extremely large factors. In contrast to the radiation width, this large spread in magnitude is associated with the unique nature of the neutron emission in each level, with only one final state being available, and as a result only a single *exit channel* existing for the reaction. Because of the single channel for neutron emission, the scattering cross section is a coherent process and its value at a given point is made up of *coherently* added contributions from various levels. Here again, as for the radiation widths, the observed behaviour of the widths is consistent with what is expected theoretically, for in the case of neutron emission a single final state is implied for energetic reasons, in contrast to the many final states for emission of radiation.

For fission the expectation had been that the process more closely resembled radiation than neutron emission, the reason being that the presence of many possible *fission products* was similar to the many possible final states in radiation rather than the single final state possible in elastic scattering. However, it is obvious that the fission width distribution of Fig. 5–2 resembles much more closely the

typical neutron width distribution than the single value typical of radiation emission. Judging from the distributions of widths only it would be concluded that fission is much more nearly like neutron emission than radiation, in spite of the large numbers of fission products.

Before turning to the question of the manner in which fission can be considered a unique process rather than an average over many final states, it is well to consider how closely the *fission width distribution* resembles that of the neutron widths. The exact shape of the neutron width distribution is of great importance in deciding the number of exit channels that are available in the reaction. The neutron width distributions of Chapter 4 for a number of non-fissionable nuclides have been discussed in detail by Porter and Thomas, in reference 5 of Chapter 4. Their discussion concerns the widths for a process in which only one exit channel (one *degree of freedom* in their notation) is possible, such as is true for the neutron widths corresponding to elastic scattering.

At the other extreme, a process in which several hundred exit channels are possible gives a distribution in which only a single width is found, as for radiation widths. If a process has a small number of exit channels, a distribution intermediate to those found for neutron widths and gamma ray widths would be expected. The fission width distribution found in U^{235} is actually slightly concave downward indicating a slight tendency toward the gamma ray distribution and leading one to expect a small number of exit channels rather than a single channel. A complete analysis of the observed fission widths of U^{235} has been carried out by Porter and Thomas who find that the most likely number of channels is $2{\cdot}3 \pm 0{\cdot}8$. It is certainly true that the number of channels in fission is small but the present data are not sufficiently accurate to fix the number of exit channels with high precision.

Another way of getting at the number of exit channels in fission is by use of a relation discussed by Wheeler in reference 5,

$$\frac{\bar{\Gamma}_F}{D} = \frac{N}{2\pi} , \tag{5–3}$$

where N is the "number of levels available to the nucleus in its critical state", i.e. the number of exit channels. If the numbers found for U^{235} are substituted into this relationship it is found that a value of $N = 0{\cdot}24$ is obtained. While the quantitative accuracy of Eq. (5–3) is probably not to be taken too seriously, the numerical result certainly seems to be that the number of exit channels is extremely small.

It should be possible to get more information on the nature of the

fission process, in particular the number of final states and exit channels involved, by means of other experiments. In general, if fission were a process that is an average over many final states in the normal sense, then it would be expected that particular properties of fission, such as the fission product mass distribution, the number of neutrons per fission, or the number of delayed neutrons, for example, would be the same in each neutron resonance.

Some evidence is available on the fission mass distribution and the delayed neutron yield as functions of neutron energy but both these quantities seem to be constant with neutron energy, implying no change from level to level. Recent accurate measurements of η, the number of fission neutrons per neutron absorbed, have been made for several fissionable isotopes. These measurements show large changes in η with energy but of course this variation is simply a matter of the different values of Γ_F from level to level. Recent direct measurements of ν reveal that it is accurately constant from level to level, hence the η variation is caused solely by changes in Γ_F from level to level. These results, as well as less precise ones indicating that fission product and delayed neutron distributions are the same in each level, indicate that fission is an *average* process, at least as far as *final* products are concerned, in spite of the small number of exit channels.

A conclusion to be drawn if the number of channels in fission is small, and one that could be checked experimentally, is the coherence between fission from level to level, leading to *resonance-resonance interference* effects. Unfortunately, these interference effects are extremely difficult to detect, and at the present time the situation is not at all clear as to the reality or amount of interference. The presence of two spin states and the possibility that only *part* of the fission components of the levels interfere, because of more than one channel, make the "theoretical" amount of interference extremely difficult to compute.

The fundamental theoretical problem that arises in connection with the experimental results is the explanation of the very small number of exit channels in fission in spite of the large number of fission products that are formed at each level. The entire fission product mass distribution is formed in each neutron resonance level, yet in spite of this large number of *final products*, the number of *exit channels* is certainly extremely small. The recent theories of fission picture the process as one that is much simpler than had been envisaged in the past, and in this way the experimental results seem more reasonable. Instead of a highly excited nuclear state, the fission process in the recent theories is one in which the nucleus has a very simple excitation, one that can be described by a very small number of quantum numbers. Corresponding to this simple

excitation there are only a few exit channels, and it is only after these exit channels are passed that the formation of the hundreds of different fission products take place. In this concept of the fissioning nucleus as "cold" at the passing of the saddle point, which defines the "exit", most of the excitation energy exists as energy of deformation. The simplicity of the excitation, similar to low-lying rotational states, predicts correctly some of the properties of fission by high energy neutrons and gamma rays, particularly the structure in the fission curve for neutrons at about one MeV energy, Fig. 5–5, and the angular distributions, as discussed in reference 2.

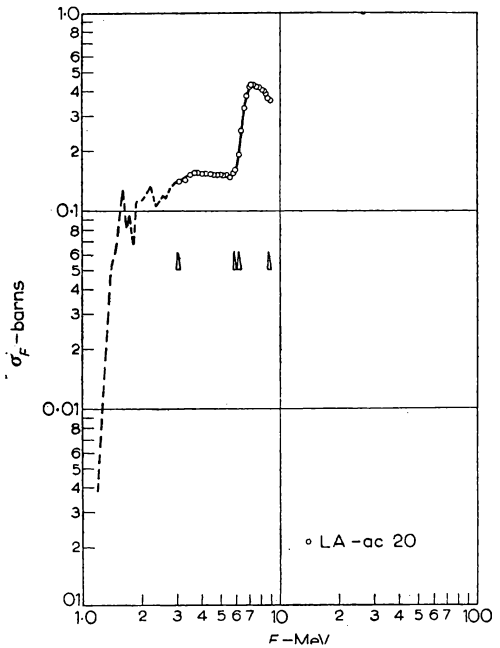

FIG. 5–5. The fission cross section of thorium for fast neutrons, illustrating the "fine structure" in the vicinity of 2 MeV and a rapid rise in cross section near 6 MeV.

Related to the simplicity of the nuclear excitation, current fission theories predict that the properties of fission will depend strongly on the spin of the compound nucleus. Thus if slow neutrons are above the *fission thresholds* for both spin states, differing in energy by about one MeV, there should be two types of levels involved. If thermal neutrons are above threshold for only one spin state, however, all the observed levels should have the same spin. From the known

results for U^{235}, however, there seems to be no evidence for two types of levels occurring in fission, all the parameters apparently being members of one smooth distribution. The other possibility that only one spin state is present unfortunately cannot be checked at the present time, but seems extremely unlikely for levels should then be seen that have zero fission width, i.e., levels with capture but no fission—and no such levels are known. Spin determinations of the various levels can be made if the scattering cross section of the resonances can be measured but this is very difficult in U^{235} because of the small value of Γ_n and hence the small peak height of the scattering resonances. Another possibility is that the levels of one spin state might have such large fission widths that they become a constant background in the fission cross section. Some such background fission cross section is present, especially in plutonium, but its magnitude is much too low to be ascribed to the spin state other than that represented by the sharp levels.

While direct measurements on a number of interesting predictions of the current fission theories unfortunately cannot be made at the present time because of experimental difficulties, the rapid accumulation of data of various types will certainly prove to be very useful in checking the detailed predictions of the recent theories. As far as practical applications of the resonance parameters of fissionable nuclides are concerned, however, experimental data are sufficiently extensive, in the case of U^{235} at least, to justify use of the results in computation of effects important to reactor design.

APPLICATIONS OF FISSION PARAMETERS

As the first nuclear reactors built were large and well-thermalized, it was not necessary to know resonance parameters of their various components with great accuracy in carrying out their design. Thermal cross sections were of greatest importance, and the absorption of neutrons during the slowing-down process, in which the dE/E spectrum was attained, was handled simply by means of *resonance integrals*. For sufficiently dilute material the resonance integral, which could usually be simply measured by a cadmium ratio for activation, gave correctly the absorption that would take place during the slowing down process. For a few materials in which self-protection was important, primarily the large, well-separated natural uranium fuel rods, the *effective resonance integral* was known sufficiently accurately from a semi-empirical formula, containing a surface term and a mass term. In none of the theoretical work was it necessary to consider the detailed resonance structure of the materials, and the necessary quantities could be measured by integral-type experiments using reactor neutrons of broad energy spread.

However, for the reactors now being designed it is extremely important to have accurate information on the detailed parameters of individual resonances. Some of these reactors contains neutrons predominantly in the intermediate energy region rather than at thermal, and for them the reactor behaviour is critically dependent on the parameters of the levels. Even for thermal reactors, however, the question of the temperature stability of modern highly enriched reactors is critically dependent on the resonance parameters. The great importance of the first level in plutonium to the temperature coefficient of a high power reactor was considered in the last chapter. The temperature coefficient is also dependent on the properties of other levels as well, in U^{235}, U^{238}, and Pu^{239}, particularly because of the way in which a large change in temperature affects the absorption of these levels via the Doppler broadening of the levels. In these calculations the necessity for accurate parameter information, rather than average cross sections alone, arises because self-absorption is very serious for the enriched fuel that is used, compared with the older type reactors in which large fuel rods of ordinary uranium, surrounded by large amounts of excellent moderators, were used. In the old geometries, various simple approximations were sufficiently accurate for reactor design. However, with modern highly enriched reactors, it is necessary to compute the details of the resonance absorption during slowing down, including self-protection effects, because simple approximations do not work for such closely spaced, highly enriched lattices.

A further difficulty in the high power reactors is that it is necessary to compute the effects of higher isotopes such as Pu^{240}, Pu^{241}, Pu^{242}, etc. These materials are not available in large amounts as yet, hence integral- or average-type experiments cannot be made with them. Even if these measurements could be made, it is much more desirable to know the actual resonance parameters so that the important effects of these higher isotopes can be accurately computed for reactors that operate at a high flux density. The long-term changes in reactivity and the changes in temperature coefficient with operation history both depend strongly on the resonance parameters of the higher isotopes, hence it is very important to obtain this information, even though it is difficult as yet because of the small amounts of the isotopes that are available.

Reactor calculations for neutron energies at which parameters are known for individual resonances can be made by utilizing the measured parameters, resonance by resonance, directly in the computations. However, it is often necessary to use various cross-section values in the calculations at energies where the resonance parameters have not been measured as yet because of insufficient

resolving power. In these higher energy regions it is necessary to resort to computations based on the knowledge of parameters at lower energy. Thus the observed distribution laws for spacings, neutron widths, radiation widths and fission widths, if assumed to apply at higher energy, can be used to calculate *average* values of such quantities as fission, capture, η, and α. The fact that average quantities are computed is no great detriment for in the reactors themselves the neutron distribution is spread over many decades and cross sections with higher resolution are hardly needed, the average quantities being sufficiently accurate for the calculations. Level parameters must still be known, even to compute the average cross section, however, because self-protection effects are usually important, and their computation requires knowledge of the parameters, though the distribution laws alone are usually sufficient, as described in reference 1.

The question of the applicability of the distributions of parameters, obtained at low energy, to higher energy causes some difficulty. For an energy change of a few kilovolts, the only known variation in level properties is an increase in neutron width in proportion to the neutron velocity, a well-established effect. The calculation made in this way of course cannot be extended with complete confidence to energies so high that higher l collisions are important, for the parameters appropriate to $l = 0$ may not apply exactly to higher angular momenta as well. However, the limitation to $l = 0$ is not extremely serious, for the most important energies for reactors are usually in the $l = 0$ region. The very high energy regions, that is several MeV, can be handled in a different way, for there the availability of Van de Graaff neutrons means that most of the important quantities, primarily fission and inelastic scattering, can be directly measured and hence made available for the calculations. Furthermore, the levels are so close and weak in the MeV region that individual levels are neither seen in the measurements nor needed in the calculations.

A particularly important quantity for the design of power reactors is η, the number of neutrons produced per neutron absorbed. The importance of η is related to its function in determining the neutron *economy*, i.e., the possibility of breeding or conversion. In terms of nuclear constants, η is given by Eq. (5–2) as $\nu/(1 + \alpha)$, with α the ratio of capture to fission. As ν is almost certainly constant it follows that knowledge of α, whether by measurement or calculation, gives the information required to obtain η. Fortunately, α is well-known for the fissionable nuclides at thermal energy as we shall see in the next chapter. The experiments to measure η (or α, if ν is constant) can be used at energies somewhat above thermal, but for energies above a few volts, direct measurements suffer difficulties inherent in

the method, such as excessive scattering. For those resonances for which all parameters are known, the value of α is of course also known automatically. However, as seen in the tables of the present chapter, there are very few resonances in the fissionable nuclides for which all the parameters have been obtained.

In view of the lack of data on resonances at high energy, it is fortunate that α can be computed from the information now available on the properties of resonance parameters of levels at low energy, that is, their average values and distribution laws. Even though these distribution laws are not known with great accuracy, the value of α thus computed as a function of energy is in reasonably good agreement with the few measured values of α at higher energy that are available. These measurements, at several keV, have been made within reactors and are averages, and rather crude averages at that, over given energy regions. However, these average values are suitable for comparison with the computed values of α and it is here that the reasonable agreement is reached. The comparison is possible only for U^{235} for it is only with this nuclide that even crude measurements are available for α in the energy region of several kilovolts. The observed agreement justifies the use of the method of calculation for the other nuclides for which α measurements are not available, and the resonance results not as complete as they are for U^{235}.

A matter of extreme importance in high-power reactors is that of the long term changes in reactivity. These changes are a result of the destruction and formation of various nuclides within the reactor, for example the burnout of strong neutron absorbers, and the buildup of fission products and of higher isotopes of plutonium, for example. Because of the limited availability of such materials as fission products and higher isotopes, it is difficult to make integral measurements on them. Fortunately, resonance parameters can usually be measured with rather small amounts of material and measurement of individual resonances in these important materials, which are available only in such small amounts, gives the required information so that their effect on reactivity as a function of time can then be calculated. Unfortunately, at the present time even the small amounts needed for resonance analysis are not available for many of these materials and the results are not known as yet. In the case of the fission products there is of course the additional complication that they are extremely radioactive and as a result their handling is difficult.

REFERENCES FOR ADDITIONAL INFORMATION

1. H. A. BETHE, article on "Theoretical Analysis of Neutron Resonances in Fissile Materials" in *Physics and Mathematics*, Vol. I, *Progress in Nuclear*

Energy Series (Pergamon Press, 1956); discussion of the theoretical implications of the observed level parameters of fissionable nuclides and the use of the parameters in predicting behaviour of these nuclides at higher energy.

2. A. BOHR, *Proceedings of International Conference on the Peaceful Uses of Atomic Energy* (United Nations, New York, 1956) Vol. 4, p. 151; the theory of fission as a process involving simple nuclear excitation and the predicted behaviour of fission parameters as a function of spin.
3. P. A. EGELSTAFF and D. J. HUGHES, article on "Resonance Structure of U^{233}, U^{235}, and Pu^{239}" in *Physics and Mathematics*, Vol. I, *Progress in Nuclear Energy Series* (Pergamon Press, 1956); a review of the experimental methods and results for level parameters.
4. J. A. HARVEY and J. E. SANDERS, article on "Summary of Data on the Cross Sections and Neutron Yields of U^{233}, U^{235} and Pu^{239}" in *Physics and Mathematics*, Vol. I, *Progress in Nuclear Energy Series* (Pergamon Press, 1956); reviews all measurements up to 1 eV. Whereas much of the material is appropriate to Chapter 6, the discussion of the measurements of η and ν as functions of energy is pertinent to the present chapter.
5. J. A. WHEELER, *Proceedings of International Conference on the Peaceful Uses on Atomic Energy* (United Nations, New York, 1956), Vol. 2, p. 155; a historical review of fission theory and discussion of possible spin effects in level parameters predicted by current theory.

CHAPTER 6

THERMAL NEUTRONS

THE AMOUNT of work that has been done with thermal neutrons is indeed impressive, especially when one recalls that they represent an extremely small spread in energy compared with the enormous range available with pile neutrons. Actually, although the energy range represented by the thermal distribution is usually considered rather wide, in absolute units it is only a few hundredths of an electron volt—thus the entire thermal spread of energy is narrower than the usual neutron resonance, typically with a 0·1 eV width. It is thus easy to realize that cross sections measured with thermal neutrons, while very important to reactor behaviour and as tools for solid state physics research, do not have an important applicability to nuclear theory. Actually, they contribute only single points on the curves of cross section versus energy hence are not of great value in determining properties of nuclear energy levels. The entire resonance cross section curves, considered in Chapters 4 and 5, are the primary sources of information for energy level parameters determined from neutron properties. However, for a few specific cases, for example the neutron-proton and neutron-electron scattering, thermal neutron measurements have an important bearing on nuclear theory.

However, even though thermal neutron cross sections are essentially only points on cross section curves, the experimental uses of thermal neutrons are widespread and constitute by far the vast majority of experimental measurements made with reactors. Here we are not concerned with the great range of *uses* of thermal neutrons, for example as sources for neutron diffraction studies of the atomic structure of matter, in the manufacture of many radioisotopes for basic research and practical applications, to promote chemical reactions, and even to treat disease.

Our concern is with the cross sections measured with thermal neutrons. While many of these are essential to the applications just mentioned, the major use of these cross sections is in connection with reactor design, in which it is often necessary to measure with great care the energy variation of cross sections within the thermal energy region itself. For certain reactor applications, it is desirable to determine special types of average cross sections, which we shall consider later. In connection with neutron diffraction applications, it is necessary to measure several special types of cross sections,

which are of particular importance in the thermal region. These cross section types refer to the optical properties of neutron scattering, properties that are predominant in the low energy region where the wave properties of neutrons are particularly evident.

We shall first consider some of the optical principles of the scattering of slow neutrons, then go on to the matters of thermal neutron sources and the types of measurements made with them. Finally, after some special attention to the thermal cross sections of fissionable nuclides, we shall conclude with a brief description of a special type of cross section, for the interaction in which the neutron gains energy from the crystal lattice vibrations in the process of being scattered. A type of thermal neutron interaction that will not be our concern here is the magnetic scattering of neutrons and the associated neutron polarization that can be produced by the magnetic effects. The main use of the magnetic scattering of neutrons is the determination of the magnetic structure of such materials as ferromagnetic iron, the ferrites, and the recently investigated anti-ferromagnetic materials, described in references 2 and 5.

OPTICS OF SLOW NEUTRON SCATTERING

In the "Thermal Cross Sections Table" of BNL 325 the particular types of cross sections that are listed are included primarily because of their applications. The coherent cross section, for instance, is used mainly in connection with neutron diffraction and, while we are not concerned with diffraction as such, it is worth our while to consider the nature of *coherent* and *incoherent* cross sections. The other types of cross sections listed, absorption, activation, bound atom, and scattering, also have definite uses, as we shall see. It is also necessary to consider to some extent the principles of measurement of the different thermal cross sections listed, because their very meaning and the accuracy of the quoted results can be understood best in connection with the description of the measurement techniques themselves.

In many respects the behaviour of slow neutrons, for which the wave characteristics predominate over those of particles, is closely analogous to that of light or X-rays. For most reactors, the neutrons present in highest intensity are those in thermal equilibrium with the graphite moderator, hence with a wavelength of about one Ångstrom. The analogy with X-ray behaviour is thus particularly close because of the similar wavelength. There are distinct differences between neutron and electromagnetic optics, however, and it is because of these differences that neutron optics has distinct applications at the present time. The two most important of these differences are the more numerous sources of incoherence and the magnetic interaction

present in neutron scattering. The incoherent scattering that arises from "spin-flipping", for instance, is a powerful tool for investigation of the neutron-proton force, as is magnetic scattering for study of ferromagnetism, antiferromagnetism, and paramagnetism.

In calculation of the X-ray intensity in crystal diffraction, the departure of the atoms from their average positions causes a decrease in the intensity of the coherently scattered X-rays present in the Bragg peaks. This same effect occurs for neutron scattering, and, in addition, there is a possible incoherence that occurs even for scattering from a single nucleus. This latter incoherence, defined as the incapability of interference for the scattered wave, is related to the possibility of change of the nuclear spin with simultaneous "flip" of the neutron spin.

The various types of incoherence in neutron scattering can be computed from the appropriate scattering *amplitudes* for each process, Eq. (2–10), representing the distance the neutron wave is shifted by the scattering nucleus. The differential scattering cross section is given by the square of the amplitude, a, and the "total scattering" cross section by $4\pi a^2$ if the scattering is isotropic, as given by Eq. (2–12). For nuclear scattering of neutrons by bound nuclei the angular distribution is isotropic if the nuclei scatter independently. Even though in practice interference effects are marked, they can be eliminated by calculation and the scattering cross section of individual "independent" nuclei obtained.

For any nucleus of nonzero spin, there will be two amplitudes, a_+ and a_-, corresponding to the two possible spins of the compound nucleus, $I \pm 1/2$, formed by combination of the neutron with the target nucleus of spin I. The compound states are not equally probable but are weighted in the ratio $(I + 1)$ to I, hence the *coherent amplitude*, which is the weighted mean of the two amplitudes, is just

$$a_{\text{coh}} = \frac{I+1}{2I+1}\, a_+ + \frac{I}{2I+1}\, a_- \ , \tag{6–1}$$

and the *coherent cross section*, neglecting interference with other nuclei, will be given by $4\pi a^2_{\text{coh}}$. As the total intensity is the sum of the contributions of the spin states, the *total amplitude* is given by,

$$a_t = \left(\frac{I+1}{2I+1}\, a_+{}^2 + \frac{I}{2I+1} a_-{}^2\right)^{\frac{1}{2}} . \tag{6–2}$$

Finally, the *incoherent amplitude* is obtained from the difference between the total intensity and the coherent intensity ($a^2_{\text{inc}} = a_t{}^2 - a^2_{\text{coh}}$),

$$a_{\text{inc}} = \frac{\sqrt{(I(I+1)}}{2I+1}\, (a_+ - a_-) \ . \tag{6–3}$$

The "total scattering" cross section and the incoherent scattering cross section will of course be given by $4\pi a_t^2$ and $4\pi a^2_{\text{inc}}$ respectively.

The amplitudes a_+ and a_- will be about the same and equal to the nuclear radius, Eq. (2–1), in the absence of resonances, for only potential scattering is present; as a result the spin-dependent incoherent scattering will be small. Near a resonance, however, the scattering amplitude will change rapidly with energy for *one* of the spin states (for the resonance has a definite spin, *either* $I + \frac{1}{2}$ or $I - \frac{1}{2}$) and marked *spin-dependent incoherence* will result because $a+$ and $a-$ differ widely. The rapid change of amplitude with energy for a single spin state can be illustrated by the *cross section* of U^{238}, Fig. 6–1, for which only one spin state occurs (because $I = 0$). The

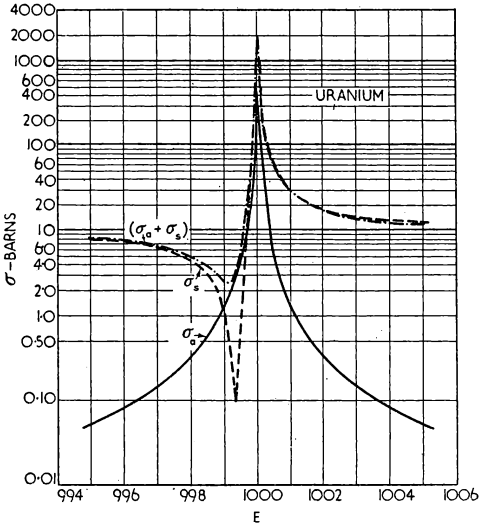

FIG. 6–1. The computed scattering, absorption, and total cross section of U^{238} for an average resonance at 1 keV showing the marked interference effect characteristic of an even-even target nucleus.

marked interference of resonance with potential scattering is shown by the dip in cross section below the potential scattering for energies just below the resonances. If the resonance is at an energy slightly above thermal, one of the amplitudes may be negative. There is a possibility that a_{coh} at thermal may by chance be zero, a situation that is almost attained for vanadium, as shown in the table of BNL 325, whose coherent cross section is only 0·032 b, with a negative amplitude. For hydrogen, the amplitude is negative because the negative amplitude of the singlet state ($I - 1/2 = 0$) is so large

that it outbalances the triplet amplitude ($I + 1/2 = 1$), in spite of the 3:1 weighting.

In addition to spin-dependent effects, incoherence may result even for a single element if it has isotopes of different amplitudes, for they are of course distributed at random in the element. The equations for this *isotopic incoherence* are just the same as those given for spin incoherence with the isotopic abundances substituted for the spin weighting factors, and we shall not quote them. In practice it is usually possible to distinguish isotopic from spin-dependent scattering by the use of separated isotopes. The incoherence resulting from temperature agitation of the atoms in the scattering sample is given by the *Debye-Waller factor* in exactly the same manner as it is computed for X-rays, and requires no further discussion.

In addition to diffraction, the optical property of *refraction* is observed for neutrons, with an index, n, given by the coherent scattering amplitude,

$$n^2 = 1 - \lambda^2 N a_{\text{coh}}/\pi \ , \qquad (6\text{–}4)$$

where λ is the neutron wavelength and N the number of nuclei per cm^3. For most materials the scattering amplitude is positive and the index less than unity, corresponding to hard sphere scattering, but for a few, notably hydrogen, the scattering amplitude is negative because of the proximity of a nuclear resonance. While refraction can be measured for neutrons, the effects are extremely small because of the weak scattering (the index differing from unity by about 10^{-6}). The critical angle for *total reflection* which occurs for materials of positive amplitude, is of the order of 20 minutes of arc for available neutron wavelengths and can be measured with good accuracy. The *critical angle*, θ_c, is very simply related to the coherent amplitude,

$$\theta_c = \lambda(N a_{\text{coh}}/\pi)^{\frac{1}{2}} \ , \qquad (6\text{–}5)$$

and this direct relationship makes the critical angle measurement a valuable approach in the determination of several fundamental constants. Because the scattering is in the forward direction, the Debye-Waller factor is unity; furthermore the critical angle is independent of the crystalline structure of the mirror. As a result of these properties, the critical angle is a sensitive measure of the coherent amplitude even when extremely large incoherent effects are present, as for the neutron-proton scattering, which has been measured with great accuracy by the mirror reflection method.

For utilization of the interference effects of slow neutrons in determination of the structure of materials by neutron diffraction, knowledge of the coherent cross sections of the nuclei present is first necessary. In addition to their use in structural work, several of

the coherent amplitudes are of great intrinsic interest in connection with basic nuclear physics. Measurements of many coherent cross sections have been performed by analysing simple crystals of known structure, for which the observed amplitudes of the Bragg peaks (the structure factors) could be used to determine the relative coherent amplitudes of the constituents of the crystals. The measurements were of a relative nature only, that is, an unknown amplitude would be determined relative to that of some standard element present in the same crystal. The amplitudes measured by diffraction have in general an accuracy of about 3 per cent, which reaches 1 per cent in a few favourable cases. The details of this type of measurement may be found in references 2 and 5.

In addition to the diffraction method, coherent amplitudes can also be determined directly from observation of the critical angle for total reflection. This *mirror method* has limited accuracy, however, for the coherent cross section depends on the fourth power of the measured critical angle and a one per cent accuracy in the latter would be necessary to give accuracy comparable to that of the usual powder diffraction work. An advantage of the mirror method is that it gives the *sign* of the scattering amplitude as contrasted to diffraction methods (which are sensitive to the square of the amplitude). At best, the direct mirror method gives an accuracy of 0·5 per cent in the critical angle or 2 per cent in the coherent cross section. Fortunately, *balancing techniques* are available for mirror reflection, and where these are applicable (for example in the coherent neutron-proton scattering to be described) the attainable accuracy is much higher. The balanced mirror technique can actually be used for gases, with an accuracy of about 10 per cent, the values given in BNL 325 for helium and nitrogen having been determined in this way. A full discussion of neutron mirror techniques is given in reference 5.

An indirect approach for coherent cross sections, based on the total cross section, sometimes results in higher accuracy than the diffraction or mirror methods. The total scattering cross section can be obtained readily by a transmission experiment if the neutron absorption is small, for the latter can then be subtracted as a minor correction. When the neutron energy used in the transmission measurement is sufficiently high so that the atom acts as if free during the collision the so-called *free atom cross section* is obtained, which is simply related to the coherent cross section. The free atom cross section is first converted to the value appropriate for a completely bound atom by multiplication by the reduced mass factor, $(A + 1)^2/A^2$, where A is the atomic mass. The *bound atom* value obtained in this way, which is listed in BNL 325, comprises the total scattering cross section, from which the coherent component is obtained by sub-

traction of the incoherent scattering. No subtraction is necessary for a monoisotopic material of zero spin (carbon and oxygen to all intents and purposes fit this description) because the bound atom and the coherent cross sections are identical. In measuring the "free atom" cross section, it might seem that very high neutron energies would be necessary, for the energy transferred to the atom is only a small fraction of the neutron energy. However, the availability of many energy states in crystals implies that the free atom cross section is already attained at an energy of a few electron volts.

The coherent cross section of carbon ($5{\cdot}50 \pm 0{\cdot}04$ b) is one that has been accurately determined from the free atom cross section. Its isotope incoherence is small because the C^{13} isotope is of very small abundance and has a coherent cross section close to that of C^{12}. The coherent cross sections of oxygen and bismuth shown in the thermal table of BNL 325 also have been obtained from the free atom values. Most of the coherent amplitudes given in this table have been determined by neutron diffraction; they have an error of the order of 3 per cent, except for a few, for example Ni, for which particular effort has resulted in a one per cent error. Higher accuracy than the diffraction results was obtained from free atom cross sections for C, Be, O, Fe, and Bi. A few of the amplitudes are negative, and in most of these cases the particular resonance whose proximity causes the negative amplitude is known.

The coherent hydrogen amplitude has received special emphasis in the last few years because of its importance to basic nuclear theory. As can be seen from Eqs. (6–1) and (6–2), the coherent scattering and the total scattering give the amplitudes for the $I + 1/2$ and $I - 1/2$ spin states, the so-called "triplet" and "singlet" states. These amplitudes, when combined with other low energy data (deuteron binding energy and neutron-proton scattering near 1 MeV), give the ranges of the neutron-proton force for the triplet and singlet configuration. Comparison of the latter range with the corresponding proton-proton range then provides an important test of the hypothesis of *charge independence* of nuclear forces, which is supported by the equality of these ranges.

SOURCES OF THERMAL NEUTRONS

The first measurements made with neutrons produced by reactors were those involving thermal neutrons and since that time measurements with thermal neutrons have advanced in types and in the accuracy of results. At present, the greatly increased source strengths relative to the early nuclear reactors make feasible a great variety of experiments that would have been extremely difficult with the first reactors and completely impossible with the natural radioactive

neutron sources that were available before the advent of chain reactions. The source of neutrons for low energy work is of course the *Maxwell distribution* of velocities, almost always at, or near, room temperature. Some efforts have recently been made to obtain neutrons from matter cooled well below room temperature. While this source of neutrons would be extremely valuable for some experiments, practically no results have been obtained with these cooled sources as yet and the usual Maxwell distribution remains the primary neutron source.

Of the wide energy range represented by pile neutrons, the highest density is for those in thermal equilibrium with matter at room temperature; the velocity of these neutrons exhibit the Maxwell distribution familiar from kinetic theory:

$$n(v)\mathrm{d}v = \frac{4n}{v_0^3\sqrt{(\pi)}}\, v^2 e^{-v^2/v_0^2}\mathrm{d}v \ . \qquad (6\text{–}6)$$

This equation, illustrated in Fig. 6–2, gives the density of neutrons

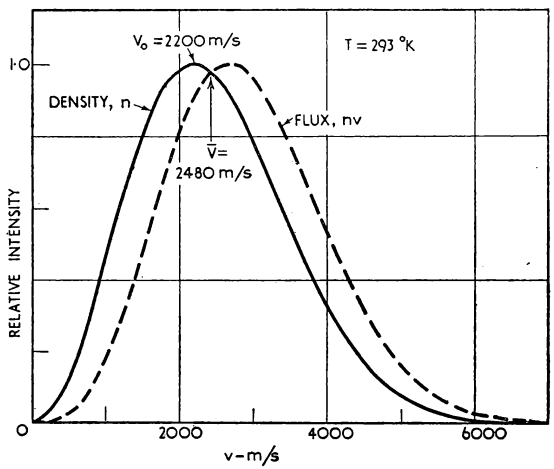

FIG. 6–2. The Maxwell density and flux distribution.

per unit volume, $n(v)$, as a function of velocity, where n is the total number per unit volume. The velocity v_0 is the *most probable velocity*, corresponding to a kinetic energy of kT(0·0253 eV); numerically it is 2200 m/sec at room temperature (293·7° K), the velocity at which thermal cross sections are quoted in BNL 325. The wavelength of the neutrons of most probable velocity is 1·80 Å, of just the order of magnitude of interatomic spacing in matter, hence the prevalence of "crystal effects" in thermal neutron scattering. The neutron *flux* is obtained by multiplying the density by the velocity;

this quantity, also shown in Fig. 6–2, gives the number of neutrons crossing a unit area per second in a neutron beam. As we shall see later, the *effective distribution* depends on the sensitivity of the particular detector as a function of neutron energy. Neutrons of the wavelength required for a particular experiment must be selected from the distribution of Fig. 6–2, which drops off rapidly both above and below v_0.

The flux in a neutron beam is easily calculated from the geometry of the hole opened into the reactor to form the beam. For example, let us assume that a hole of 10 cm by 10 cm cross section is opened into the pile to a point where the flux is 5×10^{13}. The flux in the beam formed by this hole will be given by the number of neutrons crossing a 1 cm^2 area at the point of interest in the beam, which distance will be of the order of 5 m. The beam flux will then be

$$\frac{5 \times 10^{13} \times 10^2}{4\pi(500)^2} = 1{\cdot}6 \times 10^9 \text{ neutrons cm}^{-2} \text{ sec}^{-1} .$$

The collimation (angular divergence of neutrons in the beam) in this particular case will be of the order of 10/500 or about 1°.

The angular resolution needed for neutron diffraction work is higher than that just calculated by an order of magnitude, and for mirror experiments even greater collimation is necessary (about one minute). Higher resolution is obtained by installation of diaphragms to limit the angular divergence of the beam, with an attendant reduction in intensity. Multiple slits are often used so that the intensity reduction resulting from collimation is partially counteracted. Thin sheets of cadmium suffice to stop the thermal neutrons, but it is necessary also to reduce the fast neutrons that are always present as a background. As fast neutrons are much more penetrating than thermal neutrons, collimators usually consist of large blocks of material. In actual practice, combinations of materials, for example plastic, iron, and lead, are used in order to stop the various types of radiation that are present.

The intensities in pile beams are so high that it is of utmost importance to limit the stray radiation, not only from the standpoint of interference with the experiments but to lessen the possibility of harm to the experimenters. The techniques for the formation of beams have been developed sufficiently well so that neutron fluxes of the order of 10^8 thermal neutrons are available in beams sufficiently well-collimated for diffraction experiments, while somewhat lower intensities, with correspondingly higher collimation, are used for neutron mirror research.

Whereas thermal neutron beams containing the entire Maxwell distribution have been of great value in the past, their use has been

almost completely displaced at present by the more exact measurements in which neutrons of specific energies or velocities are isolated. The velocity selection can be performed either with a *crystal monochromator* or with time-of-flight techniques using a *slow chopper*. Because of the serious interfering effect of high-order reflections when the crystal is used for slow neutrons, the chopper has usually been applied in the thermal region for cross-section work. Of course, the crystal is extensively used as a monochromator for a particular application, neutron diffraction as a means of crystal structure analysis. In this application, the monochromating crystal is permanently fixed at a favourable setting for which higher order contamination is small.

A mechanical neutron chopper operating in the thermal region is the same in principle as the fast chopper used in the resonance energy range, but the slow chopper is of much simpler mechanical design. The slow chopper bursts are of the order of 20 instead of one microsecond and, in addition, the chopping of thermal neutrons can easily be accomplished with thin layers of cadmium instead of many inches of steel or plastic. As an example, a view of the Brookhaven slow chopper equipment is shown in Fig. 6–3. The rotor

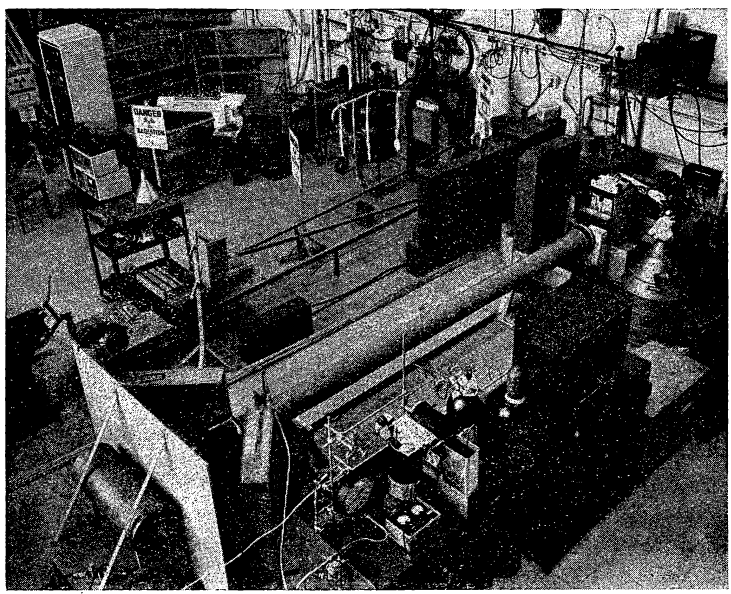

FIG. 6–3. The slow chopper equipment at the Brookhaven reactor, as used for measurement of the cross section of oxygen gas, which is contained in the long tube.

a 4″ diam. cylinder made up of parallel cadmium-plated nickel sheets, driven by an electric motor at speeds up to 15,000 rpm. The desired neutron velocities are selected by measuring electronically their time of flight to a detector, usually a well-shielded BF_3 counter, a few metres away. For cross section measurements in the 5 to 25 Å range, the background of epicadmium neutrons can be greatly reduced by insertion of neutron filters in the beam, which have a high stopping power for neutrons in and above the Maxwell distribution but are practically transparent for long wavelengths. Typical results of slow chopper measurements have already been shown as Figs. 1–4, 1–5, and 1–6, which illustrate the various cross sections that can be investigated with this type of instrument, it being particularly useful for total cross sections.

A true mechanical *monochromator* is one in which neutrons of a narrow velocity band are produced by mechanical methods, with no time-of-flight measurement involved. A monochromator has certain advantages over a time-of-flight instrument, advantages that follow from the fact that actual separation of the different velocities is not accomplished in the latter, i.e., no monochromatization occurs. For example, activation with monoenergetic neutrons is possible with the monochromator and impossible with the time-of-flight method. Because no measured flight path is involved with the monochromator, the geometrical conditions for scattering cross section measurements are also much more favourable for it than for the time-of-flight apparatus.

The obvious advantages of a mechanical monochromator for activation and scattering have led to the construction of several models, of similar design. A device of this type consists of several disks of cadmium containing radial slits, with the disks mounted on the same axis, which is parallel to the neutron beam. As the disks rotate, those neutrons in the beam will pass through the slits whose neutron velocity bears the correct relationship to the speed of rotation. While little in the way of experimental results has been obtained by the use of mechanical monochromators as yet, it seems that continued effort should produce a device capable of yielding resolutions of a few per cent in the sub-thermal region. While the variation of the capture cross section is $1/v$ for most materials in this region, the use of the monochromator seems logical for a few important materials whose cross section behaviour is not known in this energy region. The monochromator may also prove to be a useful instrument in conjunction with other equipment, for example, crystal and mirrors, especially when these are used for sub-thermal neutrons, for it can help to eliminate the effects of thermal neutrons, present in high intensity.

MEASUREMENTS WITH MAXWELL DISTRIBUTION

Because of the high fluxes of thermal neutrons in reactors it is understandable that many measurements have been made using them as a source. Even though the energy distribution is wide, it has been possible to make a large number of cross section determinations of great value using the entire Maxwell distribution. Measurements for the entire distribution are not of great value as far as comparison with theory is concerned, as we have seen, but they still have a great importance with regard to the design of nuclear reactors, especially those reactors that have sufficient moderator so that the Maxwell distribution is attained. The table of thermal cross sections in BNL 325 includes values wherever possible for the precise velocity of 2200 m/sec rather than cross sections averaged over the entire Maxwell distribution. Many of the results in the table have been obtained with monoenergetic neutrons so that the directly measured 2200 m/sec value is available. However, in the past many measurements were made for the entire distribution and its is necessary to convert the result to the monoenergetic value in order to list the cross section in the table. Conversely, a consideration of cross sections appropriate for the entire distribution is of course essential to the work done inside the reactor in which the entire distribution is effective, such as the case of production of radioisotopes, for example.

Cross-section measurements with thermal neutrons can be made using neutrons inside the reactor or present in beams emerging from it. However, measurements for the entire Maxwell distribution are not usually made in neutron beams because of the availability of velocity selectors for beam measurement. Inside the reactor, however, the entire Maxwell distribution is usually used, and it is primarily in this case that it is necessary to consider cross sections averaged over the distribution.

The total cross section, measured by transmission, is one that is now only rarely obtained using the entire distribution. The ease of total cross section measurements relative to all other types, and the ready availability of slow neutron velocity selectors means that total cross sections have been measured for practically all materials as functions of velocity in the thermal region, as demonstrated by the curves of BNL 325. In the past, though, many total cross sections were measured by transmission for the Maxwell distribution and a brief discussion of some of the difficulties involved in this type of measurement is worthwhile. Some of the first cross section measurements made with thermal neutrons involved transmissions of the complete Maxwell velocity distribution through samples. Total cross sections could easily be measured in this way because the well-collimated neutron beams ensured conditions of good geometry. The cross

section thus obtained is a particular average over the Maxwell distribution and, while it can be measured with great accuracy, its interpretation as a cross section at a definite velocity is difficult.

The correct interpretation of the measured cross section involves a careful consideration of the shape of the neutron distribution and the type of counter used in the transmission measurement. For a $1/v$ detector, the counting rate as a function of velocity varies as the Maxwell *density* (n), not *flux*, distribution, for the $1/v$ cancels the v in the flux. Hence the total counting rate I, becomes the integral of the Maxwellian density, given by Eq. (6–6)

$$I = \text{constant} \times \int_0^{0{\cdot}4\ \text{eV}} v^2 e^{-(v/v_0)^2} \mathrm{d}v \ , \qquad (6\text{–}7)$$

where v_0 is the most probable velocity, 2200 m/sec at room temperature. The counting rate would be the integral of the flux, $v^3 e^{-(v/v_0)^2}\mathrm{d}v$, if the detector were "black", i.e., if every neutron hitting the counter were detected. Because most detectors are approximately $1/v$, we shall assume a $1/v$ detector for our present purposes.

For the case of a very thin sample the transmission measurement has a simple interpretation. For then, with transmission T almost unity, the transmission equation, Eq. (1–10), becomes simply

$$1 - T = N\sigma_T x \ , \qquad (6\text{–}8)$$

and the $(1-T)$ observed obviously gives the *average total cross section*, weighted according to the neutron distribution. The essential point is that the incident distribution is undistorted by the sample and all atoms in the sample "see" the Maxwell distribution. Scattering is usually small, essentially constant with energy, and can be subtracted from the total to obtain the absorption cross section. This latter cross section is the *average absorption cross section* for a Maxwell distribution, $\bar{\sigma}_a$. If the sample has a $1/v$ absorption ($\sigma_a = k/v$), we obtain,

$$\bar{\sigma}_a = \frac{\int \sigma_a v^2 e^{-(v/v_0)^2}\mathrm{d}v}{\int v^2 e^{-(v/v_0)^2}\mathrm{d}v} = \frac{2}{\sqrt{\pi}} \frac{k}{v_0} \ , \qquad (6\text{–}9)$$

$$\bar{\sigma}_a = \frac{2}{\sqrt{\pi}} \sigma_{v_0} = 1{\cdot}128\ \sigma_{v_0} \ . \qquad (6\text{–}10)$$

Thus for a $1/v$ material (and detector), the average cross section that is obtained from a thin sample transmission measurement (with scattering subtracted) is 1·128 times the commonly listed value at the most probable velocity, v_0, usually 2200 m/sec.

Unfortunately, in practice thick samples must often be used because the statistical accuracy of the cross section obtained from a transmission near unity is very poor. The simple result just obtained is thus not often applicable. Although the cross section accuracy increases with sample thickness, the Maxwell distribution is distorted an increasing amount because of preferential absorption of the slow neutrons by $1/v$ capture, and it is necessary to consider the effect of this "hardening" on the observed cross section, $\bar{\sigma}_a$.

The increasing distortion of the spectrum with sample thickness implies that the cross section measured for a particular thickness will be an average over a distribution that changes shape as it penetrates the absorber. As a result, the measured cross section is an average over an "average" distribution. In this case, the average cross section as a function of absorber thickness cannot be evaluated directly. It was obtained by Bethe (reference 3) for the case of a $1/v$ sample and a $1/v$ detector by numerical integration, however, and his result is given in the form of a curve, Fig. 6–4. This *hardening*

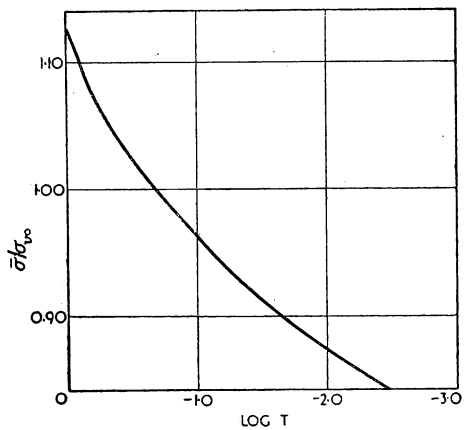

FIG. 6–4. The "hardening" curve, used for interpretation of total cross sections measured by transmission.

correction curve gives the ratio of the observed absorption cross section $\bar{\sigma}_a$ (scattering assumed to be subtracted) to the value at the most probable velocity, as a function of the transmission. Thus for unit transmission the cross section ratio has the value 1·128, as we have already computed, and it decreases with increasing $1/T$. It is interesting that the observed cross section happens to be just the value for the most probable velocity at a transmission of practically 50 per cent. This fortunate circumstance means that if transmissions

close to 50 per cent are consistently used, the observed cross sections are automatically the values at v_0, the ones always listed in tables. The correction of an observed cross section to σ_{v_0} for the transmissions normally used (log T from $-$ 0·5 to $-$ 2·0), is not large and is easily carried out.

In addition to the total cross sections, the matter of *activation cross sections* is of great practical importance. For most materials, for which there are no neutron resonances at or near thermal energy, the activation rate in a neutron flux nv is given by the simple activation formula already given as Eq. (1–17), using the 2200 m/sec cross section, even though the entire Maxwell distribution is present, and its v_0 may be different from 2200 m/sec. The use of the 2200 m/sec cross section rests on the fact that the flux is practically always determined by methods (described in reference 5) that actually measure the neutron density n independently of v (because the response of a $1/v$ detector is proportional to n rather than nv). The quoted result of a flux measurement is obtained by multiplying the measured neutron *density* by an arbitrary v, which is almost universally taken as 2200 m/sec. The actual flux may be, and probably is, different from the value obtained by assuming 2200 m/sec for v_0, because the temperature of the distribution is usually higher than room temperature. This difference is unimportant, however, when the activation of a material of approximately $1/v$ cross section is concerned. The activation of the material is, like the flux measurement, independent of v, but the cross section to be used in Eq. (1–17) *must* be the cross section at the velocity that was assumed in the quotation of the flux in the same equation (almost certainly 2200 m/sec) if the correct activation is to be obtained.

While this velocity independence of the activation holds strictly only for $1/v$ substances, most elements are $1/v$ within experimental error in the thermal region, and fortunately no further complications ensue for them. For those few materials that depart significantly from $1/v$, the calculation of reaction rate or activation in a Maxwell distribution must take into account the non-$1/v$ cross section and the neutron temperature. The simplest way to correct the non-$1/v$ behaviour is to calculate, from the known cross section curve of the material, the ratio of the actual reaction rate to that for a $1/v$ material of the same cross section value at the velocity, v_0, corresponding to the temperature of the neutron distribution, usually 2200 m/sec. This ratio, f, constitutes a *correction factor* for the non-$1/v$ effect that is easily calculated from the actual cross section as a function of velocity, for it is merely the ratio of the reaction rate of the actual cross section to a $1/v$ cross section, both integrated over the Maxwell *flux* distribution:

$$f_x = \frac{\int n(v) v \sigma_x \, dv}{\int n(v) v \, (k_x/v) \, dv} , \tag{6-11}$$

$$f_x = \frac{1}{n} \int n(v) \, \frac{\sigma_x}{k_x/v} \, dv . \tag{6-12}$$

In these equations, f_x is the correction factor for a material x of cross section σ_x and k_x/v is a $1/v$ cross section equal to that of x at v_0, k_x/v_0 being the v_0 cross section of material x listed in the table if $v_0 = 2200$ m/sec, as is usually true. In other words, f_x is just the cross section ratio weighted according to the Maxwell density (not flux) distribution.

The correction factor for a room temperature distribution is listed for those isotopes that differ appreciably from $1/v$ in the thermal cross section table in BNL 325. In use, the 2200 m/sec cross section in the table is simply multiplied by f before insertion into Eq. (1–17) to give the reaction rate or activation that will be obtained with a Maxwell distribution at room temperature. As an example of the use of f-factors we can calculate the reaction rate or number of neutron captures per second in one gramme of Cd^{113}, hence the formation rate of Cd^{114} in the Brookhaven pile ($nv = 5 \times 10^{12}$). The appropriate cross section given in BNL 325 is "19,500 b, not $1/v$, $\times$ 1·3", thus $f_{Cd} = 1{\cdot}3$. The actual 2200 m/sec cross section is 19,500 b, but because of the resonance near thermal energy, the effective value of the cross section for a Maxwell distribution is 19,500 $\times$ 1·3 = 25,300 b, and the reaction rate is

$$\frac{5 \times 10^{12} \times 25{,}300 \times 0{\cdot}602}{113} = 6{\cdot}7 \times 10^{14} \text{ captures per sec.}$$

Strictly speaking, the f-factor given is accurate for a room temperature Maxwellian only, but the change in f for a few hundred degrees C is less than the cross section error in most cases. In using f factors where the neutron distribution is not at room temperature a word of caution is necessary. If the appropriate v_0 is used instead of 2200 m/sec in Eqs. (6–11) and (6–12), then it is essential that the flux used be nv_0, *not* $n \times 2200$ m/sec as is usually quoted. The f factor then gives the ratio of the reaction rate of x to that of a $1/v$ material whose cross section at v_0 is the same as that of x; this cross section of x must be obtained from the curves in BNL 325, not the tables, which gives values at 2200 m/sec only. If the usually quoted flux is used, based on 2200 m/sec, as discussed earlier, then the 2200 m/sec cross section will give exactly the right result for a $1/v$ material regardless of the neutron temperature; for non-$1/v$, the 2200 m/sec cross section and the listed f will usually result in negligible error for

distributions within about 100° C of room temperature. For careful work, however, the cross section and flux at the appropriate v_0 should be used. For a few important heavy elements the f factor is given as a function of neutron energy with the curves of BNL 325.

Although most of the activation resulting from irradiation inside the pile lattice represents absorption of thermal neutrons, resonance neutrons do contribute a non-negligible activation. It is therefore necessary to take into account the *resonance activation* in a thermal activation cross-section measurement made inside the pile lattice. Fortunately, the resonance contribution can usually be ascertained experimentally by an additional irradiation inside cadmium. After elimination of the resonance activation by a *cadmium difference* in a thermal cross-section measurement, there are actually very few materials that cannot be considered $1/v$, as witnessed by the few f factors listed in the thermal table.

The thermal activation cross sections of the table have been obtained from the measured disintegration rate after activation by thermal neutrons, by means of Eq. (1–17), using the conventional ($v_0 = 2200$ m/sec) thermal flux, and f factors where necessary. As the flux itself is usually calibrated with a $1/v$ detector, the activation cross section resulting from Eq. (1–17) can, of course, be considered a measurement relative to the cross section of the $1/v$ standard, usually boron. The activated material is usually counted on a calibrated Geiger-Mueller counter or some other absolute β-counter and the disintegration rate is obtained from the counting rate by means of the known efficiency of the counter. Although the principle of activation measurements is quite simple, it is exceedingly difficult to obtain reproducible, accurate results in practice, with the result that activation cross sections in general are known only to about 20 per cent. By far the most significant errors arise in connection with the conversion of the counting rate to the disintegration rate I. For a sample known to disintegrate by emission of β-particles alone, it is reasonably certain that each beta entering the counter will be recorded. Even in this ideal case, however, significant error arises in the conversion of counting to disintegration rate, that is, in the estimation of the *efficiency* of the counter (fraction of disintegrations giving rise to counts).

A method of measuring the thermal *absorption cross section*, in contrast to the activation and total cross sections, by means of the effect on pile reactivity, was developed with the first nuclear reactor as a means of testing the neutron absorption of reactor components. As neutron-absorbing impurities in these components were particularly "dangerous" relative to the attainment of a chain reaction, the procedure came to be called the *danger coefficient* method of neutron

absorption measurement. As the *reproduction factor* of a pile, k, is critically dependent on the loss of thermal neutrons by absorption, the effect on the pile reactivity caused by a particular sample is thus a direct measure of its neutron absorption. Changes in the reactivity of the pile can be measured either in terms of the *period* of the pile or by means of the position of a control rod for exact *criticality* ($k = 1{\cdot}000$). In this method, the sample is placed at the centre of the pile to secure the maximum sensitivity, for the effect of a neutron absorber on reactivity is proportional to the square of the neutron flux at the point of absorption. The development and techniques of the danger coefficient method are described fully in reference 1.

The *pile oscillator* follows the same principle as the danger coefficient method, although the pile power does not reach equilibrium because of the rapid oscillation of the sample. Even though the change in pile power is a complicated function of neutron absorption when short period changes are considered, it is nevertheless true that the amplitude of the pile power variation is strictly proportional to the neutron absorption of the sample. If a sample is moved periodically in and out of the pile, or even from one point of the pile to another, and the pile flux at a particular position recorded as a function of time, the oscillating component of the pile flux will be proportional to the neutron absorption cross section of the sample. The Oak Ridge oscillator, which is operated in a part of the pile where the flux is predominantly thermal, Fig. 6–5, moves the sample in and out of the neutron detector, which is a hollow ionization chamber.

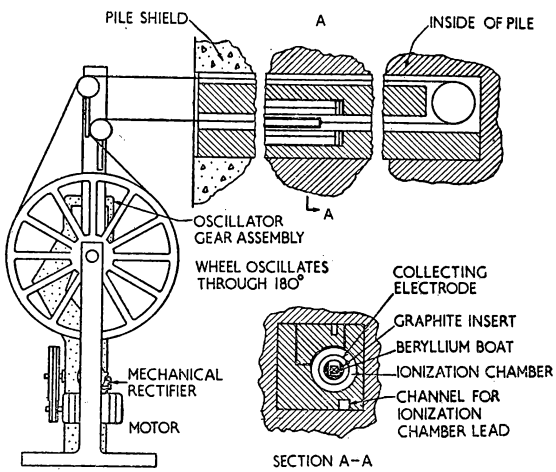

FIG. 6–5. The pile oscillator in use at Oak Ridge laboratory for measurement of absorption cross sections.

The detector is thus sensitive mainly to the local flux oscillation and the over-all pile power varies only slightly because of the limited motion of the oscillating sample. The Oak Ridge apparatus can be used with the pile operating at full power, hence without interference with other experiments (because the sample is outside the pile lattice), as contrasted to the Argonne design, which is located in the centre of the reactor core and necessitates pile operation at a level of a few watts. Many of the thermal absorption cross sections in BNL 325, particularly of the separated isotopes, have been measured with the Oak Ridge oscillator. The pile oscillators are extremely accurate because the circuits are arranged to detect only that component of the pile power oscillating with the period of the mechanical motion. The limit of detectability of the Argonne oscillator, for example, corresponds to the presence of only 25 μg of boron.

In addition to the danger coefficient and pile oscillator methods for measuring the absorption cross section, there is another method that is useful for only a very few materials, but for these it has been of extreme value. This is the method of determining the absorption cross section by measurement of the *diffusion length* of neutrons in a large block, typically of the order of metres in size. The method is useful only for materials in which the absorption cross section is very low so that the approximations of *diffusion theory* are valid. The absorption cross section is then a simple function of the measured diffusion length, L,

$$L^2 = \frac{1}{3N^2\sigma_{\bar{v}}\sigma_{tr}\left(1 - \frac{2}{5}\frac{\sigma_{\bar{v}}}{\sigma_{tr}}\right)} . \qquad (6\text{–}13)$$

Here N is the number of nuclei per cm^3, σ_{tr} is the *transport cross section*, given by $\sigma_s(1 - \overline{\cos\theta})$ with θ the scattering angle, and $\sigma_{\bar{v}}$ is the absorption cross section at the average neutron velocity, given by $\sigma_{v_0}/1{\cdot}128$. It is important to distinguish between $\sigma_{\bar{v}}$ and $\overline{\sigma_a}$, defined in Eq. (6–10). The technique of measurement of the diffusion length is quite straightforward and we shall not discuss it further at this point. The diffusion measurements are described in detail in reference 5. The outstanding examples of absorption cross sections measured by diffusion are those of the moderators graphite, beryllium, and deuterium, whose cross sections are $3{\cdot}2 \pm 0{\cdot}2$, 10 ± 1, and $0{\cdot}46 \pm 0{\cdot}10$ millibarns, respectively.

THERMAL CROSS SECTIONS OF FISSIONABLE NUCLIDES

Even though the thermal cross sections of the fissionable nuclides have been measured in the same way as the nonfissionable nuclides, they deserve special attention because of their importance to theory

as well as to reactors, and the amount of effort that has gone into their measurement. In addition, there are several types of measurements made with the fissionable nuclides, involving the process of fission, that do not apply to nonfissionable nuclides. These special techniques, involving the detection of the fission neutrons or fission fragments have already been described in Chapter 5, and we shall limit ourselves at the present time to a discussion of the results of very careful application of these methods to the thermal energy region alone.

Whereas the thermal energy region covers no resonances at all, although usually participating in the effects of several, it is still worthy of careful attention because of the great importance of thermal cross sections in the behaviour of nuclear reactors. The precise nature of the energy variation of the fission and capture cross sections determines the *temperature coefficient* of reactivity, and it is largely because of this application that careful measurements have been made in the thermal region for the principal fissionable isotopes U^{233}, U^{235}, and Pu^{239}. In connection with the cross sections throughout the thermal region, a matter of great importance is that of the cross sections for fission and capture at the single velocity 2200 m/sec. These values have great significance because many measurements are made relative to them, and in this way they become the basis for the standardization of many experimental results. In addition, they are the standard numbers for many complex reactor calculations.

Although the important 2200 m/sec cross sections have been measured in many laboratories there has been a surprisingly large amount of disagreement among the results in the past. Fortunately, at the time of the Geneva meeting in August 1955, there was an extremely good opportunity to standardize these fundamental values. The situation was unique in that they had been measured carefully in various laboratories throughout the world completely independently, because of security restrictions in effect at the time of measurement. There was thus the opportunity to see how well the cross sections would agree when measured in a completely independent manner. In connection with the Geneva meeting it was possible to have a discussion in which the scientists of each country presented what they considered the best values of their country and in this way to obtain a set of "world average" values based on the cross sections contributed by each country.

Since the time of the Geneva meeting at which the world average values were first established, it has been possible to discuss all the measurements at somewhat greater length—as a result of these discussions some small changes have occurred in the values contributed

TABLE 6–1

World values of 2200 m/sec cross sections of fissionable isotopes

The values shown for each country are the "best values" as submitted by that country; the *f*-factors have been computed from the curves in BNL 325, Supplement 1, and ν is assumed constant with energy.

		U.S.	U.K.	U.S.S.R.	France	Canada	Norway	India	World weighted averages	World consistent set
U^{233}	f									
σ_{abs}	1·001	585±10	598±10	590±20					591±7	588±7
σ_F	1·006	533±10	533±12	525±15		535±15	521±20		532±20	532±6
$1+\alpha$	0·995	1·098±0·008	1·12±0·03	1·100±0·005					1·100±0·004	1·105±0·007
η	1·005	2·28±0·03	2·25±0·04	2·31±0·02					2·29±0·02	2·28±0·02
ν	1·000	2·50±0·03	2·52±0·07	2·62±0·10					2·51±0·03	2·52±0·03
U^{235}										
σ_{abs}	0·974	689±7	725±13	695±20					697±6	694±10
σ_F	0·977	580±7	596±14	570±15	584±20		587±16	555±15	579±5	582±10
$1+\alpha$	0·997	1·188±0·008	1·21±0·03						1·189±0·008	1·192±0·008
η	1·003	2·06±0·03	2·05±0·04	2·08±0·02					2·070±0·015	2·07±0·02
ν	1·000	2·46±0·03	2·49±0·06	2·54±0·10					2·47±0·03	2·47±0·03
Pu^{239}										
σ_{abs}	1·077	1025±15	1006±25	1035±20					1025±13	1025±13
σ_F	1·052	748±15	717±16	715±30	770±20				740±9	738±9
$1+\alpha$	1·024	1·37±0·03	1·40±0·04						1·38±0·02	1·39±0·03
η	0·976	2·10±0·03	2·07±0·06	2·08±0·02					2·085±0·016	2·09±0·02
ν	1·000	2·88±0·06	2·90±0·09	3·02±0·10					2·91±0·04	2·91±0·04

by each country, hence in the final world values. The situation at the present time is presented in Table 6–1, which gives the best values as measured in each of several countries. These values have been submitted to the Brookhaven compilation group by the scientists in each country, and represent the "best values", based on all the measurements in each particular country.

The individual results and stated uncertainties for a given quantity, such as the fission cross section of U^{235}, were first used to obtain a weighted mean, with a resulting set of values for the various nuclides shown in Table 6–1. As the numbers thus obtained form an overdetermined set, these *world weighted averages* were then adjusted very slightly to obtain a *world consistent set.* Adjusting the values for consistency seems desirable, especially since the changes are small, in order to avoid confusion in their use.

An examination of the cross sections of Table 6–1 shows that, while most countries agree well on the majority of the values, there are still rather large discrepancies, particularly in the case of fission of U^{235}. The comparison of the results of different countries afforded by Table 6–1, which appears in the first supplement to BNL 325, dated January 1, 1957, is useful in that it shows the present state of agreement of these important cross sections and suggests where further work is definitely needed. Actually, and somewhat surprisingly, the agreement is not as good for the fissionable nuclides as it is for some other materials in which less effort has been expended, for example, the thermal cross section of gold. The reason for this state of affairs is probably related to the extremely difficult task of obtaining separated isotopes of high purity, hence there is always some question as to the content of the isotope in question in a particular sample.

The general shape, that is, the energy variation of the cross-section curves for U^{233}, U^{235}, and Pu^{239} is in substantial agreement for laboratories throughout the world. A good illustration is given by the total cross section of U^{235} in the thermal energy region, Fig. 6–6. In order to facilitate comparison of results, the absorption cross section is plotted in Fig. 6–7 multiplied by $E^{\frac{1}{2}}$ to remove the predominent energy variation, which is the $1/v$ energy variation. The experimental points as measured are actually total cross sections and the absorption cross section used in preparing Fig. 6–7 was obtained by subtracting the scattering cross section. This scattering cross section is not constant with energy for U^{235}, but varies from about 17 barns at zero energy to 14 barns at 1 eV, because of the effect of nearby resonances.

Even on the extended scale of Fig. 6–7 the agreement among results from various countries on the shape of the curve is quite good. The

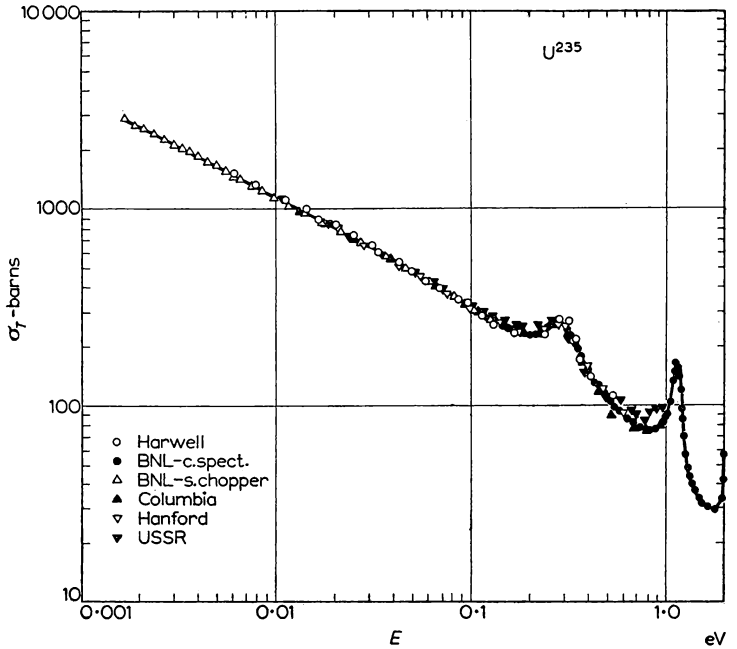

FIG. 6–6. The cross section of U^{235} in the thermal energy region, including results from laboratories throughout the world, as presented at the Geneva Conference, August 1955.

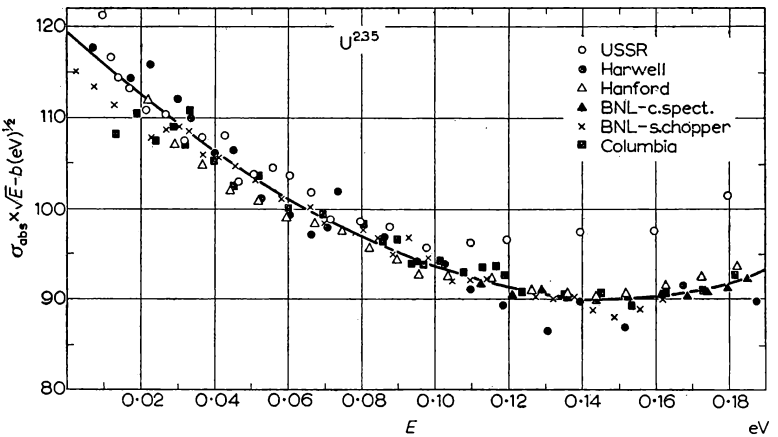

FIG. 6–7. The absorption cross section of U^{235} in the thermal region, multiplied by $\sqrt{E}$ to remove the predominant $1/v$ energy variation.

variety of instruments used in obtaining these data is impressive —the Soviet pulsed cyclotron, the Harwell linear accelerator, the Hanford and Brookhaven crystal spectrometers, the Brookhaven slow chopper and the University of Columbia pulsed cyclotron. The results of all measurements agree in showing that the U^{235} absorption decreases more rapidly with energy than $1/v$, which behaviour would appear as a horizontal line on Fig. 6–7. The departure of the U^{235} cross section from $1/v$ is a result of the presence of several nearby resonances, whose properties have already been discussed in the previous chapter.

The fission cross section, as measured in the thermal energy region by various velocity selectors, using ionization chambers to detect fission fragments is shown in Fig. 6–8, in the form $E^{\frac{1}{2}}\sigma_F$. Whereas

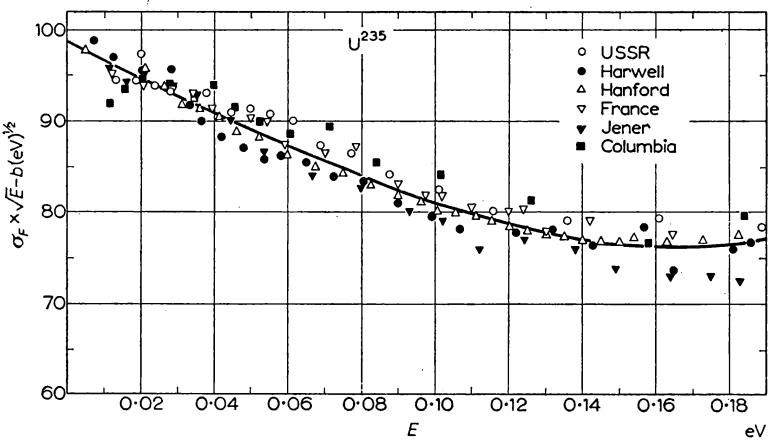

FIG. 6–8. The fission cross section of U^{235} in the thermal region multiplied by $\sqrt{E}$.

for the absorption cross section data no normalization was needed, in the case of fission the results reported by individual laboratories have been normalized to the world's best value of 582 barns at 2200 m/sec. Actually, all of the fission cross-section measurements were made relative to the 2200 m/sec value so it is felt that the best way to combine the data is to normalize all of them to a single value. Normalized in this way, the results from various laboratories are in good agreement and show departure from $1/v$ that is similar to the departure of the absorption cross section. The similarity of the shapes of the curves show that α, the ratio of capture to fission, is reasonably constant in this energy region. Further discussion of the measurements of U^{235}, and U^{233} and Pu^{239} as well, appears in reference 4.

The separate measurements of absorption and fission of course give η, but as the energy variation of η can be measured directly* a useful check on the accuracy of all measurements is obtained. In the thermal energy region the η thus determined is in very good agreement with the values computed from the absorption and fission cross sections. It is fortunate that the agreement is so good because, as we have already said, the variation of η with energy is of great importance to the understanding of the temperature coefficient of reactors. The situation in the thermal region is shown for U^{235} in

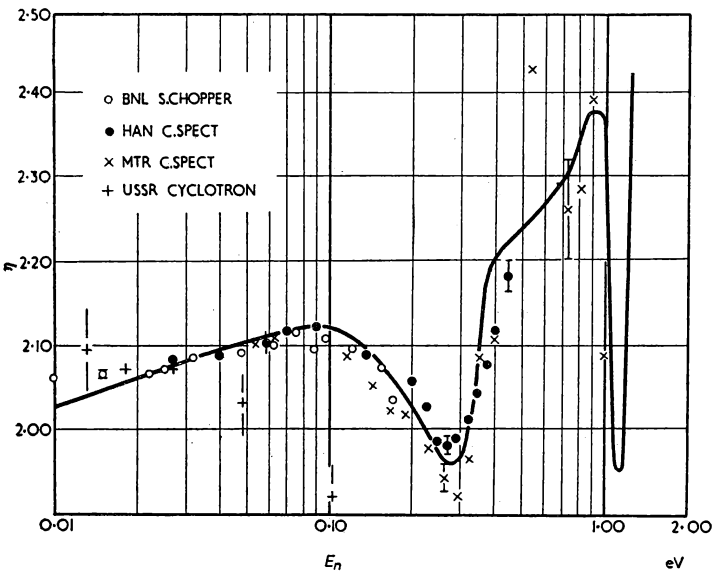

FIG. 6–9. The direct measurements of η for U^{235} in the thermal region compared with the value, shown by the solid line, computed from the world's best cross section curves for total and fission.

Fig. 6–9 in which the solid curve is computed from the "world's best" absorption and fission cross sections, found in Supplement 1 of BNL 325, while the points are direct measurements of η. In this comparison it is assumed that ν is constant with energy, an assumption which seems extremely well substantiated at the present time, as we have seen in Chapter 5. The agreement among the total, fission, and η results are not as good in the region above thermal, a situation that has already been discussed in connection with resonance parameters in Chapter 5.

* By the method of Eq. (5–1).

LATTICE VIBRATION SCATTERING

With the exception of the small changes in cross section resulting from the Doppler effect, all of the cross sections that we have been discussing show no dependence on sample temperature, as would be expected for purely nuclear interactions. However, for very low neutron energies, less than the kinetic energy of thermal agitation, there is a type of scattering whose cross section varies extremely rapidly with temperature. This type of scattering can be seen in the cross-section curve for beryllium, Fig. 1–4, in which the cross section below the crystal cutoff shows an extremely rapid temperature dependence. This rapidly varying cross section represents the *lattice vibration scattering* in which the slowly moving neutron gains a quantum of lattice vibration energy, a *phonon*, and leaves the crystal at a velocity much higher than its incident velocity. Because this process is one which the outgoing particle has a velocity independent of the incoming velocity, the resultant cross section is $1/v$, in close analogy to capture or fission, in which very rapid particles are produced.

Experimental studies of the lattice vibration scattering are important to solid state theory for they give information on the properties of the phonons in a very direct manner. At somewhat higher energies the information gained is of direct interest to reactor calculations as well. At energies slightly above thermal the lattice vibration scattering is the main process by which the neutron gives up its kinetic energy hence the process is significant to the attainment of equilibrium between neutrons and moderators. At low energies, such as shown in Fig. 1–4, the process is one of energy gain by the neutrons but the processes taking place are closely similar to those for energy loss in spite of the opposite sense of the energy exchanges.

In connection with the study of lattice scattering in relation to solid state theory the quantity of interest is not only the cross section, shown in Fig. 1–4, but the much more complicated matter of the amount of energy gained by an individual neutron as a function of the angle of emission. When studies are made of the energy gain as a function of angle for scattering by a single crystal, much information can be gained about the nature of the lattice vibrations in the crystal, such as the *dispersion* law, i.e., the relationship between the momentum (essentially the reciprocal wavelength) and frequency (i.e. energy) of the phonons. The experimental results are particularly fruitful because both momentum and energy must be conserved in the scattering process, hence information is directly gained on both momentum and energy of individual phonons. The details of the fundamental phenomena involved in the scattering process are described in reference 6.

Measurements in which the energy gain is determined are of course much more difficult than ordinary transmission measurements, which give only the total cross section, as for beryllium in Fig. 1–4. Because of this greater difficulty it is only recently that measurements of the energy have been made, and these measurements, although in their early stages, show great promise as a means of investigating fundamental properties of the spectrum of lattice vibrations in crystalline materials.

REFERENCES FOR ADDITIONAL INFORMATION

1. ANDERSON, FERMI, WATTENBERG, WEIL, and ZINN, *Phys. Rev.* **72**, 16 (1947). Describes the development and basic principles of the "danger coefficient" method of measuring neutron absorption cross sections.
2. G. E. BACON, *Neutron Diffraction* (Clarendon Press, Oxford, 1955). An extensive treatment of the theory and techniques of neutron diffraction, together with numerous applications to structure analysis.
3. H. A. BETHE, *Rev. Mod. Phys.* **9**, 69 (1937), p. 135. Theoretical treatment of "hardening" corrections for neutron transmission measurements.
4. J. A. HARVEY and J. E. SANDERS, article on "Summary of Results on σ_{abs}, σ_F, α, ν and η of U^{233}, U^{235}, and Pu^{233}" in *Physics and Mathematics*, Vol. I, *Progress in Nuclear Energy*, *Series I* (Pergamon Press, 1956). A complete description of experimental methods and evaluation of results as presented at the Geneva conference, August 1955.
5. D. J. HUGHES, *Neutron Optics* (Interscience, 1954). The fundamental principles of the optical scattering of neutrons, including magnetic scattering and brief descriptions of the techniques and results of neutron diffraction and reflection. *Pile Neutron Research* (Addison-Wesley, 1953). Methods of neutron flux standardization are described in Chapter 3 and measurement of absorption cross sections by diffusion in Chapter 8.
6. G. PLACZEK and L. VAN HOVE, *Phys. Rev.* **93**, 1207 (1954). The fundamental theory of the inelastic scattering of slow neutrons by lattice vibrations.

APPENDIX 1

CONSTANTS AND CONVERSION FACTORS

FOR convenience, the commonly used constants, and conversion factors connecting various systems of units, are collected here; they are based on the physical constants given by Cohen, Dumond, Layton, and Rollett, *Rev. Mod. Phys.* **27**, 363 (1955).

electron mass $= 9{\cdot}107 \times 10^{-28}$ g $= 0{\cdot}5110$ MeV
electron charge $= 4{\cdot}803 \times 10^{-10}$ esu
neutron mass $= 1{\cdot}008986$ atomic mass units
1 atomic mass unit $= 931{\cdot}1$ MeV $= 1{\cdot}658 \times 10^{-24}$ g
1 eV $= 1{\cdot}602 \times 10^{-12}$ ergs
1 chemical mass unit $= 1{\cdot}0027$ atomic mass units
neutron magnetic moment $= -1{\cdot}913$ nuclear magnetons
1 nuclear magneton $= \dfrac{eh}{4\pi M_p c} = 5{\cdot}050 \times 10^{-24}$ erg/gauss (where M_p is proton mass)
Planck's constant $h = 6{\cdot}625 \times 10^{-27}$ erg-sec
$\hbar = \dfrac{h}{2\pi} = 1{\cdot}054 \times 10^{-27}$ erg-sec
Boltzmann's constant $k = 1{\cdot}380 \times 10^{-16}$ erg/deg
standard gas volume $= 22{\cdot}42$ litres/mol
Avogadro's number $= 6{\cdot}026 \times 10^{23}$
velocity of light $= 2{\cdot}9979 \times 10^{10}$ cm/sec
1 curie $= 3{\cdot}70 \times 10^{10}$ dis/sec
λ (neutron) $= 0{\cdot}2860/E^{1/2}$, E in eV, λ in A
$4\pi\lambda^2 = 2{\cdot}604 \times 10^6/E$ barns
energy of 2200 m/s neutron $= 0{\cdot}02530$ eV

APPENDIX 2

ATOMIC MASSES OF LIGHT NUCLIDES

THIS table gives atomic masses M in atomic mass units (physical scale), and mass excess, $M - A$, in MeV; it is taken from A. H. Wapstra, *Physica* **21**, 367 (1955).

Element	A, mass number	$M - A$, mass excess (MeV)	M, atomic mass (amu)
n	1	8·368	1·008 986 ± 2
H	1	7·585	1·008 145 ± 2
H	2	13·726	2·014 740 ± 3
H	3	15·835	3·017 005 ± 5
He	3	15·817	3·016 986 ± 5
He	4	3·607	4·003 873 ± 3
He	5	12·932	5·013 888 ± 32
He	6	19·398	6·020 831 ± 31
Li	5	12·988	5·013 948 ± 220
Li	6	15·862	6·017 034 ± 5
Li	7	16·977	7·018 232 ± 6
Li	8	23·310	8·025 033 ± 5
Be	7	17·840	7·019 159 ± 5
Be	8	7·309	8·007 849 ± 5
Be	9	14·010	9·015 046 ± 6
Be	10	15·566	10·016 716 ± 7
B	8	24·925	8·026 768 ± 430
B	9	15·081	9·016 195 ± 6
B	10	15·010	10·016 119 ± 6
B	11	11·914	11·012 795 ± 6
B	12	16·917	12·018 168 ± 6
C	10	18·847	10·020 240 ± 110
C	11	13·895	11·014 922 ± 7
C	12	3·541	12·003 803 ± 5
C	13	6·963	13·007 478 ± 5
C	14	7·157	14·007 687 ± 3
C	15	13·187	15·014 162 ± 50
N	12	21·209	12·022 776 ± 110
N	13	9·185	13·009 864 ± 5
N	14	7·002	14·007 520 ± 3

Element	A, mass number	$M - A$, mass excess (MeV)	M, atomic mass (amu)
N	15	4·528	15·004 862 ± 5
N	16	10·402	16·011 171 ± 13
N	17	13·022	17·013 984 ± 210
O	14	12·169	14·013 069 ± 15
O	15	7·233	15·007 767 ± 6
O	16	0	16·000 000
O	17	4·222	17·004 534 ± 5
O	18	4·521	18·004 855 ± 8
O	19	8·931	19·009 591 ± 13
F	17	6·989	17·007 506 ± 4
F	18	6·188	18·006 646 ± 9
F	19	4·142	19·004 448 ± 7
F	20	5·904	20·006 340 ± 11
Ne	18	10·415	18·011 185 ± 220
Ne	19	7·398	19·007 945 ± 9
Ne	20	−1·146	19·998 769 ± 9
Ne	21	0·465	21·000 499 ± 10
Ne	22	−1·533	21·998 354 ± 12
Ne	23	1·643	23·001 764 ± 12
Na	20	14·187	20·015 236 ± 220
Na	21	3·987	21·004 281 ± 35
Na	22	1·307	22·001 404 ± 14
Na	23	−2·744	22·997 053 ± 11
Na	24	−1·336	23·998 565 ± 14
Na	25	−2·068	24·997 781 ± 180
Mg	23	1·353	23·001 453 ± 14
Mg	24	−6·853	23·992 640 ± 15
Mg	25	−5·818	24·993 752 ± 15
Mg	26	−8·569	25·990 798 ± 23
Mg	27	−6·641	26·992 868 ± 23
Mg	28	−6·784	27·992 714 ± 32
Al	24	7·161	24·007 691 ± 320
Al	25	−1·572	24·998 312 ± 60
Al	26	−4·544	25·995 120 ± 23
Al	27	−9·236	26·990 081 ± 16
Al	28	−8·594	27·990 771 ± 16
Al	29	−9·382	28·989 925 ± 110
Si	27	−4·409	26·995 265 ± 19
Si	28	−13·246	27·985 775 ± 19
Si	29	−13·353	28·985 660 ± 20
Si	30	−15·595	29·983 252 ± 19

Element	A, mass number	$M - A$, mass excess (MeV)	M, atomic mass (amu)
Si	31	−13·825	30·985 153 ± 23
Si	32	−14·773	31·984 134 ± 60
P	28	0·545	28·000 585 ± 300
P	29	−8·386	28·990 994 ± 23
P	30	−11·280	29·987 885 ± 48
P	31	−15·308	30·983 561 ± 24
P	32	−14·873	31·984 028 ± 26
P	33	−16·615	32·982 156 ± 30
S	31	−9·866	30·989 405 ± 80
S	32	−16·579	31·982 196 ± 26
S	33	−16·864	32·981 889 ± 30
Cl	32	−3·551	31·996 186 ± 430
Cl	33	−11·412	32·987 774 ± 140

APPENDIX 3

REFERENCES FOR CROSS-SECTION CURVES

THE references are arranged according to the system used in BNL 325 from which the curves in this volume were adapted.

ANL-ac (Argonne National Laboratory—accelerator)
2 — W. F. Stubbins; *Phys. Rev.* **84,** 902 (1951).
3 — Hibdon, Langsdorf and Holland; *Phys. Rev.* **85,** 595 (1952).
4 — Unpublished.
ANL-fn (Argonne National Laboratory—fission neutrons)
1 — Hughes, Garth, and Levin; *Phys. Rev.* **91,** 1423 (1953).
ANL-γn (Argonne National Laboratory—photo-neutrons)
2 — V. Hummel and B. Hamermesh; *Phys. Rev.* **82,** 67 (1951).
ANL-sc (Argonne National Laboratory—slow chopper)
1 — T. Brill and H. V. Lichtenberger; *Phys. Rev.* **72,** 585 (1947).
Bar (Bartol Research Foundation)
1 — S. C. Snowdon and W. D. Whitehead; *Phys. Rev.* **90,** 615 (1953).
2 — C. P. Swann and F. R. Metzger; *Phys. Rev.* **100,** 1329 (1955).
BNL-ac (Brookhaven National Laboratory—accelerator)
1 — Poss, Salant, Snow, and Yuan; *Phys. Rev.* **87,** 11 (1952).
2 — Hafner, Hornyak, Falk, Snow, and Coor; *Phys. Rev.* **89,** 204 (1953).
BNL-cs (Brookhaven National Laboratory—crystal spectrometer)
4 — H. H. Landon and V. L. Sailor; *Phys. Rev.* **93,** 1030 (1954).
8 — Wood, Landon, and Sailor; *Phys. Rev.* **98,** 639 (1955).
11 — V. L. Sailor; *Proc. Int. Conf. on Peaceful Uses of Atomic Energy,* UN, New York, 1956, Vol. 4, Paper 586.
BNL-fc (Brookhaven National Laboratory—fast chopper)
3 — Unpublished.
5 — Pilcher, Harvey, and Hughes; *Phys. Rev.* **103,** 1342 (1956).
BNL-sc (Brookhaven National Laboratory—slow chopper)
3 — Unpublished.
4 — Palevsky, Hughes, Zimmerman, and Eisberg; *J. Nucl. Energy,* **3,** 177 (1956).
Cal (University of California. Radiation Laboratory)
1 — Cook, McMillian, Peterson, and Sewell; *Phys. Rev.* **75,** 7 (1949).
2 — J. De Juren and N. Knable; *Phys. Rev.* **77,** 606 (1950).
3 — R. H. Hildebrand and C. E. Leith; *Phys. Rev.* **80,** 842 (1950).
5 — W. I. Linlor and B. Ragent; *Phys. Rev.* **92,** 835 (1953).
6 — Unpublished.
Cav (Cavendish Laboratory)
3 — E. Bretscher and E. B. Martin; *Helv. Phys. Acta* **23,** 15 (1950).
4 — G. H. Stafford; *Proc. Phys. Soc.* (*London*) A **64,** 388 (1951).
Col (Columbia University)
13 — Unpublished.
CR (Chalk River Laboratory)
1 — E. B. Paul and R. L. Clark; *Can. J. Phys.* **31,** 267 (1953).
3 — Unpublished.

Duke (Duke University)
3 — H. Marshak and H. W. Newson; *Phys. Rev.* **98,** 1162 (1955).
4 — J. H. Gibbons; *Phys. Rev.* **102,** 1574 (1956).
5 — Newson, Gibbons, Marshak, Williamson, Mobley, Toller, and Block; *Phys. Rev.* **102,** 1580 (1956).
Fr (France)
2 — Auclair, Galula, Hubert, Jacrot, Joly, Netter, and Vendryes; *Proc. Int. Conf. on Peaceful Uses of Atomic Energy*, UN, New York, 1956, Vol. 4, Paper 354.
Han (Hanford)
1 — Unpublished.
Har (Harwell)
4 — Unpublished.
5 — J. E. Lynn and N. J. Pattenden; *Proc. Int. Conf. on Peaceful Uses of Atomic Energy*, UN, New York, 1956, Vol. 4, Paper 423.
6 — B. T. Price; *J. Nucl. Energy* **2,** 128 (1955)
Har-ac (Harwell—accelerator)
2 — A. E. Taylor and E. Wood; *Phil. Mag.* **44,** 95 (1953).
Hrv (Harvard University)
1 — R. Sherr; *Phys. Rev.* **68,** 240 (1945).
2 — V. Culler and R. W. Waniek; *Phys. Rev.* **95,** 585 (1954).
3 — Hillman, Stahl and Ramsey; *Phys. Rev.* **96,** 115 (1954).
4 — V. Culler and R. W. Waniek; *Phys. Rev.* **99,** 740 (1955).
JENER (Joint Establishment for Nuclear Energy Research, Norway)
3 — D. Popovic; *J. Nucl. Energy* **1,** 3 (1954).
LA (Los Alamos)
3 — N. Nereson and S. E. Darden; *Phys. Rev.* **89,** 775 (1953).
4 — N. Nereson and S. E. Darden; *Phys. Rev.* **94,** 1678 (1954).
5 — Unpublished.
LA-ac (Los Alamos—accelerator)
3 — F. L. Ribe; *Phys. Rev.* **87,** 205 (1952).
4 — Coon, Graves, and Barschall; *Phys. Rev.* **88,** 562 (1952).
5 — Phillips, Davis, and Graves; *Phys. Rev.* **88,** 600 (1952).
6 — Brolley, Fowler, and Schlacks; *Phys. Rev.* **88,** 618 (1952).
7 — S. G. Forbes; *Phys. Rev.* **88,** 1309 (1952).
8 — M. E. Battat and F. L. Ribe; *Phys. Rev.* **89,** 80 (1953).
10 — R. B. Day and R. L. Henkel; *Phys. Rev.* **92,** 358 (1953).
11 — Martin, Diven, and Taschek; *Phys. Rev.* **93,** 199 (1954).
15 — E. R. Graves and R. W. Davis; *Phys. Rev.* **97,** 1205 (1955).
17 — Day, Mills, Perry, and Scherb; *Phys. Rev.* **98,** 279 (1955).
19 — Beyster, Henkel, Nobles, and Kister; *Phys. Rev.* **98,** 1216 (1955).
20 — Unpublished.
21 — Beyster, Walt, and Salmi; *Phys. Rev.* **104,** 1319 (1956).
24 — Frye, Rosen, and Stewart; *Phys. Rev.* **99,** 1375 (1955).
25 — R. B. Day; *Phys. Rev.* **102,** 767 (1956).
Mex (Mexico)
2 — Mazari, Alba, and Serment; *Phys. Rev.* **100,** 972A (1955).
Minn (University of Minnesota)
2 — Freier, Fulk, Lampi, and Williams; *Phys. Rev.* **78,** 508 (1950).
MIT (Massachusetts Institute of Technology)
8 — C. L. Storrs and D. H. Frisch; *Phys. Rev.* **95,** 1252 (1954).
9 — R. M. Kiehn and C. Goodman; *Phys. Rev.* **95,** 989 (1954)
10 — J. B. Guernsey and A. Wattenberg; *Phys. Rev.* **101,** 1516 (1956).
11 — Unpublished.

MTR-cs (Materials Testing Reactor—crystal spectrometer)
7 — L. G. Miller and J. E. Evans; *Bull. Am. Phys. Soc.* Ser. II, **1,** 247 (1956).
MTR-fc (Materials Testing Reactor—fast chopper)
5 — Simpson, Fluharty, and Simpson; *Phys. Rev.* **100,** 1266A (1955).
NWU (Northwestern University)
1 — J. B. Weddell and J. H. Roberts; *Phys. Rev.* **95,** 117 (1954).
ORNL-ac (Oak Ridge National Laboratory—accelerator)
2 — Johnson, Willard, and Bair; *Phys. Rev.* **96,** 985 (1954).
3 — P. H. Stelson and E. C. Campbell; *Phys. Rev.* **97,** 1222 (1955).
4 — Unpublished.
ORNL-cs (Oak Ridge National Laboratory—crystal spectrometer)
2 — Allen, Stephenson, Stanford, and Bernstein; *Phys. Rev.* **96,** 1297 (1954).
Oxf (Oxford University)
2 — R. G. P. Voss and R. Wilson; *Proc. Roy. Soc.* (*London*) A **236,** 41 (1956)
Rice (Rice Institute)
3 — C. F. Cook and T. W. Bonner; *Phys. Rev.* **94,** 651 (1954).
5 — Unpublished.
6 — Taylor, Lönsjö, and Bonner; *Phys. Rev.* **100,** 174 (1955).
9 — T. W. Bonner and J. H. Slattery; *Bull. Am. Phys. Soc.* Ser. II, **1,** 175 (1956).
Switz (Switzerland)
6 — Baldinger, Huber, and Proctor; *Helv. Phys. Acta* **25,** 142 (1952).
Tex (University of Texas)
3 — I. L. Morgan; *Phys. Rev.* **103,** 1031 (1956).
USSR
1 — V. S. Dementi and D. V. Timoshuk; *Compt. Rend. Acad. Sci. U.S.S.R.* **27,** 929 (1940).
5 — Nikitin, Galanina, Ignatiew, Okorow, and Suchorutchkin; *Proc. Int. Conf. on Peaceful Uses of Atomic Energy,* UN, New York, 1956, Vol. 4, Paper 646.
6 — Adamchuk, Gerasimov, Yefimov, Zenkevich, Mostovoi, Pevzner, Chernyshov, and Tsitovich; *Proc. Int. Conf. on Peaceful Uses of Atomic Energy,* UN, New York, 1956, Vol. 4, Paper 645.
7 — Nikitin, Sukhoruchkin, Ignatyev, and Galanina; *Proc. Conf. Acad. Sci. U.S.S.R. on Peaceful Uses of Atomic Energy,* July 1955, p. 81.
Wis (University of Wisconsin)
2 — Barschall, Bockelman, and Seagondollar; *Phys. Rev.* **73,** 659 (1948).
6 — Barschall, Bockelman, Peterson, and Adair; *Phys. Rev.* **76,** 1146 (1949).
10 — Peterson, Adair, and Barschall; *Phys. Rev.* **79,** 935 (1950).
12 — C. K. Bockelman; *Phys. Rev.* **80,** 1011 (1950).
13 — R. L. Henkel and H. H. Barschall; *Phys. Rev.* **80,** 145 (1950).
19 — Bockelman, Miller, Adair, and Barschall; *Phys. Rev.* **84,** 69 (1951).
20 — Miller, Adair, Bockelman, and Darden; *Phys. Rev.* **88,** 83 (1952).
22 — Walt, Becker, Okazaki, and Fields; *Phys. Rev.* **89,** 1271 (1953).
24 — Fields, Becker, and Adair; *Phys. Rev.* **94,** 389 (1954).
26 — R. L. Becker and H. H. Barschall; *Phys. Rev.* **102,** 1384 (1956).

INDEX